Technische Universität München

TUM School of Natural Sciences

Profiling cellular E3 ubiquitin ligase networks

Lukas Teoman Henneberg

Vollständiger Abdruck der von der TUM School of Natural Sciences der Technischen Universität München zur Erlangung eines **Doktors der Naturwissenschaften (Dr. rer. nat.)** genehmigten Dissertation.

Vorsitz: **Prof. Dr. Matthias Feige**

Prüfende der Dissertation:

1. **Hon.-Prof. Dr. Brenda A. Schulman**
2. **Prof. Dr. Stephan A. Sieber**
3. **Prof. Dr. Matthias Mann**

Die Dissertation wurde am 05.04.2024 bei der Technischen Universität München eingereicht und durch die TUM School of Natural Sciences am 01.07.2024 angenommen.

Table of Contents

List of publications

1) Activity-based profiling of cullin-RING ligase networks by conformation-specific probes, **Henneberg LT**, Singh J, Duda DM, Baek K, Yanishevski D, Murray PJ, Mann M, Sidhu SS, Schulman B., bioRxiv. 2023 Jan 17:2023.01.14.524048. doi: 10.1101/2023.01.14.524048. Preprint.
   *Thesis contains work from this published paper.

2) Systemwide disassembly and assembly of SCF ubiquitin ligase complexes, Baek K, Scott DC, **Henneberg LT**, King MT, Mann M, Schulman BA., Cell. 2023 Apr 27;186(9):1895-1911.e21. doi: 10.1016/j.cell.2023.02.035. Epub 2023 Apr 6.
   *Thesis contains work from this published paper.

3) Identification of orphan ligand-receptor relationships using a cell-based CRISPRa enrichment screening platform, Siepe DH, **Henneberg LT**, Wilson SC, Hess GT, Bassik MC, Zinn K, Garcia KC., Elife. 2022 Sep 30;11:e81398. doi: 10.7554/eLife.81398.

4) The tissue protective functions of interleukin-22 can be decoupled from pro-inflammatory actions through structure-based design, Saxton RA, **Henneberg LT**, Calafiore M, Su L, Jude KM, Hanash AM, Garcia KC., Immunity. 2021 Apr 13;54(4):660-672.e9. doi: 10.1016/j.immuni.2021.03.008.

5) Decoding the messaging of the ubiquitin system using chemical and protein probes, **Henneberg LT**, Schulman BA., Cell Chem Biol. 2021 Jul 15;28(7):889-902. doi: 10.1016/j.chembiol.2021.03.009. Epub 2021 Apr 7.

6) Structure-based decoupling of the pro- and anti-inflammatory functions of interleukin-10, Saxton RA, Tsutsumi N, Su LL, Abhiraman GC, Mohan K, **Henneberg LT**, Aduri NG, Gati C, Garcia KC., Science. 2021 Mar 19;371(6535):eabc8433. doi: 10.1126/science.abc8433.

Summary

The complexity of biological live relies on the dynamic organization of proteins into functional networks. Understanding these systems is critical in gaining insights into the regulatory mechanisms shaping cellular function in physiological and pathophysiological conditions. One of these systems are cullin-RING ubiquitin E3 ligases, which regulate virtually all eukaryotic processes and are comprised of over 300 unique complexes. Their modular nature allows them to dynamically adjust to the needs of the cell based on external and internal stimuli, but our understanding of the molecular mechanism of this reshaping and what CRL complexes are assembled and active at a given moment is lacking. To better elucidate the process of CRL assembly and disassembly, we validate the structural mechanism by which CAND1 enables dynamic assembly in cells, by examining how mutations of CAND1 affect degradation of CRL1 substrates and the cellular CRL1 landscape. To enable probing of active CRLs, we developed a suite of synthetic antibodies recognizing active cullins. These probes target active cullins by detecting both their modification with NEDD8 and them assuming the active structural conformation. Implementing our probe to profile the networks of activated CUL1-4-containing E3s in cells revealed the complexes' responses to various stimuli. By profiling several cell types, we observed variations in their baseline neddylated CRL repertoires, which directly impact the efficiency of targeted protein degradation. Moreover, our probe unveiled the differential rewiring of CRL networks across distinct primary cell activation pathways. These findings underscore the importance of conformation-specific probes, which enable nonenzymatic activity-based profiling across a network of varied multiprotein complexes. In the case of neddylated CRLs, this approach reveals widespread regulation and has the potential to facilitate the development of degrader drugs.

Zusammenfassung

Die Komplexität des biologischen Lebens beruht auf der dynamischen Organisation von Proteinen in funktionellen Netzwerken. Diese Systeme zu verstehen ist wichtig, um Einblicke in die Regulierungsmechanismen zu gewinnen, die Zellfunktionen unter physiologischen und pathophysiologischen Bedingungen bestimmen. Eines dieser Systeme sind Cullin-RING-Ubiquitin-E3-Ligasen, die praktisch alle eukaryontischen Prozesse regulieren und aus über 300 einzigartigen Komplexen bestehen. Ihre modulare Natur ermöglicht es ihnen, sich dynamisch an die Bedürfnisse der Zelle anzupassen, aber unser Verständnis des molekularen Mechanismus dieser Umgestaltung und der CRL-Komplexe, die zu einem bestimmten Zeitpunkt zusammengesetzt und aktiv sind, ist unzureichend. Um den Prozess des Auf- und Abbaus von CRLs besser zu verstehen, validieren wir den strukturellen Mechanismus, durch den CAND1 das dynamische Zusammenkommen von CRL-Komplexen in Zellen ermöglicht, indem wir untersuchen, wie Mutationen von CAND1 den Abbau von CRL1-Substraten und die zelluläre CRL1-Landschaft beeinflussen. Um die Untersuchung aktiver CRLs zu ermöglichen, haben wir eine Reihe von synthetischen Antikörpern entwickelt, die aktive Cullins erkennen. Diese Sonden zielen auf aktive Cullins ab, indem sie sowohl deren Modifikation mit NEDD8 als auch deren aktive strukturelle Konformation erkennen. Die Anwendung unserer Sonden zur Erstellung von Profilen zellulärer Netzwerke aktivierter CUL1-, CUL2-, CUL3- und CUL4-haltiger E3s zeigt wie diese Komplexe auf verschiedene Stimuli reagieren. Durch die Erstellung von Profilen verschiedener Zelltypen konnten wir Variationen in ihrem Basisrepertoire an neddylierten CRLs feststellen, die sich direkt auf die Effizienz des induzierten Proteinabbaus auswirken. Darüber hinaus enthüllte unsere Sonde die unterschiedliche Neuverdrahtung von CRL-Netzwerken bei verschiedenen Aktivierungssignalwegen in Primärzellen. Diese Ergebnisse unterstreichen die Bedeutung konformationsspezifischer Sonden, die eine nicht-enzymatische,

aktivitätsbasierte Profilierung in einem System bestehend aus zahlreichen Multiproteinkomplexen ermöglichen. Im Fall von neddylierten CRLs zeigt dieser Ansatz eine weit verbreitete Regulierung auf und hat das Potenzial, die Entwicklung von Degrader-Medikamenten zu erleichtern.

Acknowledgments

I am profoundly grateful to all who have been instrumental in my journey. None of the work described in this thesis would have been possible without the contributions and support of the many people I crossed paths with during my time in the Schulman and Mann groups.

First and foremost, I would like to thank Brenda Schulman and Matthias Mann for giving me the opportunity to pursue research at the intersection of their labs research focus. Thank you for allowing me to pursue my research interests and giving me the liberties to do so. This has allowed me to learn new cutting-edge technologies and grow both as a scientist and a person. I am very thankful for being a part of both your teams. I would like to extend my gratitude to Wade Harper for being a valuable member of my TAC committee and a great source of advice.

I would like to thank David Duda, Jespal Singh and Sachdev Sidhu for laying the foundation for the Fab project and Kheewoong Baek and Daniel Scott for allowing me to be a part of the CAND1 story. Kheewoong Baek I would also like to thank for being a great "roommate" when we shared our lab-space and the constant flow of ideas and knowledge during that time.

I also extend a general thanks to the members, past and present, of the Schulman and Mann research groups, for creating a vibrant research environment where scientific advice is readily available.

From the Schulman lab I would like to thank: Josef Kellermann, Rajan Prabu, Marianne Schuster and Stephanie Ammann-Mwathi for keeping the lab running and well organized; Jakob Farnung for being a great baymate and a constant source of

Abbreviations

Acetyl-CoA	acetyl coenzyme A
ACN	Acetonitrile
ADP	Adenosine diphosphate
AGC	automatic gain control
AP-MS	affinity purification mass spectrometry
APPBP2	Amyloid Beta Precursor Protein Binding Protein 2
APS	Advanced Photon Source
ARIH1	Ariadne RBR E3 Ubiquitin Protein Ligase 1
ATP	Adenosine triphosphate
BET family	bromodomain and extraterminal domain family
BSA	Bovine serum albumin
BTRC	Beta-Transducin Repeat Containing E3 Ubiquitin Protein Ligase
C, Cys	L-cysteine
CAA	2-Chloroacetamide
CAND1	Cullin-associated NEDD8-dissociated protein 1
CAND2	Cullin-associated NEDD8-dissociated protein 2
CCNE	Cyclin E
CDKN1b	Cyclin Dependent Kinase Inhibitor 1B
CDR	Complementarity-determining region
CHUK	Component Of Inhibitor Of Nuclear Factor Kappa B Kinase Complex
CID	collision-induced dissociation
COP9	Constitutive photomorphogenesis 9
CRBN	Cereblon
CRL	cullin-RING E3 ligase
CSF1	Colony Stimulating Factor 1
CSN	COP9 signalosome
CTD	C-terminal domain
DCAF	DDB1 And CUL4 Associated Factor
DCAF15	DDB1 And CUL4 Associated Factor 15
DCN1	Defective In Cullin Neddylation 1 Domain Containing 1
DDA	Data-dependent analysis
DDB1	Damage Specific DNA Binding Protein 1
DIA	Data-independent analysis
DMEM	Dulbecco's Modified Eagle Medium
DMSO	Dimethyl sulfoxide
DNA	Deoxyribonucleic acid
DTT	1,4-dithiothreitol
DUB	Deubiquitylating enzyme

EDTA	Ethylenediaminetetraacetic acid
ELISA	enzyme-linked immunosorbent assay
ELOB	Elongin B
ELOC	Elongin C
EM	electron microscopy
ESI	Electrospray ionization
et al.	et alia
FA	Formic acid
FAC	ferric ammonium citrate
FBS	Fetal bovine serum
FBXL5	F-Box And Leucine Rich Repeat Protein 5
FBXW11	F-Box And WD Repeat Domain Containing 11
FBXW7	F-Box And WD Repeat Domain Containing 7
FDA	Food and Drug Administration
FDR	false discovery rate
FEM1B	Fem-1 Homolog B
FEM1C	Fem-1 Homolog C
GABARAP	Gamma-aminobutyric acid receptor-associated protein
GAN	Gigaxonin
GAPDH	Glyceraldehyde-3-Phosphate Dehydrogenase
GST	Glutathione S-transferase
HCD	Higher-energy collisional dissociation
HECT	homologous to E6-AP C terminus
HEPES	4-(2-hydroxyethyl)-1-piperazineethanesulfonic acid
HPLC	High-performance liquid chromatography
HRP	Horseradish peroxidase
IKZF	IKAROS Family Zinc Finger 1
IL-13	Interleukin 13
IL-4	Interleukin 4
IP	immunoprecipitation
IP-MS	immunoprecipitation mass spectrometry
IPTG	Isopropyl b-D-1-thiogalactopyranoside
IREB2	iron regulatory protein 2
ISG15	Interferon-stimulated gene 15
KCTD9	Potassium Channel Tetramerization Domain Containing 9
KEAP1	Kelch Like ECH Associated Protein 1
KLHDC10	Kelch Domain Containing 10
KLHDC2	Kelch Domain Containing 2
KLHDC3	Kelch Domain Containing 3
KLHL12	Kelch Like Family Member 12
L, Lys	L-lysine

LB	Lysogeny broth
LC	liquid chromatography
LCMS	Liquid chromatography–mass spectrometry
LFQ	label-free quantification
LPS	Lipopolysaccharides
MES	2-(N-morpholino)ethanesulfonic acid
MFI	mean fluorescence Intensity
MPB	Maltose-binding protein
mRNA	Messenger RNA
MS	mass spectrometry
NEDD8	Neural precursor cell expressed developmentally down-regulated protein 8
NFKBIA	Nuclear Factor Of Kappa Light Polypeptide Gene Enhancer In B-Cells Inhibitor, Alpha
NFKBIE	Nuclear Factor Of Kappa Light Polypeptide Gene Enhancer In B-Cells Inhibitor, Epsilon
NGS	next-generation sequencing
NHS Ester	N-Hydroxysuccinimide ester
PARKIN	Parkin RBR E3 Ubiquitin Protein Ligase
PBS	Phosphate-buffered saline
PDB	Protein Data Bank
PMSF	phenylmethylsulfonyl fluoride
POI	Protein of interest
PROTAC	proteolysis targeting chimera
PTM	Post translational modification
PVDF	Polyvinylidene fluoride
RBR	RING-in between-RING
RBX1	Ring-Box 1
RBX2	Ring-Box 2
RCR	RING-Cys-Relay E3 Ligase
RCR	RING Cys relay
RING	really interesting new gene
RNA	Ribonucleic acid
RPMI	Roswell Park Memorial Institute
RZ-finger	RNF213–ZNFX1 finger
SBM	substrate binding module
SCF	SKP, cullin, F-box containing complex
SDB-RPS	styrene divinylbenzene reversed phase sulfonate
SDC	Sodium Deoxycholate Detergent
SDS	Sodium dodecyl sulfate
SDS-PAGE	sodium dodecyl sulfate–polyacrylamide gel electrophoresis

SEC	size-exclusion chromatography
SEM	standard error mean
SKP1	S-Phase Kinase Associated Protein 1
SUMO	small-ubiquitin like modifiers
TB	Terrific broth
TBST	tris-buffered saline Tween 20
TCEP	tris(2-carboxyethyl)phosphine
TEV	Tobacco Etch Virus nuclear-inclusion-a endopeptidase
TFA	Trifluoroacetic acid
TNF	Tumor necrosis factor
Tris	tris(hydroxymethyl)aminomethane
tRNA	Transfer RNA
Ub	Ubiquitin
UBE2D	Ubiquitin Conjugating Enzyme E2 D
UBE2L3	Ubiquitin Conjugating Enzyme E2 L3
UBE2M	Ubiquitin Conjugating Enzyme E2 M
Ubl	Ubiquitin like protein
UCE	ubiquitin carrying enzyme
UFM1	Ubiquitin Fold Modifier 1
UPS	ubiquitin proteasome system
VCP	Valosin Containing Protein
VHL	Von Hippel-Lindau Tumor Suppressor
VME	vinyl methyl ester
VS	vinyl sulfone
WHB domain	winged-helix B domain
WT	wild type

Introduction

Biological systems

Multicellular organisms are complex entities composed of specialized tissues, each harboring a myriad of cell types arranged in elaborate hierarchies[1]. These cells perform crucial physiological functions, with each cell type possessing unique functional and morphological attributes. These characteristics are determined by a sophisticated interplay among the genome, transcriptome, proteome, and other regulatory molecules that make up the cell[2]. The precise coordination of spatiotemporal expression patterns of the different molecules necessary for generating specific cell types is governed by the inherent genetic program present in each cell. But individual cells are not following a static program, instead they are dynamic systems that are able to change their form and function in response to their environment and internal needs by modulating the nonlinear interactions among genes, proteins, and metabolites in time and space (Figure 1). The cellular state at a particular time is a product of the abundances of the components and their interplay, with changes causing the cellular state to shift.
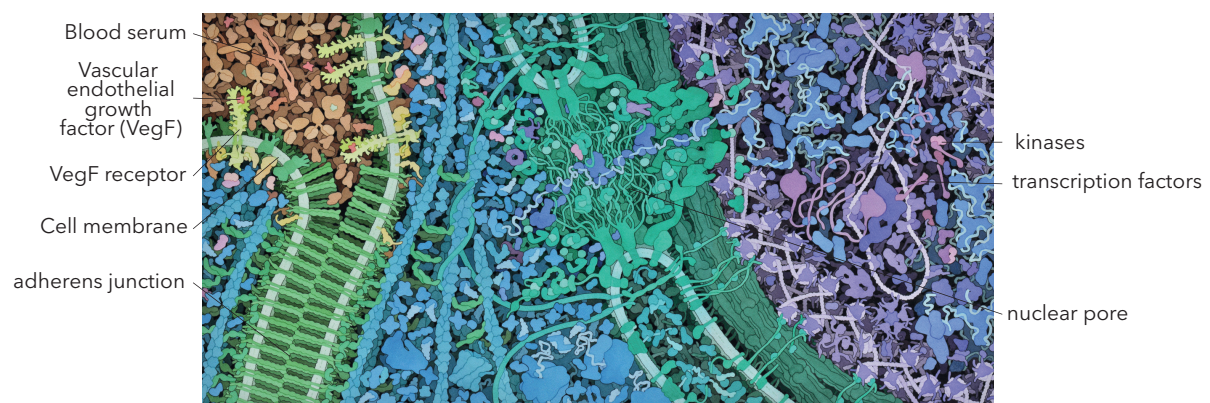
Figure 1 Cellular complexity. Cells are crowded systems relying on the precise transfer of information across and between cells. Illustration by David S. Goodsell, RCSB Protein Data Bank. doi: 10.2210/rcsb_pdb/goodsell-gallery-041

Unraveling the underlying principles resulting in a specific cell state, or phenotype, has been a long-standing core objective in molecular life science research. Beadle and Tatum's groundbreaking work on the genetic foundations of biochemical

reactions in *Neurospora crassa* gave rise to the "one gene, one protein, one function"-paradigm[3]. This paradigm suggests that there is a one-to-one relationship between a gene and the function of the protein it produces, indicating that the complexity of a biological system's functions is directly proportional to the number of its protein-coding genes.Further, the model requires that the expression of one gene product does not affect the expression or function of any other gene product.

The advent of genomic technologies allowed scrutinizing the molecular composition of cells with greater precision revealing that the "one gene, one protein, one function"-paradigm falls short in elucidating the multifaceted functional phenotypes of organisms. The Human Genome Project revealed that humans possess approximately 20,000 protein-coding genes[4], considerably fewer than initial estimates. Subsequent large-scale screening methods, including genome-wide association studies and RNA interference screens, have struggled to establish straightforward links between genotype and phenotype[5,6]. While these techniques have identified single-gene defects with high penetrance, the genetic underpinnings of many studied phenotypes are more intricate than anticipated, often involving a network of genomic changes or mechanisms across various molecular layers such as the transcriptome, proteome, and interactome, and the non-linear crosstalk between them[5-8].

Gaining insight into the complex functional dynamics of living systems has prompted a paradigm shift towards an approach that challenges the assumptions that the functional diversity of a cell stems solely from its genome. This new approach emphasizes the necessity to study molecules and their relationships within integrated systems to gain a comprehensive understanding of intricate biological processes. These strategies rely on detecting and precisely quantifying

molecular diversity across multiple levels, including the transcriptome, proteome, and interactome.
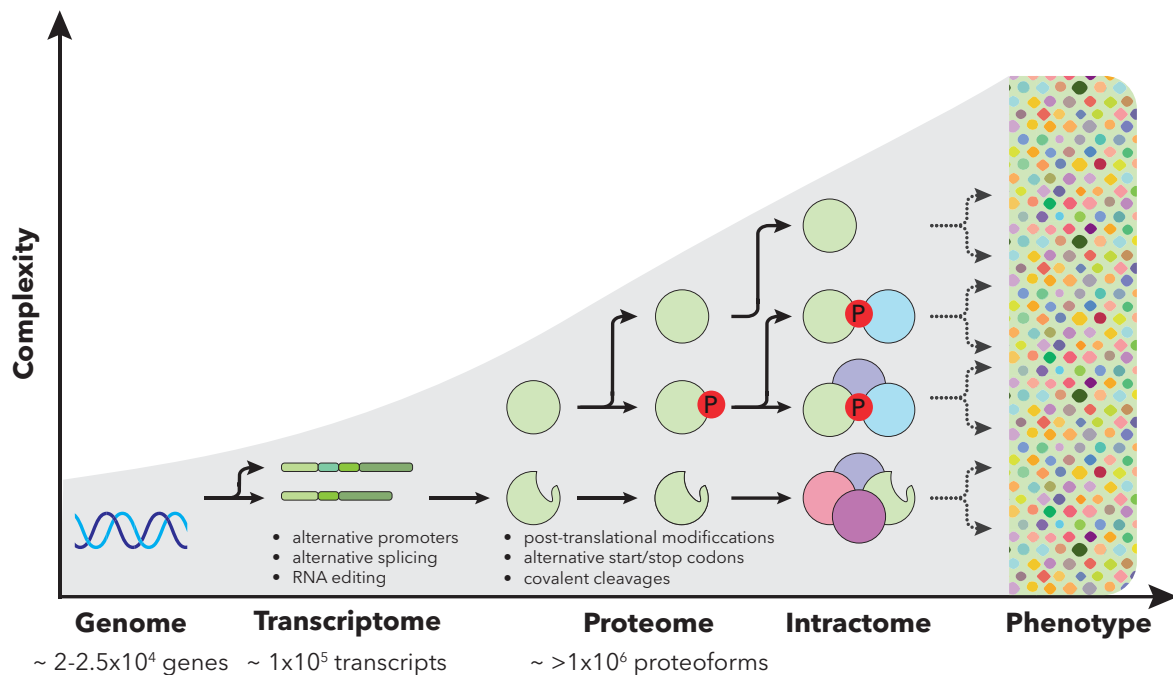
Extending the functional complexity of the genome

With the genome of a cell, and even the whole organism, being mostly stable the ability to react to environmental perturbations stems primarily from variations in the transcriptome and beyond (Figure 2). Regulatory elements enable adjusting transcript composition and quantity in response to external and internal conditions[9,10]. Additionally, eukaryotic cells have the ability to expand transcript sequence diversity by mechanism such as alternative splicing[11-30]. The collective impact of these regulatory mechanisms results in an estimated >83,000 mRNA transcripts emerging from approximately 20,000 human genes[23,31,32].

While the synthesis of a new protein depends directly relies on the production of its corresponding mRNA transcript, protein production is affected by elements beyond transcript availability, such as mRNA sequence features, codon bias, epitranscriptomic modifications, and interactions with regulatory elements like microRNAs, as well as the availability of tRNAs and uncharged ribosomes. The proteome is further shaped by protein degradation rates, affected by factors such as protein localization, stability, three-dimensional conformation, and integration into stable complexes[33-38]. In healthy cells, there is a delicate balance between protein synthesis and degradation. mRNA abundance variations are often buffered at the protein level, meaning substantial changes in mRNA do not necessarily lead to significant changes in the levels of the corresponding protein[33,38]. This buffering effect is particularly notable for proteins forming stable complexes, indicating that stoichiometric ratios of complex subunits play a crucial role in directing protein abundance. This protein-level buffering mechanism aids cells in reducing the

functional effects of variations in the genome and transcriptome that are caused by random events or genotypes that may promote disease.

During steady-state these effects only marginally distort the correlation between mRNA abundance and protein level. However, transitions in cell state or rapid adaptations to stimuli can temporarily disrupt this agreement. During such periods, a short term drastic increase in translation or rapid protein degradation allow cells to quickly adapt their quantitative proteome without substantial changes in mRNA levels[39,40].

Genome	Transcriptome	Proteome	Intractome	Phenotype
~ 2-2.5x10^4 genes	~ 1x10^5 transcripts	~ >1x10^6 proteoforms		

Figure 2 Sources of cellular complexity. Cellular complexity is the product of numerous mechanisms that vastly extend molecular diversity beyond what is encoded in the protein-coding genome. Mechanism increasing the cellular diversity can act on transcription (e.g. usage of alternative promotors), translation (e.g. alternative splicing), or post-translationally (e.g. post-translational modifications like phosphorylation). Adapted from Bludau and Aebersold, 2020[2].

Beyond variations of protein levels, proteome diversity is expanded beyond transcript diversity via a number of processes[41-43]. The most significant source of diversity at the proteome level arises from post-translational modifications (PTMs)[44].

These modifications can be either covalent cleavages or alterations of proteins through various chemical additions[45-47]. Human cells house a repertoire of over 460 catalytically active proteases[47], capable of modifying a protein's primary amino acid sequence by cleaving specific segments, thereby influencing protein localization and activity. Virtually all human proteins undergo covalent modification through PTMs at some point. While certain PTMs are permanent, the majority are reversible and subject to dynamic alterations. Out of the 20 common amino acids in proteins, 15 are susceptible to modification, and currently, approximately 400 distinct PTMs are known. The modular PTM cascades can be separated into 'writers', that catalyze the modification, 'readers' which detect the modification and induce the correct cellular response and 'erasers' that remove the PTM. The three most prevalent modifications in cells involve attaching sugar molecules to asparagine residues (N-linked glycosylation), adding phosphate groups to serine, threonine, and tyrosine residues (phosphorylation), and introducing acetyl groups to lysine residues (acetylation). N-linked glycosylation is mediated by glycosylatransferase, which attaches a glycosyl group to the asparagine side-chain amine, which can then be further modified by addition of multiple glycosyl groups to create a complex glycan-modification, which is commonly observed for secreted or membrane proteins (Figure 3). Phosphorylation is catalyzed by kinases in an ATP-dependent manner and can induce a wide array of downstream effects such as activity and protein-protein interactions. Modification of the e-amino group of lysines performed by acyl-transferases in an acetyl-CoA dependent manner, with, amongst others, important effects on transcription. The ability of PTMs to reshape their target proteins makes them critical for cellular signaling pathways. Disruptions to the machinery governing these modifications, can lead to severe disease phenotypes[48].

Glycosyl-Asparagine   Phospho-Serine   Phospho-Threonin   Phospho-Tyrosine   Acetyl-Lysine
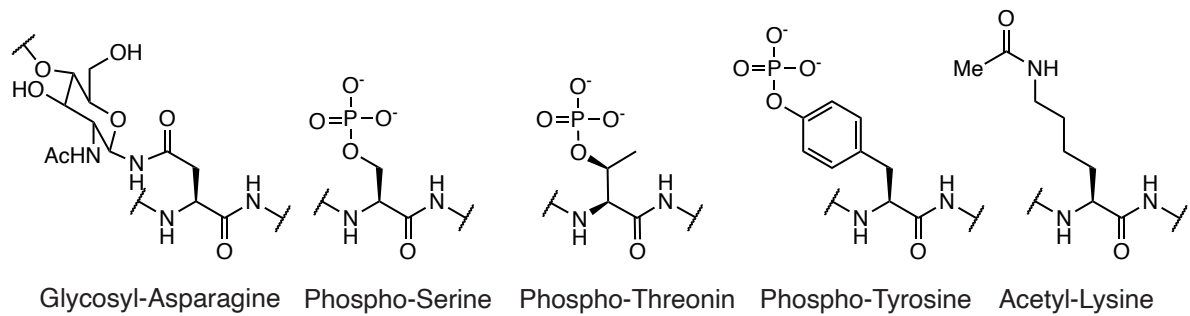
Figure 3 Frequently encountered post-translational modifications (PTMs) on proteins. These modifications, including glycosylation, phosphorylation and acetylation are orchestrated by specific enzymatic cascades. PTMs play a pivotal role in modulating protein structure and function, contributing to the intricate regulatory networks within cells.

Combined, the mechanisms introducing variation at the transcriptome and proteome level are estimated to generate over 1 million different proteoforms[49], each with a unique amino acid sequence or PTMs. Different PTM sites on the same protein or across different proteins are connected via molecular crosstalk leading to a complex network that governs cellular function. The proteome's functional capacity is further enriched by some single proteoform being able to adopt multiple three-dimensional conformations. A protein changing its conformation can significantly affect its stability, localization, and molecular function.

Besides changing their structural features proteins can also change the proteins and other macromolecules they interact with.   Many proteins do not function by themselves but perform their biochemical functions as part of diverse macromolecular assemblies. This network of molecular interactions, the cells interactome, exhibits greater diversity and adaptability to environmental signals compared to the transcriptome and proteome as it does not rely on the synthesis of new molecules. Cellular functions depend on the dynamic organization of proteins in networks of physical interactions. These interactions are crucial for many proteins to perform their biological functions and their disruption can result in disease[50,51]. The dynamic nature of the interactome, causes it to vary between different cell lines,

cellular compartments, different cellular stimulation[30,52], or in disease-relevant contexts[53,54]. Interactions between proteins can be very transient, such as the interactions between kinases and their substrate, or be retained over longer timescales such as those seen for molecular machines like the ribosome and proteasome. Besides being co-expressed at the right stoichiometry and colocalizing within the cell, interactions between proteins may require the involved proteins to assume a specific three-dimensional conformation[55,56]. Protein interactions are also frequently dependent on specific proteoforms or vice versa. Furthermore, certain PTMs only occur upon complex formation. The cell frequently employs proteoform-dependent rearrangements of its interactome to swiftly adapt its functional landscape in response to varying environmental conditions[57-59].

Proteins cannot just transiently interact with each other. Besides protein modifications based on small chemical moieties eukaryotic cells have additionally evolved a cascade that involves the covalent modification of a protein with another protein – ubiquitin.

Ubiquitin

First identified in 1975, ubiquitin was described as "a universal constituent of living cells" by Goldstein and colleagues[60]. Named after its ubiquitous presence among eukaryotes, with homologues also found in some bacteria, ubiquitin was soon after found to be covalently conjugated to other proteins[60-65]. Initially proposed as a signal for downstream proteases, in the early 1980s Aaron Ciechanover, Avram Hershko, and Irwin Rose first described the multistep enzymatic cascade involved in the tagging of ubiquitin to proteins[66-70]. This groundbreaking work was honored with the Nobel Prize in 2004. Subsequent investigations revealed that the proteasome is the ATP-dependent protease responsible for ubiquitin-dependent protein degradation[71-73].
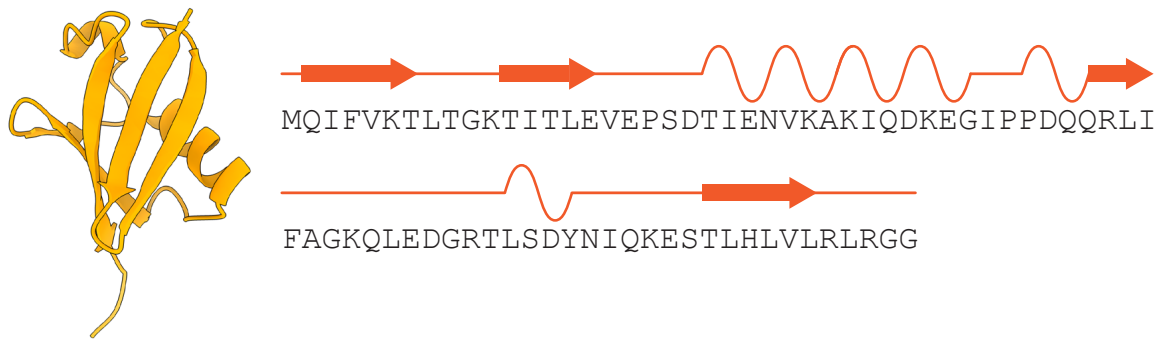
Figure 4 Ubiquitin. Cartoon representation of the structure of human ubiquitin (PDB 1UBQ, left) and the sequence of ubiquitin with secondary structural elements indicated (right). Arrows indicate β-sheets and a wavy line α-helices.

Ubiquitin is a 76-amino acid protein with a molecular weight of 8.5 kDa (Figure 4). It assumes a compact globular protein fold known as the ubiquitin- or β-grasp fold. This structure is characterized by four β-sheets tightly embracing an α-helix[74]. Notably stable, the ubiquitin fold is resilient against high temperatures and acidic conditions[60]. Modification of proteins with ubiquitin occurs through a specialized cascade where the C-terminus of ubiquitin is attached to the ε-amino group of a lysine side-chain via an isopeptide-bond[64]. Ubiquitin can also be attached to N-termini[75], or serine and threonine side-chains[76], although this is less common. Ubiquitylation is controlled by a complex enzymatic network, which in humans is thought to involve more than 1,000 proteins[77,78]. Comprehensive proteomics studies indicate that a major fraction of eukaryotic proteins is subject to ubiquitylation[79-81]. Ubiquitin is attached to targets, in a context-dependent manner, by cascades of E1 (activating), E2 (conjugating), and E3 (ligating) enzymes (Figure 5). For attachment to a target protein ubiquitin is first activated by an E1 enzyme such as UBA1. In an ATP dependent process, the C-terminal carboxylate of G76 is activated and transferred onto a cysteine of the E1 enzyme. The charged E1 enzyme, then recruits a conjugating enzyme (E2) and transfers the activated ubiquitin onto the catalytic cysteine of the E2 enzyme via a trans-thioesterification reaction. Humans encode for approximately 40 different E2 enzymes. E2s bind to E3 ubiquitin ligases, which mediate substrate recruitment and allow ubiquitin

transfer from the activated E2~ubiquitin thioester complex to the target lysine by various mechanisms[82]. Depending on their mechanism ubiquitin transfer and general structure ubiquitin E3 ligases are categorized into multiple families[83]. The largest family with over 500 members is called RING ligases[84]. They act as
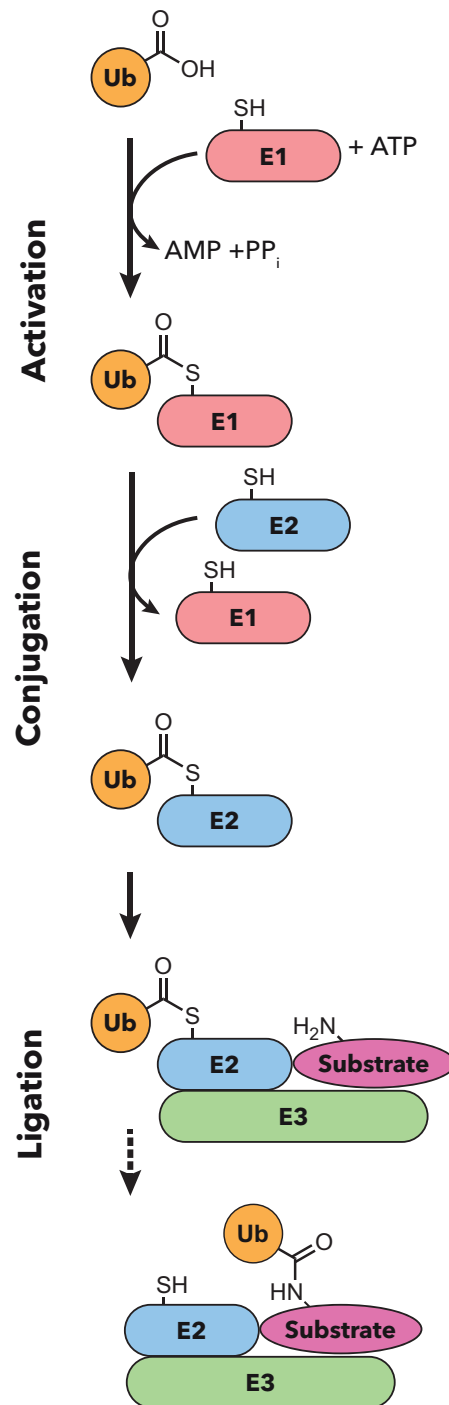
Figure 5 The ubiquitin conjugation machinery. An overview of the chemical processes involved in the enzymatic steps of ubiquitylation.
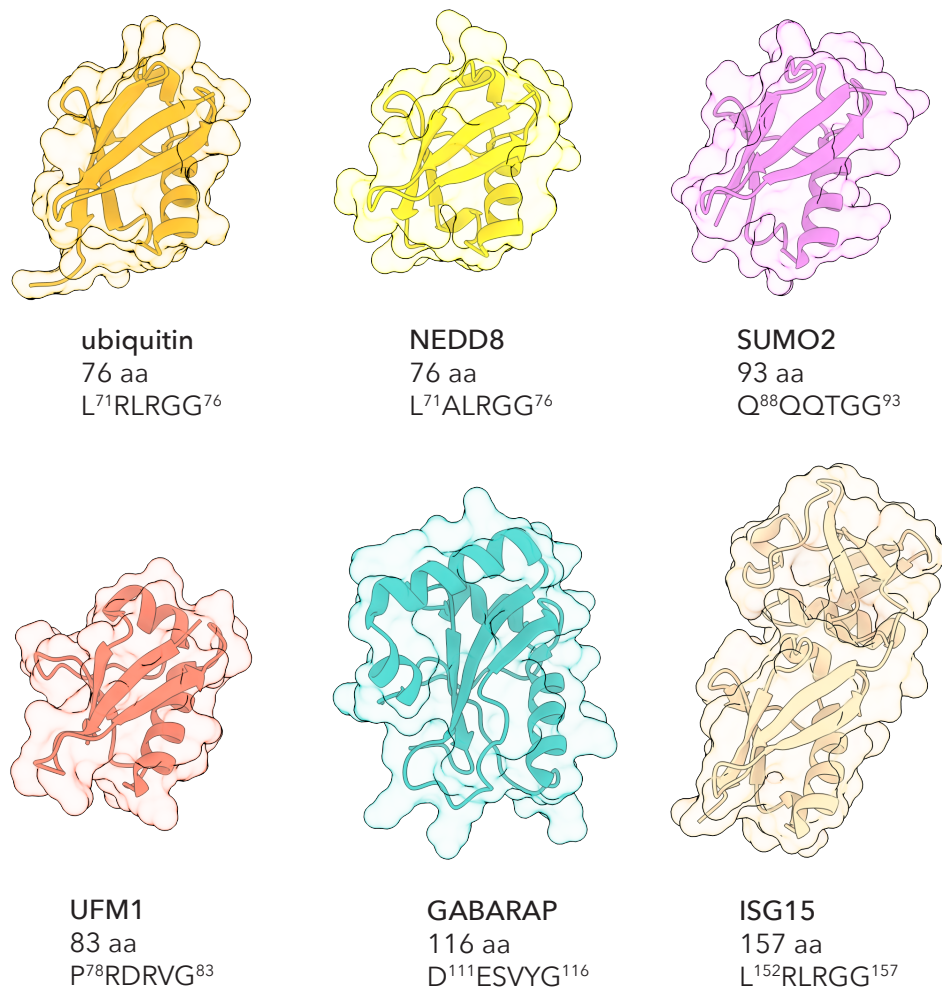
scaffolding proteins, bringing the activated E2~ubiquitin thioester and substrate into close proximity in a reactive conformation enabling ubiquitin transfer. The remaining E3 ligases are subdivided into multiple families, such as HECT, RBR, RCR and RZ-finger[85-87], which while structurally diverse all share a related transfer mechanism. E3s in these families contain catalytic cysteines which accept ubiquitin from the E2 and catalyze transfer to the substrate themselves. As with other enzymatic post-translational modifications, ubiquitin is reversible. A class of protease called deubiquitylases selectively cleaves the ubiquitin isopeptide-bond, regenerating unconjugated ubiquitin and removing the modification from the substrate[88].

Given the involvement of numerous proteins, the ubiquitin system often becomes dysregulated in various pathological conditions, such as cancer, inflammation, and neurodegenerative diseases[89]. Pathogens have been found to exploit the Ub system by either mimicking or hijacking the host's Ub system components. This strategy helps them evade detection by the immune system[90-92].

Including ubiquitin, eukaryotic cells encode for nearly 20 proteins that are attached to various macromolecules as post-translational modifications (Figure 6). These proteins all adopt the characteristic β-grasp fold of ubiquitin[93]. Despite the strong structural and sequence similarities these ubiquitin-like proteins regulate a strikingly diverse set of cellular processes, including nuclear transport, proteolysis, translation, autophagy, and antiviral pathways. While sharing a similar fold, the sequences of Ubl diverge. NEDD8 exhibits the highest sequence homology with ubiquitin, sharing 58% similarity. In contrast, members of the small-ubiquitin like modifiers (SUMO) have limited sequence similarity with ubiquitin and include an N-terminal extension. The Ubl GABARAP, crucial for autophagy, features two additional N-terminal helices. Unlike ubiquitin, NEDD8, or SUMO, UFM1 lacks a C-

terminal GG motif but instead has a VG motif. ISG15 resembles a linear fusion of two β-grasp domains.

Despite sharing a conserved structure, the enzymatic cascades responsible for modifying proteins with different Ubls operate independently, enabling them to perform distinct cellular functions[78]. This independence, or orthogonality, is maintained through highly selective protein-protein interactions that prevent Ubls from being activated and entering the cascade of a non-cognate Ubl. The unique C-terminus of each Ubl and a specific hydrophobic patch, known as the I44 patch for ubiquitin, are instrumental in this exclusion[94]. While ubiquitin's hydrophobic

ubiquitin
76 aa
$L^{71}RLRGG^{76}$

NEDD8
76 aa
$L^{71}ALRGG^{76}$

SUMO2
93 aa
$Q^{88}QQTGG^{93}$

UFM1
83 aa
$P^{78}RDRVG^{83}$

GABARAP
116 aa
$D^{111}ESVYG^{116}$

ISG15
157 aa
$L^{152}RLRGG^{157}$

Figure 6 Selection of ubiquitin-like proteins. The structures of selected ubiquitin-like proteins are shown as cartoons with transparent surface view. The number of amino acids and the last six C-terminal residues of the mature ubiquitin-like proteins are shown.

region is crucial for interactions in the ubiquitylation cascade and with ubiquitin-readers[95], each Ubl possesses a distinct hydrophobic patch, allowing them to function separately and regulate physiological processes different from ubiquitin's role.
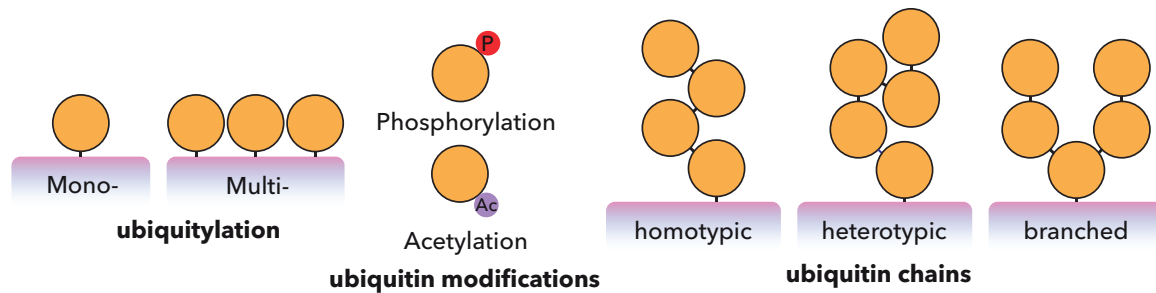
Figure 7 The ubiquitin code. Schematic representation showing some examples of the various modifications making up the 'ubiquitin code'.

The ubiquitin code

Other than most post-translational modifications ubiquitylation is not a binary modification[96]. Instead, the exact makeup of a single ubiquitin modification site of a protein serves as a versatile signal that regulates protein-based communication in and between eukaryotic cells[97]. Besides modification of one site of the substrate with a single ubiquitin, ubiquitin itself possesses seven lysine residues (K6, K11, K27, K29, K33, K48, and K63) or its N terminus (M1) which can be further ubiquitylated. The resulting polyubiquitin chains can involve a single type of linkage, or result in branched chains, when multiple sites on a single ubiquitin are modified (Figure 7). Remarkably, each linkage type has specific enzymes that write (assemble), recognize (read) and hydrolyze (erase). While different linkage types have different prevalence within cells, proteomic studies have shown that all possible linkage types can be found in cells[79,80,97-101].

Beyond additional modification with ubiquitin, ubiquitin, being a protein itself, can also be the target of other post-translational modifications such as acetylation[102-105], phosphorylation[81,106-111] and addition of ubiquitin-like proteins[112-114]. Six out of seven lysine residues of ubiquitin can be acetylated[102-105] and a broad array of serin and threonine sites can be phosphorylated[81,106-111] (Figure 8). The combination of diverse linkage types, chain lengths, and other post-translational modifications give rise to a plethora of distinct messages. Ubiquitin-binding proteins serve as decoder, discerning between various chain architectures and initiate the appropriate cellular response.
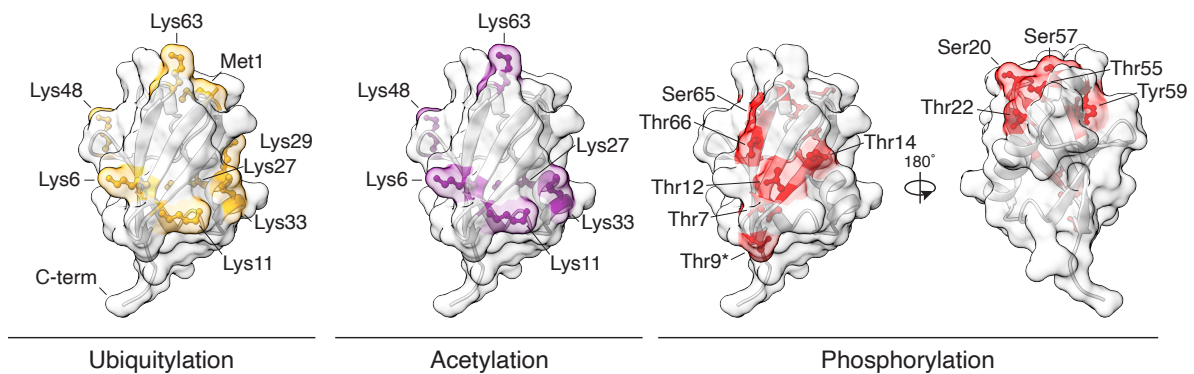
Figure 8 Possible modifications of ubiquitin. Cartoon representations of ubiquitin under a semi-transparent surface with modifiable residues are colored and shown in ball-and-stick representation. The eight residues able to be targeted for ubiquitylation are shown on the left and colored orange. In the middle the six lysine residues that have been identified to be acetylated are shown in purple. Possible serine, threonine, and tyrosine residues of ubiquitin that can be phosphorylated are shown on the right and colored red. To display all phosphorylation sites the structure is rotated 180 degrees. The asterisk on Thr9 indicates that this site has been ambiguously assigned.

Deciphering the code

Due to the large size of ubiquitin compared to others PTMs, ubiquitylation significantly affects a protein's structure and function[115]. With the complexity of the ubiquitin code, modification with ubiquitin can have a multitude of effects, including causing the controlled degradation of proteins, transforming intermolecular interactions, and altering localization or activity[96]. Which of these effects occur for a specific protein is determined by a class of proteins called ubiquitin-readers[116,117]

(Figure 9), which can detect defined ubiquitin chain-types or ubiquitylated substrates via specific ubiquitin-binding domains or other domains[118]. These proteins can recognize and distinguish a substrate modified with a single ubiquitin, one carrying a specific chain-type or specific chain topology. After binding their targets ubiquitin-readers, often function as effector proteins or mediate a specific downstream effect in accordance to the specific ubiquitin-message by recruiting the correct effector-proteins. Additional proteins recruited can be E2s, E3s, DUBs, or other proteins that continue the signaling cascade.
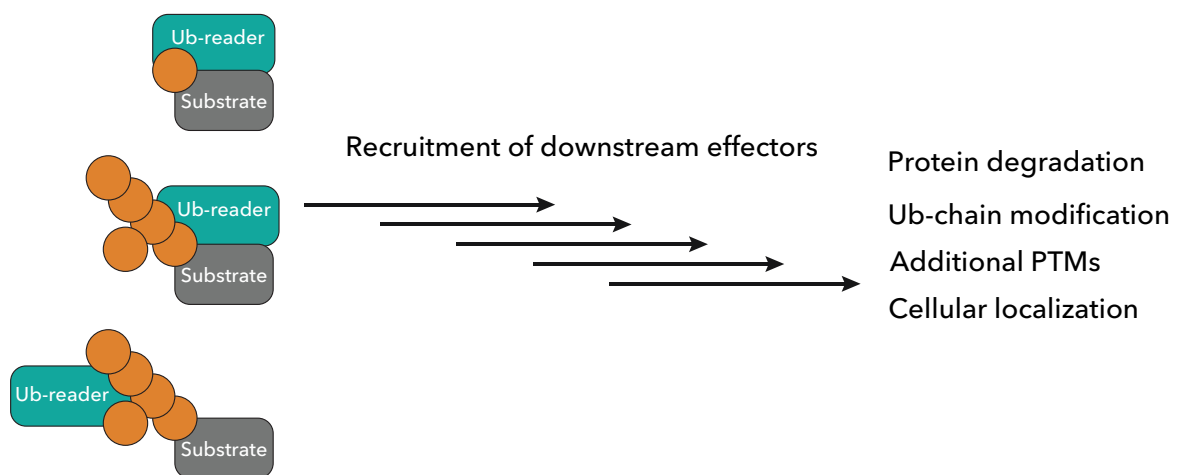
Figure 9 Effects of ubiquitylation are initiated by reader proteins. Different ubiquitin-messages are detected and deciphered by different reader proteins which then initiate the correct downstream response.

Inducing the controlled degradation of proteins was the first identified function of ubiquitylation[68,119]. Proteins tagged with ubiquitin are efficiently recognized and degraded by the 26S proteasome in an ATP dependent process. Being a multiprotein complex, the 26S proteasome possess multiple ubiquitin receptors that recognize the correct ubiquitylated substrates based on chain topology, folding state, and the presence and location of initiation regions[120] (Figure 10). A pivotal observation in ubiquitin-induced protein degradation was the necessity of multiple ubiquitins being attached to the substrate prior to its degradation.

Traditionally, a K48-linked ubiquitin chain of at least 4 molecules has been considered the canonical degradation targeting signal, although recent studies suggest that other ubiquitin modifications can also channel proteins to the proteasome[120]. During the targeted degradation of substrates by the proteasome, ubiquitin molecules are typically not degraded but instead removed from the substrate by proteasome-resident DUBs, enabling the recycling of ubiquitin molecules[121]. This allows the ubiquitin proteasome system (UPS) to degrade individual proteins in a highly regulated fashion allowing it to degrade misfolded, damaged, or unneeded cellular proteins.
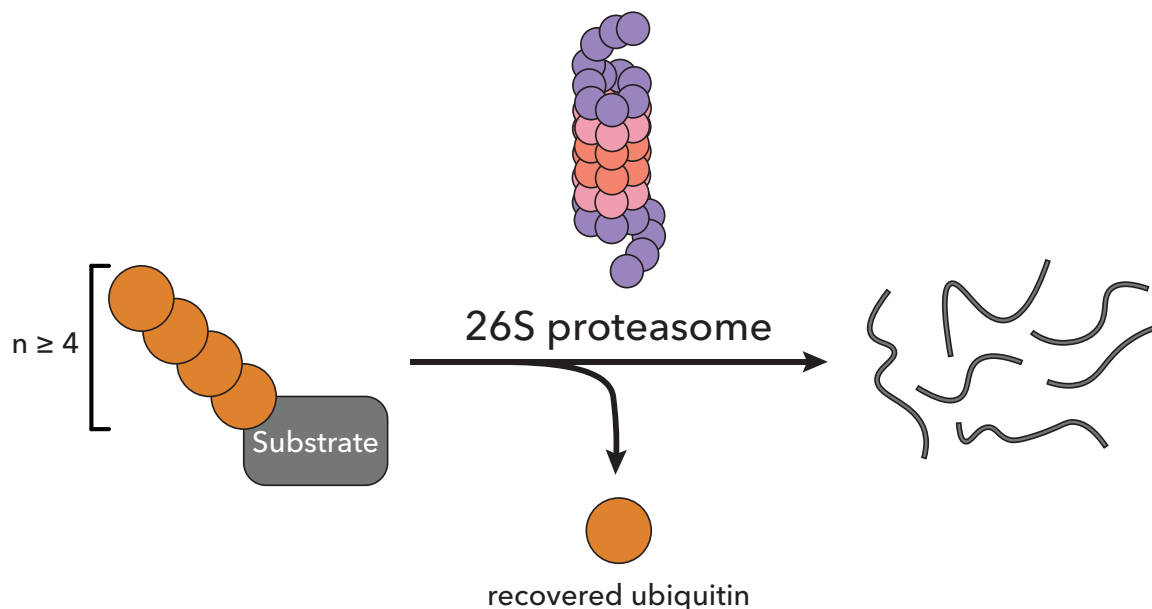
Figure 10 The ubiquitin-proteasome-system. Specific ubiquitin-messages containing at least 4 ubiquitins lead to association and subsequent degradation of the substrate by the 26S proteasome.

Protein degradation is crucial for more than just removing aged or damaged proteins; it also enables cells to adapt dynamically to their environment and internal needs. The speed at which a cell reaches a new steady state in response to a stimulus is directly tied to the half-life of the proteins involved[122]. For example, a protein with a 200-minute half-life would take a long time to reach a new steady state if its synthesis were reduced tenfold (Figure 11). On the other hand, a protein

with a one-minute half-life would adjust to a new steady state quickly. This principle is also applicable when there's a sudden tenfold increase in a protein's production. This property is vital for using transcription or translation regulation to swiftly control biological processes. In such scenarios, the instability of the regulated protein is essential, allowing for rapid adjustments to achieve a new steady state. Many key cellular regulators, such as transcription factors, signal transduction proteins, cell cycle control proteins, and those involved in cell death and apoptosis, exhibit high instability. This inherent instability allows for quick responses to changes in gene transcription and protein synthesis, which contributes to the dynamic regulation of cellular processes.
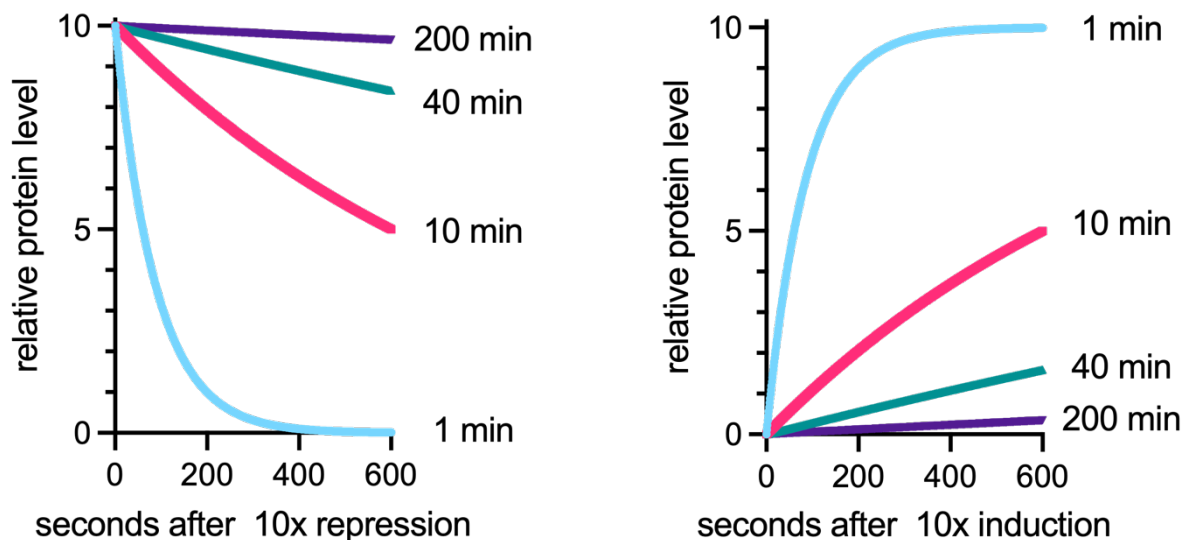
Figure 11 Protein turnover allows for dynamic regulation. Graphs showing the relative protein level of hypothetical proteins with half-lives of 1, 10, 40, and 200 minutes after 10-fold repression of synthesis or a 10-fold induction of production. Adapted from Alberts et. al, Mol. Bio. Cell, 6th ed (2015)

E3 ubiquitin ligases

With these wide-ranging effects ubiquitylation on cellular function, targeting ubiquitin to the correct proteins is critical. With them mediating the final step in transferring ubiquitin to the substrate protein this is the responsibility of ubiquitin E3 ligases. As such E3 ligases serve dual roles: they attract specific proteins for modification and facilitate the transfer of ubiquitin from an E2 enzyme to the targeted substrate or a ubiquitin-linked substrate. The catalysis process of E3

ligases primarily adheres to one of two primary mechanisms. Certain E3 ligases, including those with Homologous to E6AP C Terminus (HECT) and Really Interesting New Gene (RING)-between-RING (RbR) domains, possess catalytic cysteines (Figure 12). These E3s initially acquire Ub from an E2~Ub intermediate, where "~" signifies a reactive thioester bond between the enzyme's catalytic cysteine and Ub's C terminus. Subsequently, they directly transfer Ub to a distally recruited substrate. Conversely, RING E3 ligases do not form a covalent intermediate with Ub. Instead, they act as structural facilitators that bring the activated E2~Ub intermediate and the target protein together (Figure 12). This mechanism allows RING E3s to enable the transfer of Ub from E2 to the substrate without forming a direct bond between the E3 and Ub, thereby facilitating a more flexible and dynamic interaction between the E2 enzyme, the Ub-containing E3, and the target protein.

HECT E3 ligase

RBR E3 ligase

RCR E3 ligase
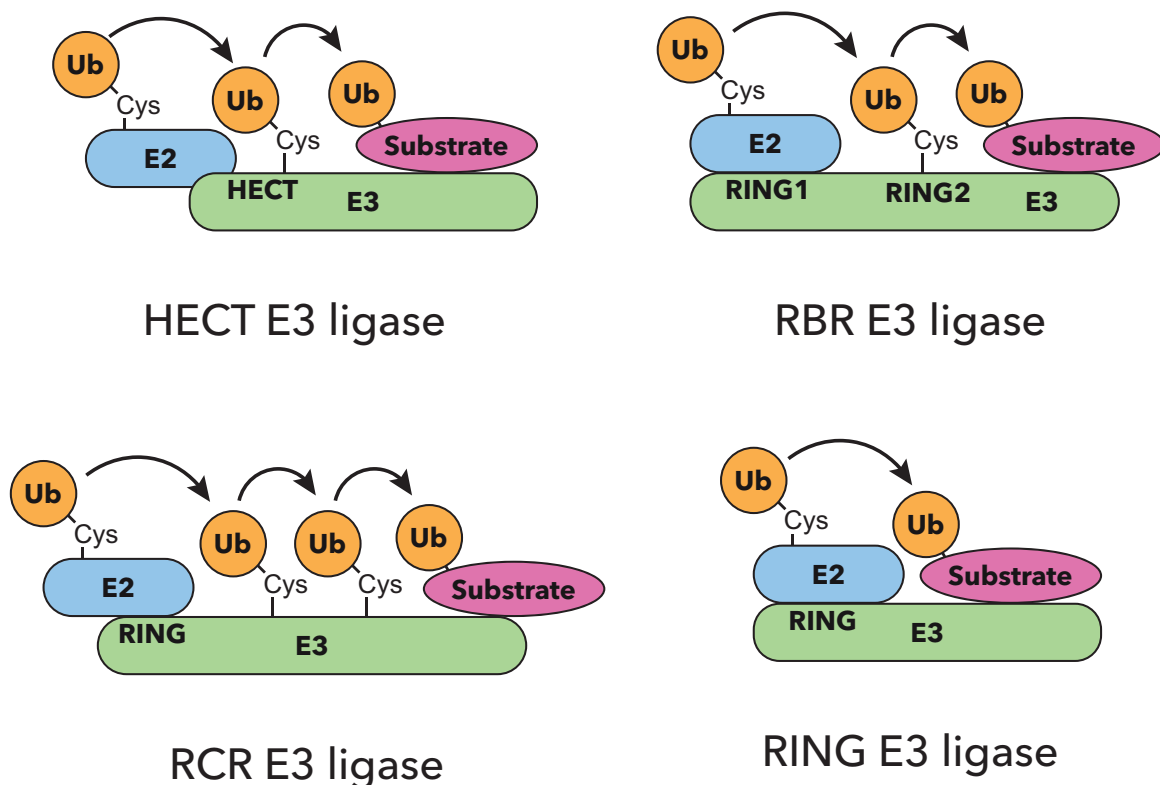
RING E3 ligase

Figure 12 E3 ligase families. Cartoon representations of HECT (homologous to E6-AP C terminus), RBR (RING-in between-RING), RCR (RING Cys relay), and RING (really interesting new gene) families of E3 ligases. HECT, RBR, and RCR E3 ligases feature a catalytic Cysteine (Cys) that is charged with ubiquitin by an E2 enzyme. Subsequently, these E3s then catalyze transfer of ubiquitin to the substrate. Members of the RING family mediate direct transfer of ubiquitin from the charged E2 to the substrate.

The ~600 different E3 ligases encoded by the human genome differ greatly in how many proteins they modify. Some E3 ligases target only a single substrate[123-125], while others have the capability to modify dozens of proteins[126,127]. Moreover, E3 ligases often specialize in constructing specific types of ubiquitin modifications on their target substrates[128]. Collaboration and the formation of super-assemblies between multiple E3 ligases enhance the efficiency of ubiquitylation or enable the creation of more complex heterotypic ubiquitin chains[129,130]. To ensure the correct timing and location of ubiquitylation, E3 ligases recognize specific motifs referred to as degrons. Degrons can take multiple forms, such as linear sequences stretches that are constitutively accessible to the E3 ligase, or can be produced by PTMs such as phosphorylation[131], acetylation[132,133], hydroxylation[134,135], ADP ribosylation[136], or arginylation[137]. Besides dynamic activation of degrons, degrons can also be dynamically inactivated, for example by oxidation[138]. Certain substrates may have multiple copies of a degron, facilitating multivalent and high-affinity recognition[139-141]. While degrons comprised of short linear motifs are best understood, structural degrons where a shape instead of a sequence is recognized also exist[142,143]. Additionally, some E3 ligases predominantly function by extending ubiquitin chains, recognizing ubiquitin itself as a substrate[144-147].

Cullin-RING ubiquitin E3 ligases
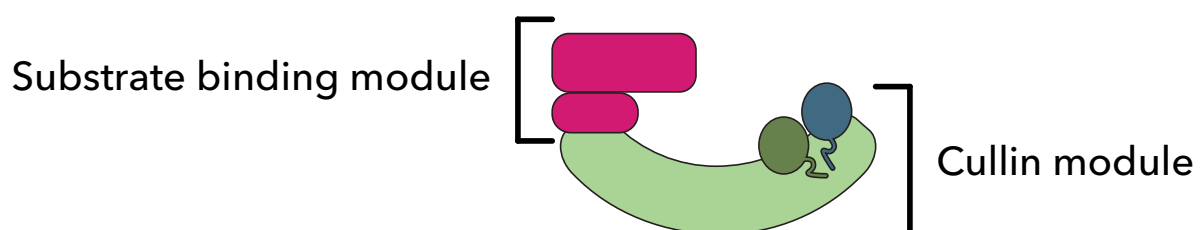
Figure 13 Cullin-RING ligase architecture. Cullin-RING ubiquitin E3 ligases are composed of a cullin core, composed of a cullin (green) and RBX protein, which can bind numerous, dedicated, and interchangeable substrate binding modules.

The largest family of E3 ligases are cullin-RING ligases (CRLs) with ~300 members in humans, making up ~50% of all E3 ligases[83]. CRLs share a common architecture, characterized by cores consisting of a cullin protein and a RING domain-containing RBX protein (in humans, CUL1, CUL2, CUL3 or CUL4 pair with RBX1, and CUL5 with RBX2)[148-150] (Figure 13). The assembly of CRL complexes involves the binding of the cullin's N-terminal domain with one of its dedicated substrate-binding modules (SBMs)[151-155]. Each cullin-RBX core can interchangeably associate with numerous SBMs (Figure 14). For example, CUL1 can bind approximately 70 distinct SKP1-F-box-protein complexes, while CUL4 can associate with around 60 different DDB1-DCAF complexes. The cullin's C-terminal region and RBX1 then partner with a ubiquitin carrying enzyme (UCE), housing a catalytic cysteine responsible for transferring ubiquitin to the SBM-bound substrate. This modular architecture, coupled with diverse UCE partners and numerous SBMs, generates a vast array of unique E3 ligase complexes, allowing the targeting of a diverse range of substrates with a broad spectrum of functions.
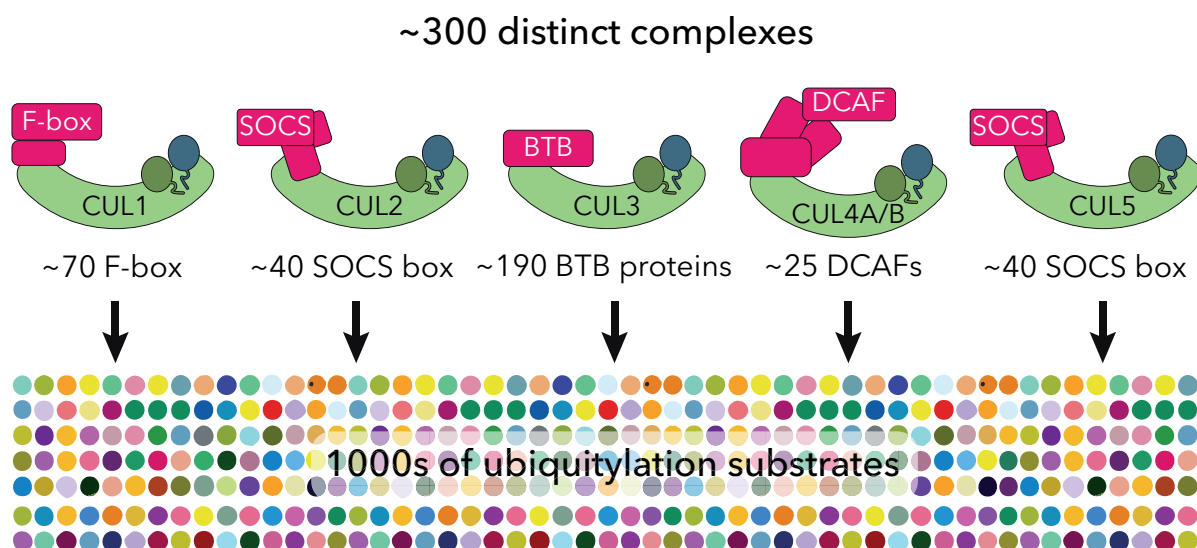
Figure 14 cullin-RING ligase diversity. The modular nature of cullin-RING ligases allows for ~300 different complexes to form based on five (or six if CUL4A/B are included separately) different canonical backbones. The formed cullin-RING ligases are responsible for ubiquitylation of thousands of substrates.

The cullin-RING ligase cycle

Maintaining cellular homeostasis relies on precise control of CRL activity. Cellular cullin concentrations are significantly lower than the total pool of available substrate receptors. This disparity prevents simultaneous access to all substrate receptors and restricts the occupancy of a specific receptor at any given moment. To overcome this limitation and accommodate the multitude of substrate receptors needed for ubiquitination, cullins employ the CRL assembly factor CAND1 (Figure 15). Originally identified as a neddylation inhibitor[156-159], CAND1 facilitates the assembly and disassembly of various substrate receptors as needed. CAND1 can catalyze the dissociation of F-box proteins from CUL1, transforming a complex that would typically remain stable for days into one that changes within seconds. This remarkable ability of CAND1 ensures access to different substrate receptor complexes for the catalytic cullin-RING complex, allowing dynamic regulation of ubiquitination processes[160-165].
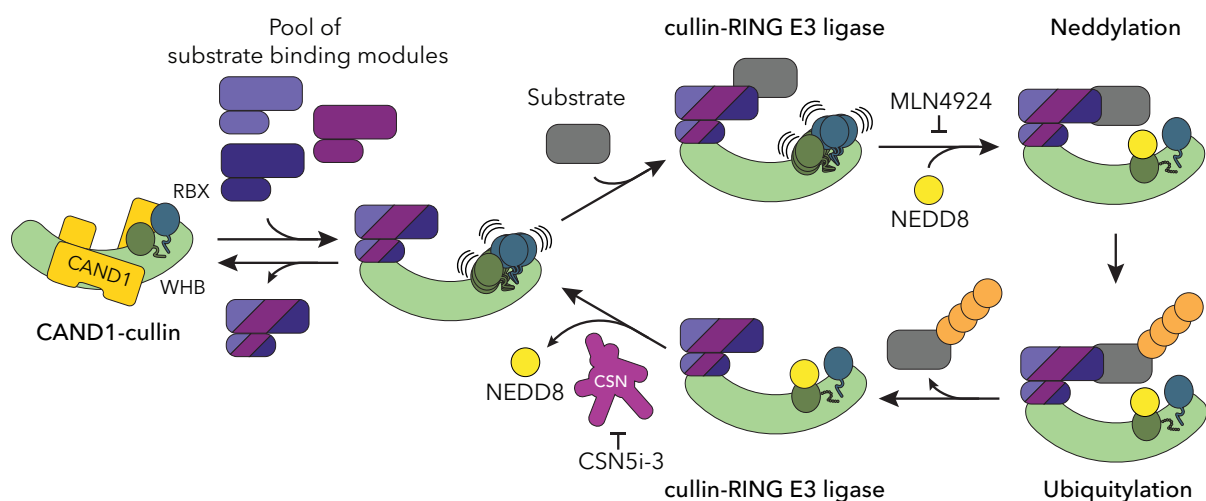
Figure 15 The cullin-RING ligase cycle. Cullin-RING E3 ligases are tightly regulated by a controlled sequence of neddylation, substrate ubiquitylation, removal of the NEDD8-modification and substrate binding module exchange. This ensures a dynamic equilibrium in response to cellular demands. Steps inhibited by MLN4924 (neddylation) and CSN5i-3 (deneddylation) are indicated.

A CRLs ubiquitylation function is activated when the ubiquitin-like protein NEDD8 is inked to a specific conserved lysine on the cullin C-terminal WHB subdomain[166-171]. This process is facilitated by the E2s UBE2M/UBE2F and the co-E3 ligase DCN[169,172-174]. Research on CUL1 has demonstrated that modification with NEDD8 results in a remarkable 1,000-fold increase in ubiquitylation efficiency[170]. This enhancement is attributed to the adoption of a specific conformation by NEDD8 and CUL1's WHB subdomain, facilitating the binding and activation of UCEs[170,171] (Figure 16). The homologous nature of WHB domains in CUL1, CUL2, CUL3, and CUL4 suggests that they form structurally similar complexes when covalently linked to NEDD8[175,176]. Mutational data further underscore the significance of the NEDD8–CUL4 interface, particularly in drug-induced ubiquitylation triggered by degraders[170]. Neddylation hinders the cycling of substrate receptors onto and off a CRL complex by directly clashing with CAND1 binding, thereby activating the complex for ubiquitination[161]. However, for neddylation to take place, CAND1 must disassociate from a CRL before or during the neddylation process, and vice versa[177].
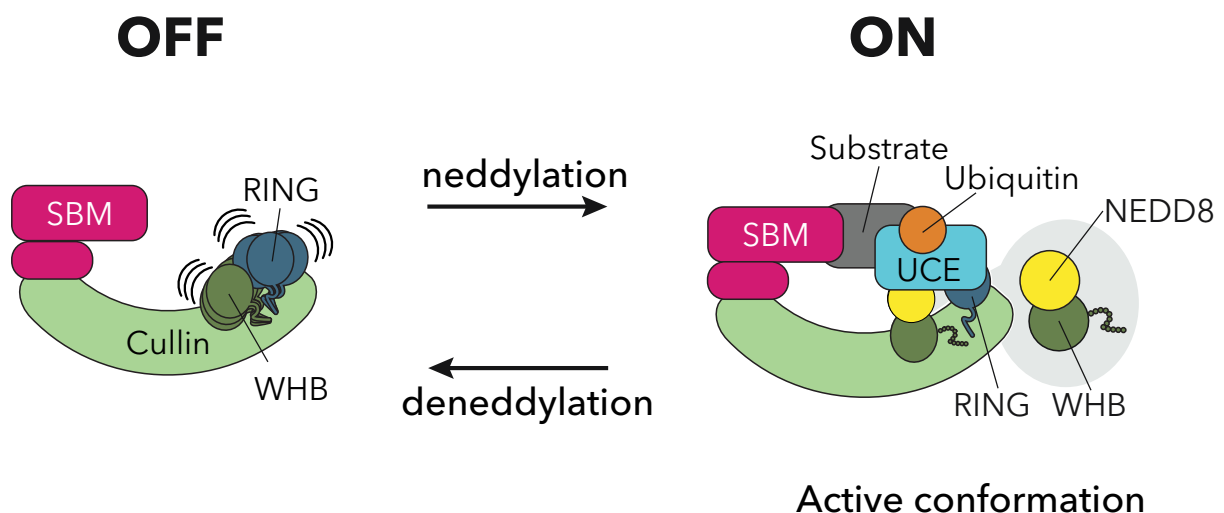
Figure 16 CRLs are activated by NEDD8. Site-specific NEDD8 linkage to the cullin's WHB domain switches CRLs on. Modification with NEDD8 allows the complex to assume the active conformation required for ubiquitylation (SBM: Substrate binding module, UCE: ubiquitin carrying enzyme)

With neddylation determining CRL activity, it is highly controlled. The COP9 signalosome (CSN) plays a crucial role in deconjugating NEDD8 from cullins, unless

a CRL is shielded by binding a substrate[178-183]. This mechanism ensures that after substrate degradation, most CRLs are deneddylated. Studies on CUL1- and CUL4-based CRLs have shown that only when deneddylated are these CRLs, and presumably others, subject to a pathway that promotes the dissociation of the SBM from its cullin–RING partners[160,162,163,184]. Additionally, some CRLs undergo further controls in the absence of substrate, including SBM autoubiquitylation and/or the formation of autoinhibited self-assemblies[183,185-187]. This dynamic process of assembly, activation, deactivation, and disassembly reshapes the cellular CRL repertoire. Consequently, the linkage of NEDD8 to a cullin typically marks an assembled, active CRL[150,188].
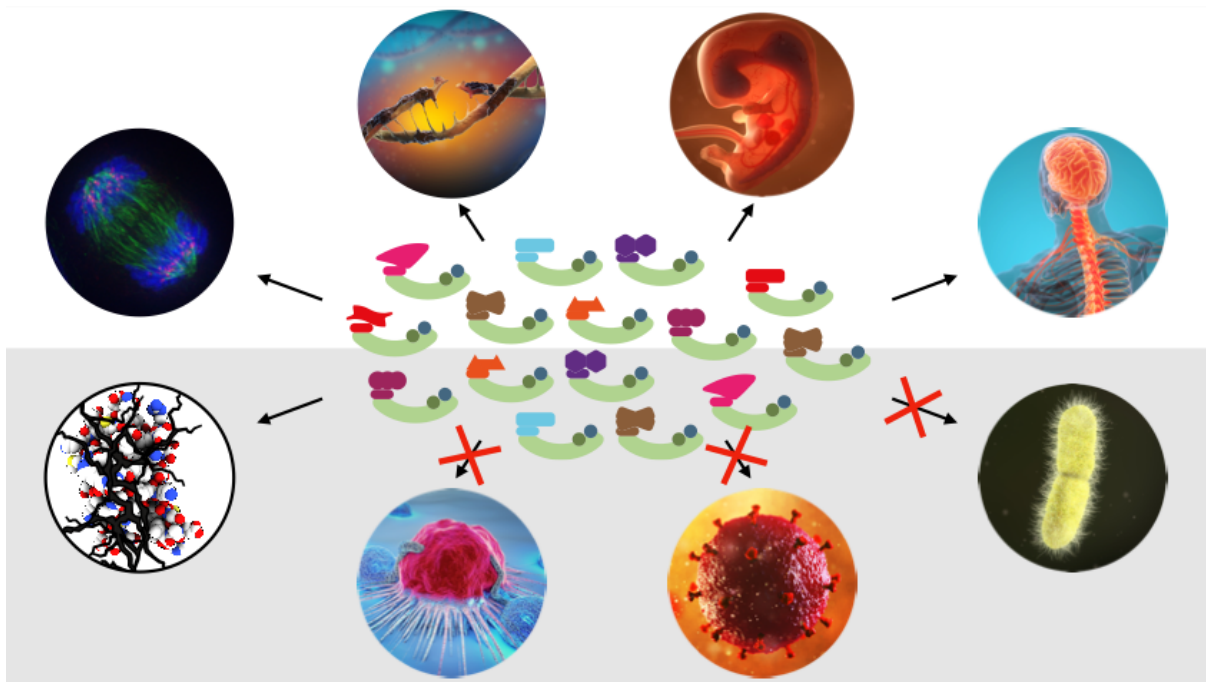
Figure 17 Roles of CRLs. CRLs play pivotal roles in a multitude of biological processes, spanning cell cycle regulation, DNA repair mechanisms, and embryonal and neuronal development. Additionally, CRLs are frequently misregulated in cancer and hijacked by pathogens such as bacteria and viruses. Moreover, the majority of currently available targeted protein degradation strategies rely on CRLs, underscoring their significance as versatile and druggable targets in therapeutic interventions. Image credit starting top left, going clockwise: Roy van Heesbeen, Mirsad (Adobe Stock), unlimit3d (Adobe Stock), magicmine (Adobe Stock), gaetan (Adobe Stock), artegorov3@gmail (Adobe Stock), Christoph Burgstedt (Adobe Stock).

The regulation of the CRL network through neddylation has been linked to various cellular processes, including cell division, immune signaling, DNA replication and repair, responses to redox stress and hypoxia, tumorigenesis, and pathogen hijacking[126,149,189] (Figure 17). Neddylation is also crucial for CRL-dependent targeted protein degradation[183,190,191]. Recent findings based on inhibiting neddylation for CUL1- and CUL4 based complexes suggest an 'adaptive exchange hypothesis,' where the landscape of NEDD8-activated CRLs is rewired in response to changes in cellular conditions[160,162,163].

Chemical Probes to target enzymatic networks

How can complex and diverse biological pathways like the ubiquitin system and its related Ubl systems be effectively studied? Besides biochemical and molecular biological approaches, chemistry offers opportunities for gaining new insights and control of PTMs and their associated protein networks[192]. For instance, small molecule inhibitors targeting kinases, histone-acetyltransferases, and histone-deacetylases have significantly advanced our understanding of phospho and acetyl regulation[193-195]. These systems are conducive to chemical approaches as the enzymes involved in catalyzing these PTMs adhere to common principles, and the reactants are relatively small organic molecules.

The Ub-system and its related Ubl-systems hold equal or even greater significance and show larger variety in potential messages, in part to the modifications being proteins themselves. The wide range of potential messages encoded by these systems and the numerous messengers (E1, E2, and E3 enzymes) involved makes understanding the molecular intricacies a formidable yet crucial challenge. The complexity is further increased by the dynamic nature of the Ub modification and the enzymatic processes responsible for modifying proteins with ubiquitin relying

on transient multiprotein complexes. Unraveling this complexity presents a promising opportunity for pharmacological exploitation.

Addressing these challenges is greatly aided by the development of tools that enable observing and controlling the information transfer across the Ub system, offering new opportunities to understand the inner workings of E1-E2-E3 cascades. These approaches frequently depend on the selective modification of a target protein[196]. Possible modifications include, but are not restricted to, fluorophores, affinity handles, bioconjugation handles, or reactive functional groups that allow such desired downstream applications such as imaging, enrichment, or target labelling (Figure 18). For most applications it is desirable to target specific residues. For this purpose, multiple strategies to target different amino acids have been developed.
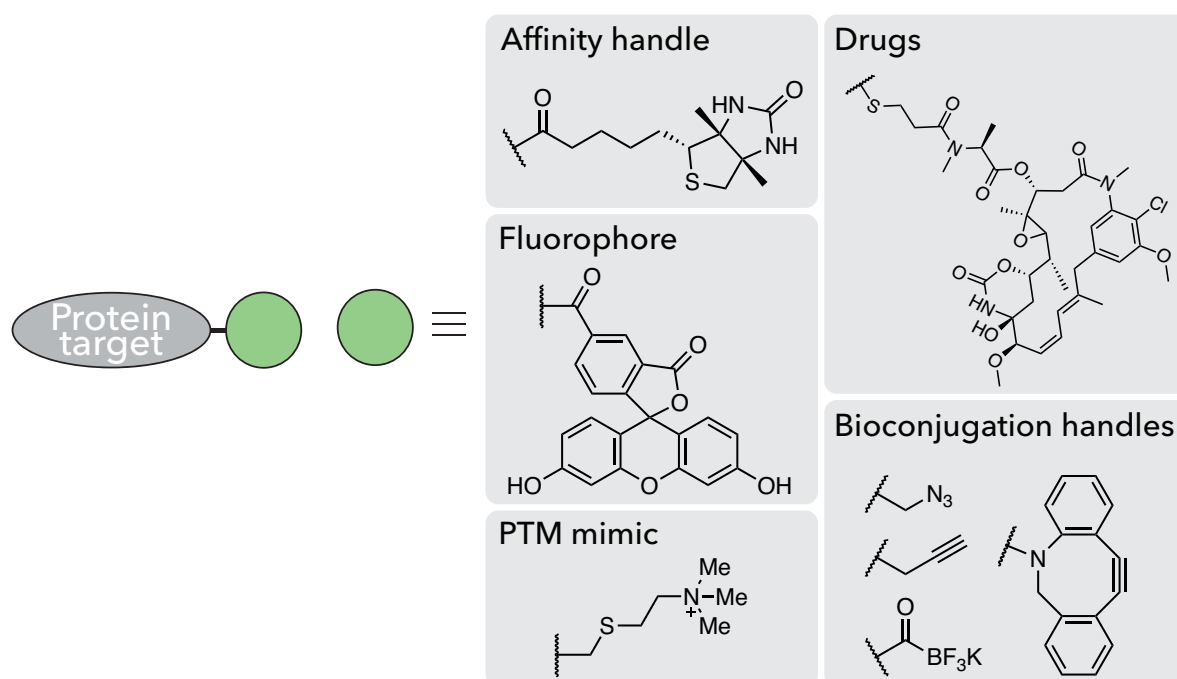
Figure 18 Protein conjugates. Proteins selectively modified with chemical groups can be used as therapeutics or for investigating biological systems. Modifications can include affinity handles (e.g. biotin), fluorophores (e.g. fluorescein), PTM mimics (e.g. trimethylammonium), drugs (e.g. Mertansine), or bioconjugation handles (e.g. azides, alkynes, trifluoroborates, or Dibenzocyclooctyne-amines).conjugates

The E1-E2-E3 conjugation cascade of the Ub- and Ubl-systems relies on thiol chemistry, making it amenable to probing. Further, in most currently known ubiquitylation events, Ub's C-terminus is transferred between the catalytic cysteines of E1, E2, and sometimes E3 enzymes, before reaching its target substrate. Many significant advancements have utilized thiol-reactive compounds to capture catalytic cysteines in E1, E2, or E3. A widely employed and adaptable method involves introducing a reactive group onto the C terminus of Ub, either entirely through synthetic means or semi-synthetically[197,198]. These activity-based probes (ABPs) emulate Ub substrates in catalytic reactions, forming covalent bonds with the active site of the targeted enzyme. ABPs consist of three key components: (1) a reactive group, or warhead, capturing the enzyme's catalytic cysteine; (2) a recognition element or targeting group establishing noncovalent interactions with the specific protein target; and (3) a reporter, such as an affinity handle or fluorescent label, facilitating detection and/or enrichment of labeled proteins (Figure 19). The selection and arrangement of the reactive group and recognition element govern the ABP's specificity and reactivity[199]. Ub can either be integrated into reactive enzyme~Ub complex ABPs, or be used effectively mimic such complexes in non-reactive probes. ABPs can be used to assess the activity of some E3 ligases, such as those belonging to the HECT, RBR, RCR and RZ-finger families can be assessed using probes reacting with the catalytic cysteine. This made cysteine-reactive probes useful in understanding the mechanisms of autoinhibition and activation of RbR E3 ligases ARIH1 and ARIH2. Reaction with a Ub-vinyl methyl ester probe (Ub-VME) acted as a marker for activity, enabling the detection of their activation by neddylated cullin-RING ligases[200] and a Ub-vinyl-sulfone probe (Ub-VS) was utilized to demonstrate the inhibitory effects of a regulatory domain found in PARKIN.

Targeted protein degradation

Small molecules can also be used to alter the specificity of E3 ligases, causing them to ubiquitylate proteins of interest (POIs) different from their natural substrates[191]. These molecules, collectively referred to as degraders, were initially exemplified by proteolysis-targeting chimeras (PROTACs). PROTACs consist of two moieties—one binding to an E3 enzyme and the other to a POI—connected by a linker. By bringing together the E3 and POI, PROTACs facilitate ubiquitylation and subsequent degradation of the POI (Figure 20). In contrast to traditional inhibitors, small-molecule degraders operate catalytically, allowing them to exert their effects at lower concentrations. Unlike inhibitors that selectively target one activity of a protein, degraders interfere comprehensively with all functions. This allows, in principle, for the pharmacological targeting of virtually any cellular protein, even those lacking clear enzymatic function, provided a small molecule can be identified to bind it. Early experiments utilized peptide-based PROTACs, demonstrating target protein degradation but suffering from poor potency due to low

Activity based probe
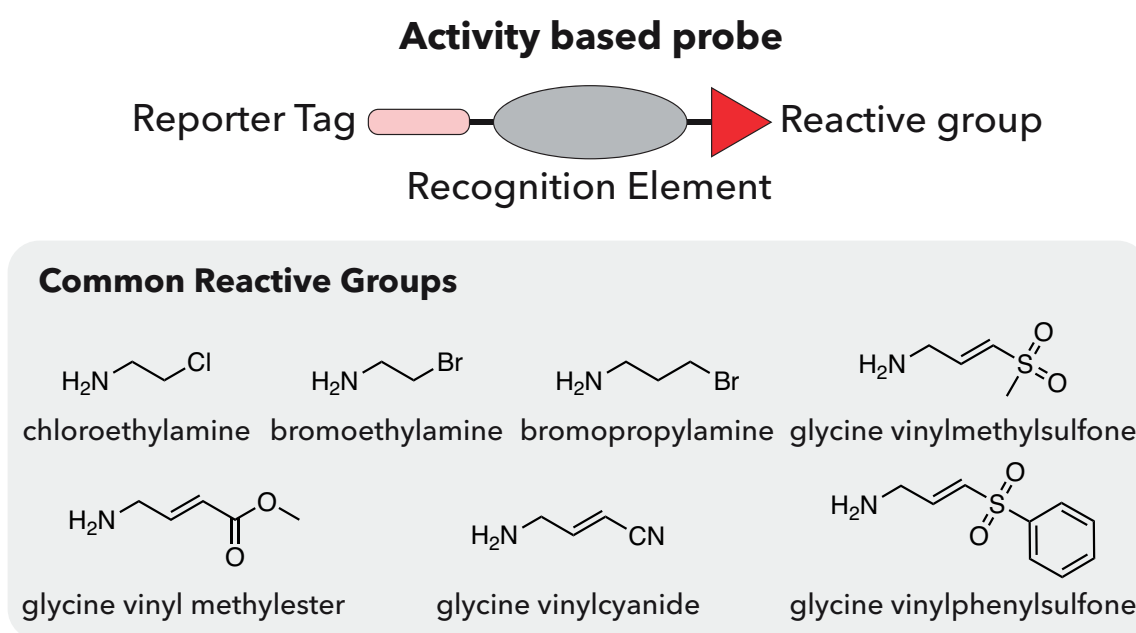
Figure 19 Activity based probes. Cartoon of the common architecture of activity-based probes. The chemical structures of commonly used reactive groups are shown.

bioavailability[201-203]. Significantly improved potency was achieved with the development of the first entirely small molecule PROTAC[204]. The concept of targeted protein degradation reached new heights when FDA-approved immunomodulatory imide drugs (IMiDs) like thalidomide, lenalidomide, and pomalidomide were found to induce degradation of neo substrates (Figure 20). These compounds, termed molecular glues, sandwich the E3 ligase and substrate by mediating new interactions[205-208]. While the discovery of IMiDs and more recent molecular glue degraders occurred serendipitously, new screening platforms have been designed to systematically identify these compounds[190,209,210].
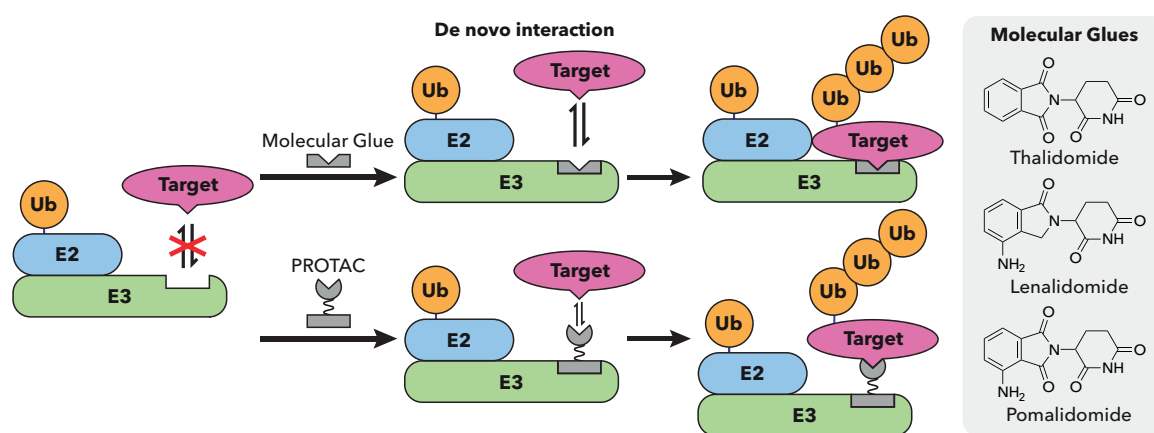
Figure 20 Targeted protein degradation strategies. Overview of the molecular glue and proteolysis targeting chimera (PROTAC) strategies of recruiting neo-substrates to ubiquitin E3 ligases for ubiquitylation. Chemical structures of the molecular glues Thalidomide, Lenalidomide, and Pomalidomide are shown.

Induced protein degradation has emerged as a novel therapeutic approach, offering a promising modality to tackle targets that were previously considered undruggable. However, currently only a small fraction of the ~600 E3 ligases encoded by the human genome have been successfully used for targeted protein degradation strategies. While current efforts are extending the range of E3 ligases that can be recruited to target POIs[211,212], most successful degrader molecules still rely on only two E3 ligases: CUL4[CRBN] and CUL2[VHL 213]. Additionally, information on which E3 ligase would work best against a specific target in a specific environment is currently lacking. Expanding the E3 ligase toolbox and our understanding of

which E3 ligases are best suited to degrade a POI under certain conditions is imperative to unlock the full therapeutic potential of induced protein degradation.

In vitro selection of antibodies

Besides small-molecules, antibodies and other protein-based binders have been essential in delineating the complex mechanisms governing biology. Classically, such binders against desired targets have been produced in the form of antibodies by immunizing animals with an antigen and extracting the produced antibodies from the animal's blood after multiple injections. This method relies on the animals immune system's ability to recognize and respond to foreign substances, leading to the production of specific antibodies by B cells that can neutralize the pathogen or initiate an immune response. Antibodies generated by this approach are polyclonal, recognizing multiple epitopes. To produce antibodies recognizing only a singular epitope traditionally the hybridoma approach developed by Kohler and Milstein in 1975 has been used[214]. While many antibodies of incredible value for therapeutic, diagnostic, and research use have been developed this way and the hybridoma approach is currently still used to produce most antibodies, there are a number of aspects that have room for improvement: 1) reliance on experimental animals, 2) not compatible with high-throughput screening methods, 3) high cost, 4) long process to yield antibodies, and 5) low control over epitope selection process[215,216].

As an alternative, *in vitro* selection methods, predominantly phage display, have been established[217]. The phage display method relies on the ability to fuse polypeptides to bacteriophage coat proteins, which can then be displayed on phage particles, linking genotype and phenotype[217-219] (Figure 21). This allows the usage of extremely diverse libraries ($>10^{11}$) of DNA-encoded peptides or proteins, where the pool of phages can be amplified through a bacterial host. Instead of using

libraries of antibodies most phage display strategies rely on using single-chain variable fragments (scFvs) or antigen-binding fragments (Fabs). Alternatively non-classical antibody-based binder backbones such as nanobodies, DARPINs[220], or peptides[221] can be used. By employing selections with immobilized ligands, library pools can be enriched for proteins possessing specific binding characteristics. Most importantly, the fact that selections are performed *in vitro* allows fine control over the antigen/target protein and target specific adjustments to the selection conditions. This permits targets that would be difficult or impossible to be used with strategies based on animal immunization, such as toxic proteins or preformed
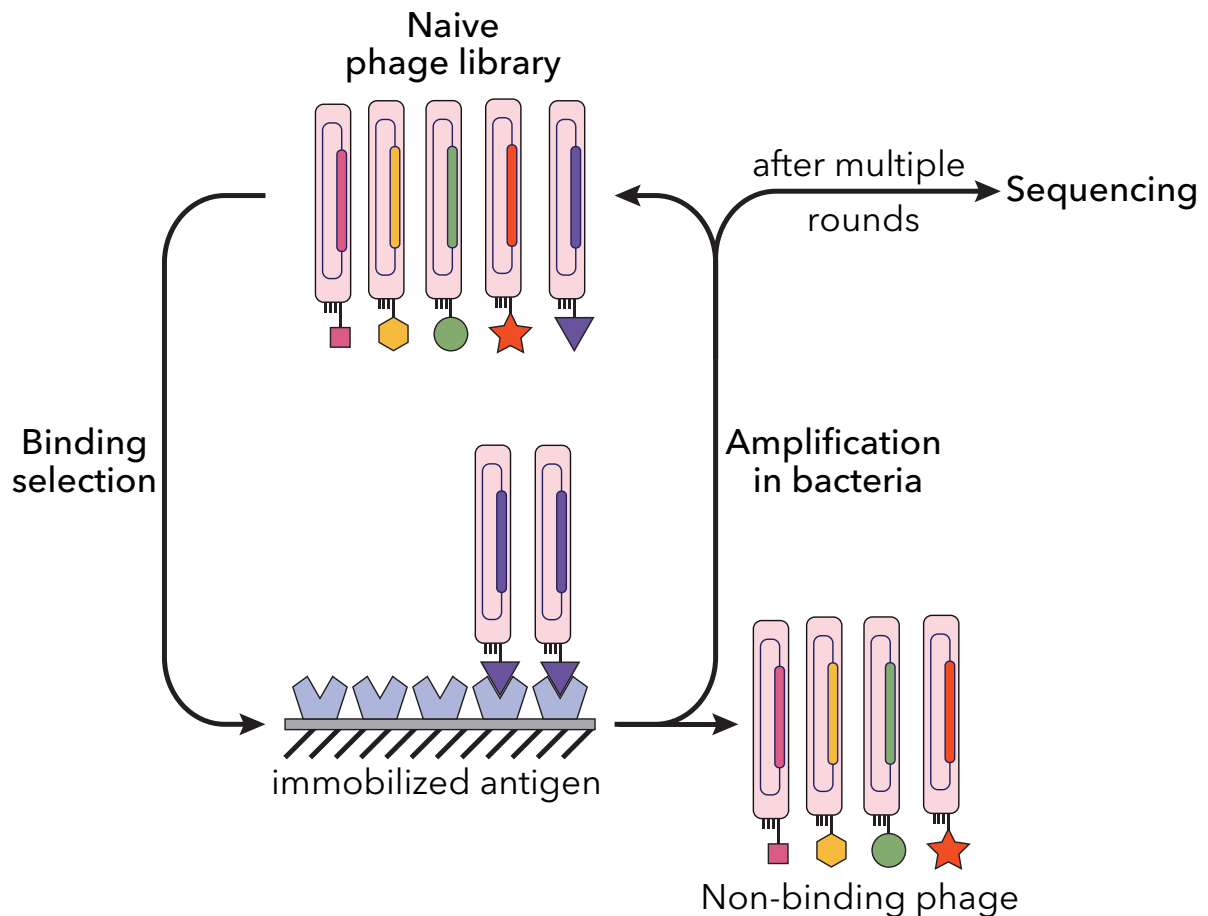
Figure 21 Selection of binders using phage display. Libraries of proteins (depicted in various colors) are presented on phage particles through fusion with coat proteins (shown in black). Proteins are fused to coat proteins on phage particles, allowing each phage to display a unique protein and encapsulate its encoding DNA. By screening highly diverse libraries (>10[10] clones) antigen-specific clones can be identified by performing multiple rounds of selections with an immobilized antigen, which include washing to eliminate non-binding phage. Phages binding the antigen can be amplified by infecting a bacterial host. With this amplified pool additional rounds of selections can be performed to enrich for antigen-binders. Ultimately, binding clones are sequenced to recover the sequences of the antigen binding proteins. Figure adopted from Sidhu and Koide 2007

protein complexes. Additionally, the selection against binders of a desired target can be preceded by negative selections against targets that the binder is not supposed to bind. After the selection process, individual clones from these enriched pools can be examined using enzyme-linked immunosorbent assays (ELISAs) to measure binding in a high-throughput manner. Most crucially, the amino acid sequence of any clone can be easily determined by sequencing the DNA contained within the phage particles. This also These factors make the phage display method well suited for adaptation to a high-throughput pipeline.

Mass spectrometry-based proteomics

While small molecule or protein probes enable the targeting of individual proteins for diagnostic or therapeutic purposes, they provide only a limited view of the intricate relationships within cells. To obtain a comprehensive understanding of the complex protein networks governing cellular function, methods enabling quantitative profiling of proteins, their interactions, and modifications are essential. Mass spectrometry stands out as a powerful tool for unbiased system-wide characterization and quantification of the proteome, including the site-specific posttranslational modifications contained within[222-224]. Consequently, it emerges as the method of choice for investigating complex biological functions and addressing clinical questions.
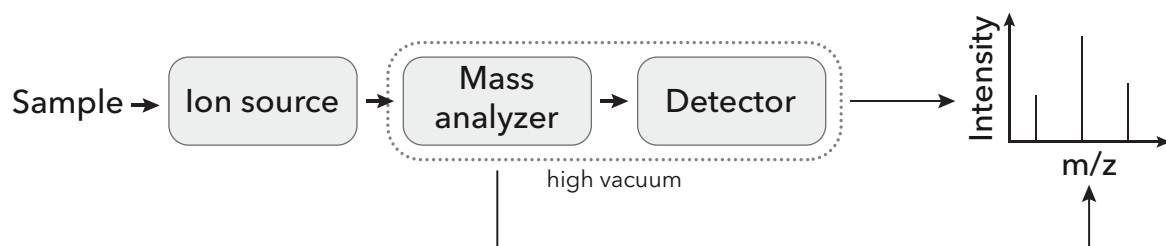
Figure 22 Components of a mass spectrometer. A typical mass spectrometer comprises three main components: an ion source, a mass analyzer, and a detector. Figure adopted from Banerjee and Mazumdar 2011[225].

Mass spectrometry relies on detecting the mass-to-charge ratios (m/z) of analyte ions[226-231]. MS-based experimental strategies for proteomics classically distinguish between bottom-up and top-down approaches. Top-down approaches involve the analysis of intact proteins, offering high sequence coverage and the ability to differentiate between proteoforms without inferring protein information from peptides[232]. However, it is experimentally and computationally challenging, especially for complex samples. On the other hand, bottom-up or shotgun proteomics involves inferring protein information from identified peptides. This approach is the most commonly applied technique for in-depth system-wide proteome analysis. While the analysis of peptides over intact proteins comes with many advantages, bottom-up approaches may be limited by low protein coverage and protein inference problems.

While MS can be used as a stand-alone analysis technique[233-236], it is often coupled with liquid chromatographic (LC) separation to reduce sample complexity[237]. From the LC separated peptides are continuously sprayed into the mass spectrometry instrument. The mass spectrometer comprises an ionization source, a mass analyzer, and a detector (Figure 22). Peptides separated by LC are converted into gaseous ions using methods like electrospray ionization (ESI)[228] before entering the mass spectrometer. Ions are then resolved according to their mass-to-charge (m/z) values by a mass analyzer. Prominent mass analyzers include quadrupoles[238,239], Orbitrap[240,241] and time-of-flight[238] analyzers, which are often combined in modern MS instruments. Peptide ions enter the final stage of the instrument that contains the detector – allowing the assessment of their m/z values. The detector is typically a variant of an electron multiplier that amplifies the low signal originating from only few analyte ions or a detector that records an induced charge by oscillating ions in e.g. an Orbitrap[242,243].

To sequence and identify peptides in mass spectrometry, precursor ions with a specific mass-to-charge ratio (m/z) are first isolated and then fragmented using techniques like collision induced dissociation (CID), electron capture/transfer methods, or photodissociation[244-250]. The resulting fragments' m/z values are
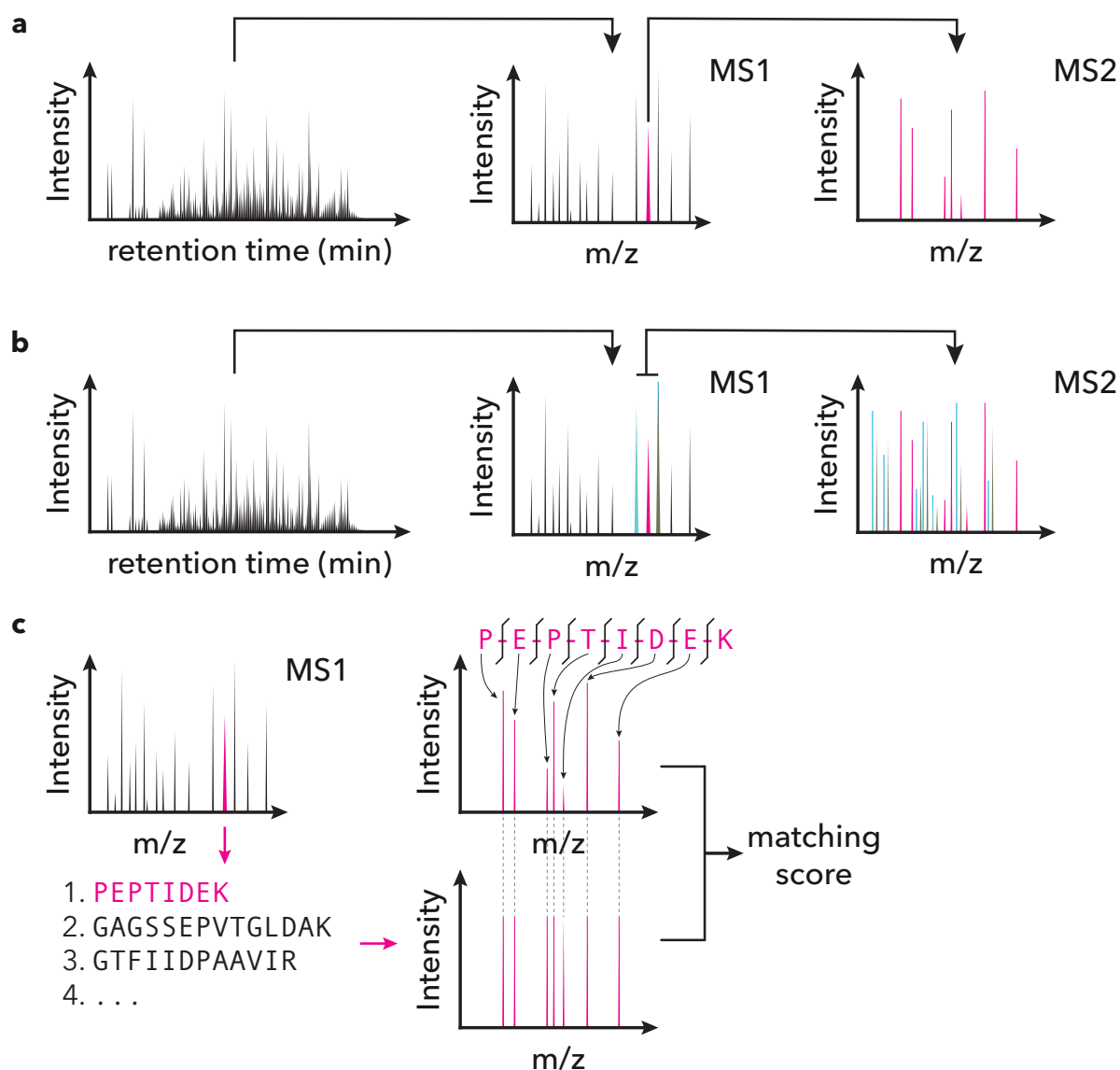
Figure 23 Data acquisition strategies in shotgun proteomics. (a) For data-dependent acquisition (DDA), a peptide ion is selected from the numerous ions detected in the MS1 scan at a specific retention time based on certain criteria. The selected peptide ion then undergoes fragmentation and the resulting data is recorded as MS2 spectra. (b) In data-independent acquisition (DIA), several peptide ions are selected at a specific retention time based on defined m/z windows. The selected peptide ions are then fragmented, resulting in the generation of complex MS2 spectra. (c) Peptide sequence assignment entails the *in silico* prediction of possible peptides followed by the generation of their theoretical MS2 spectra. Fragment ion data are extracted from the most closely matching theoretical MS2 spectra. Figure adapted from Sinha and Mann 2020

recorded in the MS/MS (or MS2) scan, creating a peptide fingerprint. This highly specific information is utilized for peptide sequence identification. Even a short sequence of amino acids along with their flanking masses, known as a peptide sequence tag, is sufficient for identifying a peptide within the entire human proteome. More commonly, all possible fragmentation spectra are generated based on a database and statistically scored against the experimental spectra to determine the peptide sequence.

During acquisition hundreds of peptides are ionized and enter the mass spectrometer simultaneously. Up until recently, these peptides were analyzed using data-dependent acquisition (DDA), where the instrument selects peptides based on user-defined rules such as mass-to-charge ratio (m/z), charge, intensity, and cross-section, aiming to acquire as many MS/MS spectra as possible (Figure 23a). However, DDA is partly stochastic, leading to missing values due to the large number of peptides compared to the analysis time. In contrast, data-independent acquisition (DIA) methods involve the continuous cycling[251-254] (64-67) across the entire m/z range by splitting it into several mass windows (Figure 23b). This results in complex MS/MS spectra, which include overlapping fragmentation patterns from co-isolated peptide ions. Modern software can deconvolute these spectra to identify multiple peptides. This process often involves comparing the spectra to a previously acquired 'peptide library,'[255], but more recently, it's becoming possible to do so without the need for a reference library[256].

Peptide quantification strategies can be broadly classified into two categories: label-free and label-based approaches. In label-free quantification (LFQ), peptide signals are extracted from raw data, usually at the MS1 level, and then normalized and compared between different proteomic conditions. LFQ is more straightforward and economical, offering flexibility in project design. However, it

may variations between measurements can impact comparisons between samples if not carefully addressed. On the other hand, label-based approaches utilize stable isotopes to encode different proteome states. These approaches rely on the labeled peptides having the same physiochemical behavior while having predictable differences in mass.

The primary objective of classical MS experiments in proteomics is to identify and quantify proteins within the proteome. In bottom-up proteomics, protein information is deduced from the peptide level. Regardless of the quantification and scan modes employed, mass spectrometers generate outputs comprising MS1 and MS2 spectra. Numerous software tools allow processing the data, from identifying the signals (feature finding) to matching MS2 spectra to peptide sequences using search engines and quantification at both peptide and protein levels[257,258] (Figure 23c). The simplest output from proteomics analysis is a matrix that lists proteins and their abundances in different samples, with the data filtered using false-discovery rate cut-offs. Recent advancements in this field include the integration of standard or proteomic-specific bioinformatics pipelines, which for instance incorporate machine learning techniques. Additionally, there's a trend towards integrating proteomic data with other omics-type data, such as various forms of next-generation sequencing (NGS)

Aim of this study

Eukaryotic biology depends on widespread ubiquitylation by E3 ligases. Understanding when and how E3 ligases are activated is critical to elucidate pathways of biological regulation and develop new therapeutic strategies. With ≈300 family members in humans, cullin-RING ligases (CRLs) comprise nearly half of all E3 ligases; they mediate ≈20% of all protein degradation, regulate virtually every eukaryotic process, and are amongst the hottest platforms for targeted protein degradation[149,150,183,189-191]. Thus, it is of great interest to be able to probe the cellular repertoires of active CRLs in different settings.

CRLs are modular systems, that are dynamically formed and dismantled on a systemwide level[160-165]. The assembly/disassembly factor CAND1 (Cullin-associated NEDD8-dissociated protein 1) has been identified as a key player in regulating this dynamic process. However, the precise mechanism by which CAND1 shapes the cellular repertoire of CRL complexes remains unclear. Cryo-EM studies performed in the lab have revealed the structural mechanism by which CAND1 enables dynamic assembly and disassembly. In the first part of this work, we validated this structural mechanism in cellular systems by profiling how different mutations of CAND1 affect the cellular CRL repertoire and the cell's ability to respond to degradation-inducing stimuli.

Apart from CAND1, the activity of CRLs is intricately regulated by a complex cycle involving multiple proteins[156-158,161,164,177-179,182,259-262]. This cycle critically includes activation of CRL complexes via modification of the cullin module with the ubiquitin-like protein NEDD8 (Neural precursor cell expressed developmentally down-regulated protein 8). Unlike active complexes of some E3s (e.g., HECT and RBR E3s) that can be surveyed with probes reacting with their catalytic cysteine, CRLs lack an

active site and instead bridge substrates and ubiquitin-carrying enzymes (UCEs), necessitating alternative methods to target their active pool selectively.

Prior efforts to probe the cellular CRL repertoire have used an indirect, laborious approach requiring endogenous tagging of individual cullin subunits. The current state-of-the-art is limited to single cullins, restricted to the engineered cell system (including the limitations associated with making them) and does not distinguish between active and inactive CRL complexes. Moreover, the current technology fails to allow simultaneous comparisons between different cullins (e.g. CUL1 *and* CUL2, etc.) in a single cell type, nor comparisons between which CRLs are active in different cell types. Furthermore, to our knowledge, there are no methods to quantify the repertoires of active CRLs in primary cells.

In this work, we developed a suite of antigen-binding fragments (Fabs) that specifically recognize active neddylated CRLs using phage display, utilizing NEDD8 as a marker of activated cullins. Structural studies confirmed the binding of one of the Fabs to neddylated CUL1 in its active conformation during ubiquitylation. Employing biochemical and proteomics approaches revealed it not only recognizing NEDD8-linked cullin proteins but also capturing assembled neddylated CRL1, CRL2, CRL3 and CRL4 complexes with high specificity. By combining this activity-based probe with quantitative proteomics, we were able to profile distinct active CRL complex landscapes and their responses to cellular signaling pathways and degrader drugs.

Results

CAND1 mediated systemwide CRL assembly

Cullin-RING ubiquitin ligases are essential for proper function of eukaryotic systems. To ensure their correct function, CRL-dependent ubiquitylation is regulated by a multimodal mechanism that activates and labels substrate-bound complexes. One level of this regulation is neddylation. A conserved lysine on the WHB-domain of cullins gets modified with the small ubiquitin-like protein NEDD8 greatly increasing the efficiency of the ubiquitylation reaction[170]. CRL complexes not needed at a given moment are deneddylated by the COP9 signalosome (CSN). Substrate-bound complexes are protected from CSNs activity leaving them in the active, neddylated state. Another major factor regulating CRLs is CAND1, which binds non-neddylated CRL complexes and keeps them in their inactive state by preventing their neddylation. Despite their seemingly inhibitory roles both CSN and CAND1 are required in cells for degradation of many CRL substrates.

The beneficial effect on CRL function of CSN and CAND1 is a result of them allowing a specific CRL complex to be assembled when needed i.e., the cognate substrate is available. The cellular concentrations of substrate receptors vastly exceed those of cullin backbones[163,263]. Additionally, purified CUL1-RBX1-SKP1-Fbp complexes are highly stable with day long half-lives[153,159,161]. In combination this would lead to a fraction of available SKP1-Fbp complexes sequestering all CUL1-RBX1 preventing the formation of new CUL1-RBX1-SKP1-Fbp complexes needed under specific cellular conditions. CAND1 prevents this from happening. When provided with CAND1, uneddylated CUL1-RBX1-SKP1-Fbp complexes partly release their SKP1-Fbp module[161]. Furthermore, CAND1 partially releases from CAND1-CUL1-RBX1 complexes when mixed with SKP1-Fbp[161]. This indicates a role of CAND1 in controlling the assembly and disassembly of CRL complexes by promoting the swapping of substrate binding modules[161,163]. Proteomic studies could support this

function of CAND1 by profiling human CUL1-RBX1-SKP1-Fbp complexes and showing that their composition depended on CAND1 and neddylation and deneddylation[163].

While data from *Arabidopsis thaliana*[264] and biochemical experiments[161] suggested that CAND1 has a positive role in CRL1 activity, structural studies indicated an inhibitory role. Crystal structures of CAND1 in complex with CUL1-RBX1 showed CAND1 wrapped around CUL1 with CAND1's first two HEAT repeats (making up CAND1's "anti-neddylation domain) blocking the neddylation site of CUL1's WHB domain and a β-hairpin motif of CAND1 ("anti-SKP1" domain) blocking the SKP1-Fbp binding site[156]. Reversely, in structures of CUL1-RBX1-SKP1-Fbp complexes both SKP1 and the Fbp occlude the CUL1 site bound by CAND1's β-hairpin. Together this indicates that CUL1-RBX1 binding to CAND1 or SKP1-Fbp is mutually exclusive. In an attempt to reconcile these seemingly contradictory findings, an intermediate complex involving all components – CUL1, RBX1, CAND1, and SKP1-Fbp – was proposed[163]. However, the underlying structural mechanism has never been characterized.

To resolve this conflict and elucidate the structural mechanism of CAND1 mediated CRL-remodeling Dr. Kheewoong Baek performed single-particle cryo-EM studies for CUL1-RBX1 in complex with different SKP1-Fbs and CAND1. The resulting structures showed several different conformations of the CAND1-CUL1-RBX1 complex, indicating that instead of forming a singular unstable intermediate CAND1-CUL1-RBX1 assumes multiple forms as either CAND1 or SKP1-Fbp dissociate from CUL1-RBX1.

Other than previous structures showed, SKP1-Fbp can still bind a CAND1-CUL1-RBX1 complex with fully engaged CAND1 by assuming a slightly rotated

conformation with a reduced interface ("rocked"). Further, CAND1 could bind in a way that leaves the SKP1-Fbp binding site of CUL1 free by only interacting with CUL1's C-terminal halve ("rolling"). Biochemical assays performed by Dr. Daniel Scott could show that SKP1-Fbp modules in the "rocked" conformation are more susceptible to displacement, whereas CAND1 in the "rolling" conformation has reduced contacts to the cullin with its "anti-neddylation"-domain. Together this suggests a mechanism where instead of going through a single intermediate, CAND1 and CUL1-RBX1-SKP1-Fbp complexes go through an assemble of conformations that enables the reversible formation of both CAND1-CUL1-RBX1 and CUL1-RBX1-SKP1-Fbp complexes.

To test if the proposed structural mechanism can explain CRL function in a cellular environment, we tested TNF depended degradation of phosphorylated NFKBIA by CUL1[BTRC]. A previous study had shown the importance of CAND1 in the function of CUL1[BTRC] in degrading NFKBIA in a TNF dependent manner using cells bearing a knockout of CAND1 and its compensatory homolog CAND2[160]. The severely impaired degradation efficiency of the CAND null cells could be restored by expressing WT CAND1. Re-expressing a CAND1 variant with the β-hairpin deleted instead of wildtype CAND1 failed to restore phospho-NFKBIA degradation efficiency (Figure 24a,b). Importantly, cells expressing a CAND1 mutant (β-hairpin++) with key residues mutated (M1068W P1070Q) that is only deficient in dissociating SKP1-Fbp while retaining wildtype like CUL1 binding also showed severely impaired degradation of phospho-NFKBIA.
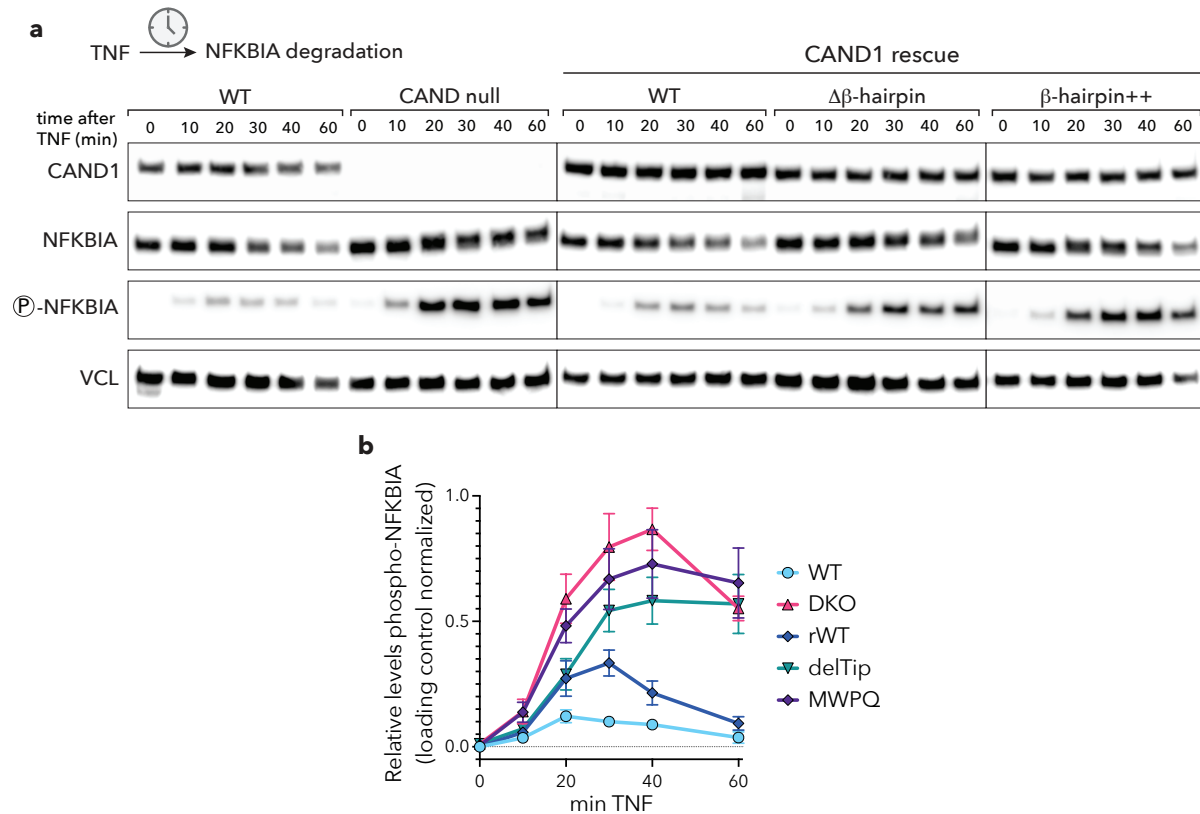
Figure 24 CAND1-CUL1-SKP1 interface critical in production of degradation-competent SCFs.
(**a**) Expression of CAND1 β-hairpin mutants in CAND-null 293 cells does not rescue TNF-induced degradation of phosphorylated NFKBIA. Immunoblots (IBs) detecting CAND1, total- or phospho NFKBIA, or vinculin (VCL) as a loading control at specific time points post-TNF treatment are shown. The chemiluminescent signal is displayed with adjusted brightness and contrast. (**b**) Graph showing the relative levels of phosphorylated NFKBIA (normalized to vinculin loading control as plotted in (a) (n = 3, errors bars SEM). Figure adapted from Baek, Scott et. al 2023.

By employing a cell line containing endogenously tagged 3xFLAG-CUL1 we explored the effects of the CAND1 mutants on the cellular composition of CUL1-RBX1-SKP1-Fbp complexes. Deshaies and colleagues used this cell line to profile endogenous CRL repertoires when preventing post-lysis CAND1 mediated exchange[162,163]. We assessed the effects of rescue in the same parental cell line with wild-type or mutant CAND1 WT on the repertoire of CUL1-associated proteins by performing anti-FLAG immunoprecipitations followed by mass spectrometry (Figure 25). This methodology allowed us to scrutinize the impact of CAND1 mutants on the occupancy levels of 44 Fbps and SKP1. The reintroduction of WT CAND1 successfully reinstated the cellular SCF repertoire of the CAND1/2 knockout cells, mirroring that of the corresponding parental cells. The observed

differences between cells originally containing CAND1 and CAND1 WT rescues are likely a result of adaptive changes in Fbp expression level caused by the CAND1/2 knockout and our results align with earlier studies indicating CAND1-dependent SCF complex formation. In contrast to WT CAND1, the expression of β-hairpin mutants had minimal influence on the cellular SCF repertoire. Together this is consistent with the structural model, where CAND1 is required to assume its "engaged" and promote the "rocking" of the CUL1-SKP1-Fbp interface to regulate the formation of CUL1-SKP1-Fbp complexes at a systemwide level in cells.
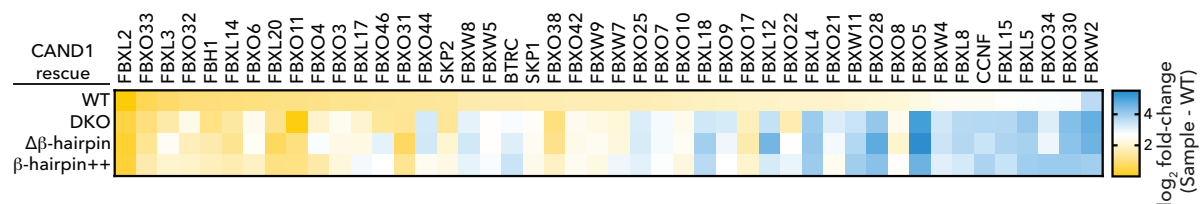
Figure 25 Systemwide SCF assembly. The WT CAND1-dependent SCF steady-state repertoire is not restored upon expression of CAND1 β-hairpin mutants in CAND null-cells. Endogenous FLAG-CUL1 was immunoprecipitated in presence of recombinant GST-RBX1-CUL1, acting as a "sponge" to sequester free CAND1 and Fbp, and MLN4924 and CSN5i-3 to suppress exchange. The SCF proteome in CAND-null 293 cells stably expressing either WT CAND1 (top row) or the specified CAND1 mutants (bottom two rows) was determined using mass spectrometry. The log2 fold-change for CUL1-association of each Fbp relative to WT cells is shown in the heatmap. Figure adapted from Baek, Scott et. al 2023.

Neddylation as a marker of active cullins

The CRL assembly cycle critically depends on modification of the cullin backbone with the small ubiquitin-like protein NEDD8[166-168,170,171,265]. The ubiquitin ligase function of a CRL is activated through the linkage of NEDD8 to a specific site conserved across the C-terminal WHB subdomains of cullins. Kinetic studies with CUL1-based complexes have shown that modification with NEDD8 results in a more than 1,000-fold increase in ubiquitylation efficiency[170]. This effect of NEDD8-modification is a result of NEDD8 and CUL1's WHB subdomain adopting a specific conformation together that activates ubiquitin conjugating enzymes[170,171]. The highly conserved sequences of the WHB subdomains of CUL1, CUL2, CUL3, and CUL4 suggests that they form structurally similar complexes when modified with NEDD8[175,176]. This is further supported by mutational data based on CUL1

complexes confirming the significance of the NEDD8-CUL4 interface in degrader-drug induced ubiquitylation[170].

The precise regulation of the cullin-RING E3 ligase network via neddylation is pivotal for orchestrating diverse cellular processes, spanning cell division, immune signaling, DNA replication and repair, responses to redox stress and hypoxia, tumorigenesis, and engagements with bacterial and viral pathogens[126,149,189]. Furthermore, cullin-RING ligases are the predominant ubiquitin E3 ligases harnessed for targeted protein degradation strategies[183,190,191]. Investigation into the consequences of neddylation inhibition on the substrate receptors associated with CUL1 and CUL4 has given rise to the 'adaptive exchange hypothesis'[160,162,163]. This hypothesis proposes that the landscape of NEDD8-activated CRLs undergoes rewiring to adeptly respond to alterations in cellular conditions[162,163].

Consequently, there is a significant interest in investigating NEDD8-activated CRLs. However, the current method for assessing active CRL repertoires necessitates endogenous tagging of cullin, a process that is laborious, may introduce artifacts, confines studies to the engineered cell line, and poses challenges for primary cells[162,163]. Targeting NEDD8 directly is also complicated, as a substantial proportion of cellular NEDD8 exists in an unconjugated state[266,267]. Using anti-NEDD8 antibodies may present challenges, given that a considerable portion of NEDD8's surface is obscured by interactions with a cullin[170,171,268]. Furthermore, previous studies utilizing tagged NEDD8 identified only a limited subset of SBMs in affinity purification mass spectrometry (AP–MS) experiments, significantly fewer compared to the same workflow applied to identically tagged cullins[269,270]. Additionally, it is noteworthy that several hundred proteins, beyond cullins, undergo neddylation[266,267].

In order to tackle these issues, we drew inspiration from the successful targeting of ubiquitin chains with affinity reagents and thought out to generate antigen-binding fragments (Fabs) via phage display that specifically target neddylated cullins[271-274]. In order to generate probes selectively binding neddylated CRLs, we implemented a negative>negative>positive selection strategy to enrich specific binder from a Fab phage library[275] (Figure 26a, 27a,b,c,d). First, phages carrying Fabs binding to a cullin-RING complex or NEDD8 separately were removed from the library. Subsequently, a neddylated cullin-RING complex served as the bait for a positive selection. As baits we selected the minimal complex that can be enzymatically neddylated, composed of the cullin C-terminal region and RBX1[166]. Conducting separate selections with CUL1 or CUL2 resulted in two and three Fab sequences, respectively.
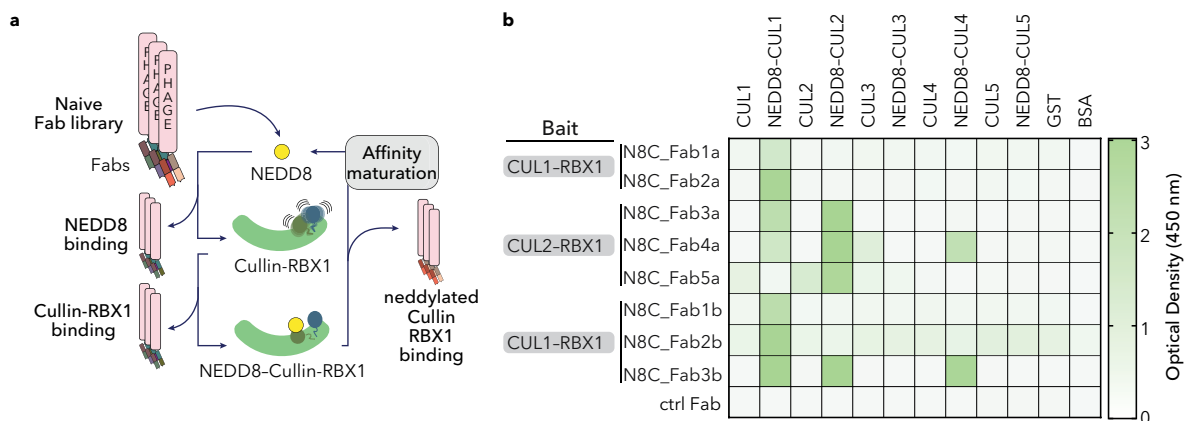
Figure 26 Generating synthetic antibody fragments (Fabs) specifically targeting neddylated cullins. a, To select Fabs specifically binding neddylated cullins over non-neddylated cullins or NEDD8 alone a negative>negative>positive selection strategy was used. Baits used for selection include the neddylated C-terminal regions of CUL1 or CUL2 bound to RBX1. b, ELISA to determine binding specificity of the generated Fabs against non-neddylated and neddylated CUL1-CUL5, GST and BSA at a concentration of 50 nM (full titrations in Figure 28).The baits used for individual Fabs are indicated. Figure adapted from Henneberg, Duda, Singh et. al 2023.

To characterize the affinities and specificities of the Fabs resulting from the selection we performed enzyme-linked immunosorbent assays (ELISAs) (Figure 28a and c). All selected Fabs bound neddylated over non-neddylated cullins, GST, or BSA with high specificity (Figure 26b). Testing binding to different cullin backbones, showed

that multiple Fabs specifically bound the cullin used as bait during their selection. Surprisingly, two Fabs resulting from a selection using neddylated CUL2-RBX1 as

b Fab light chain V$_L$

```
  1  atg aaa aag aat atc gca ttt ctt ctt gca tct atg ttc gtt ttt tct att gct aca aac gcg tac gct gat atc  75
      M   K   K   N   I   A   F   L   L   A   S   M   F   V   F   S   I   A   T   N   A   Y   A   D   I
 76  cag atg acc cag tcc ccg agc tcc gcc tct gtg ggc gat agg gtc acc atc acc tgc cgt gcc agt cag        150
      Q   M   T   Q   S   P   S   S   L   S   A   S   V   G   D   R   V   T   I   T   C   R   A   S   Q
151  tcc gtg tcc agc gct gta gcc tgg tat caa cag aaa cca gga aaa gct ccg aag ctt ctg att tac tcg gca tcc  225
      S   V   S   S   A   V   A   W   Y   Q   Q   K   P   G   K   A   P   K   L   L   I   Y   S   A   S
226  agc ctc tac tct gga gtc cct tct cgc ttc tct ggt agc cgt tcc ggg acg gat ttc act ctg acc atc agc agt  300
      S   L   Y   S   G   V   P   S   R   F   S   G   S   R   S   G   T   D   F   T   L   T   I   S   S
301  ctg cag ccg gaa gac ttc gca act tat tac tgt cag caa tct tct tat tct ctg atc acg ttc gga cag ggt acc  366
      L   Q   P   E   D   F   A   T   Y   Y   C   Q   Q   S   S   Y   S   L   I   T   F   G   Q   G   T
     aag gtg gag atc aaa
      K   V   E   I   K
```

Fab heavy chain V$_H$

```
  1  atg aaa aag aat atc gca ttt ctt ctt gca tct atg ttc gtt ttt tct att gct aca aac gcg tac gct gag gtt  75
      M   K   K   N   I   A   F   L   L   A   S   M   F   V   F   S   I   A   T   N   A   Y   A   E   V
 76  cag ctg gtg gag tct ggc ggc ggc ctg gtg cag cca ggg ggc tca ctc cgt ttg tcc tgt gca gct tcc gga ttc  150
      Q   L   V   E   S   G   G   G   L   V   Q   P   G   G   S   L   R   L   S   C   A   A   S   G   F
151  aac ttt tct tct tct tct ata cac tgg gtg cgt cag gcc ccg ggt aag ggc ctg gaa tgg gtt gca tct att tct  225
      N   F   S   S   S   S   I   H   W   V   R   Q   A   P   G   K   G   L   E   W   V   A   S   I   S
226  tct tct tat ggc tat act tat tat gcc gat agc gtc aag ggc cgt ttc act ata agc gac gac aca tcc aaa aac  300
      S   S   Y   G   Y   T   Y   Y   A   D   S   V   K   G   R   F   T   I   S   A   D   T   S   K   N
301  aca gcc tac cta caa atg aac agt cta aga gct gag gat act gcc gtc tat tat tgt gct cgc act gtt cgt ggc  375
      T   A   Y   L   Q   M   N   S   L   R   A   E   D   T   A   V   Y   Y   C   A   R   T   V   R   G
376  tcc aaa aaa ccg tac ttc tct ggt tgg gct atg gac tac tgg ggt caa gga acc ctg gtc acc gtc tcc tcg      447
      S   K   K   P   Y   F   S   G   W   A   M   D   Y   W   G   Q   G   T   L   V   T   V   S   S
```
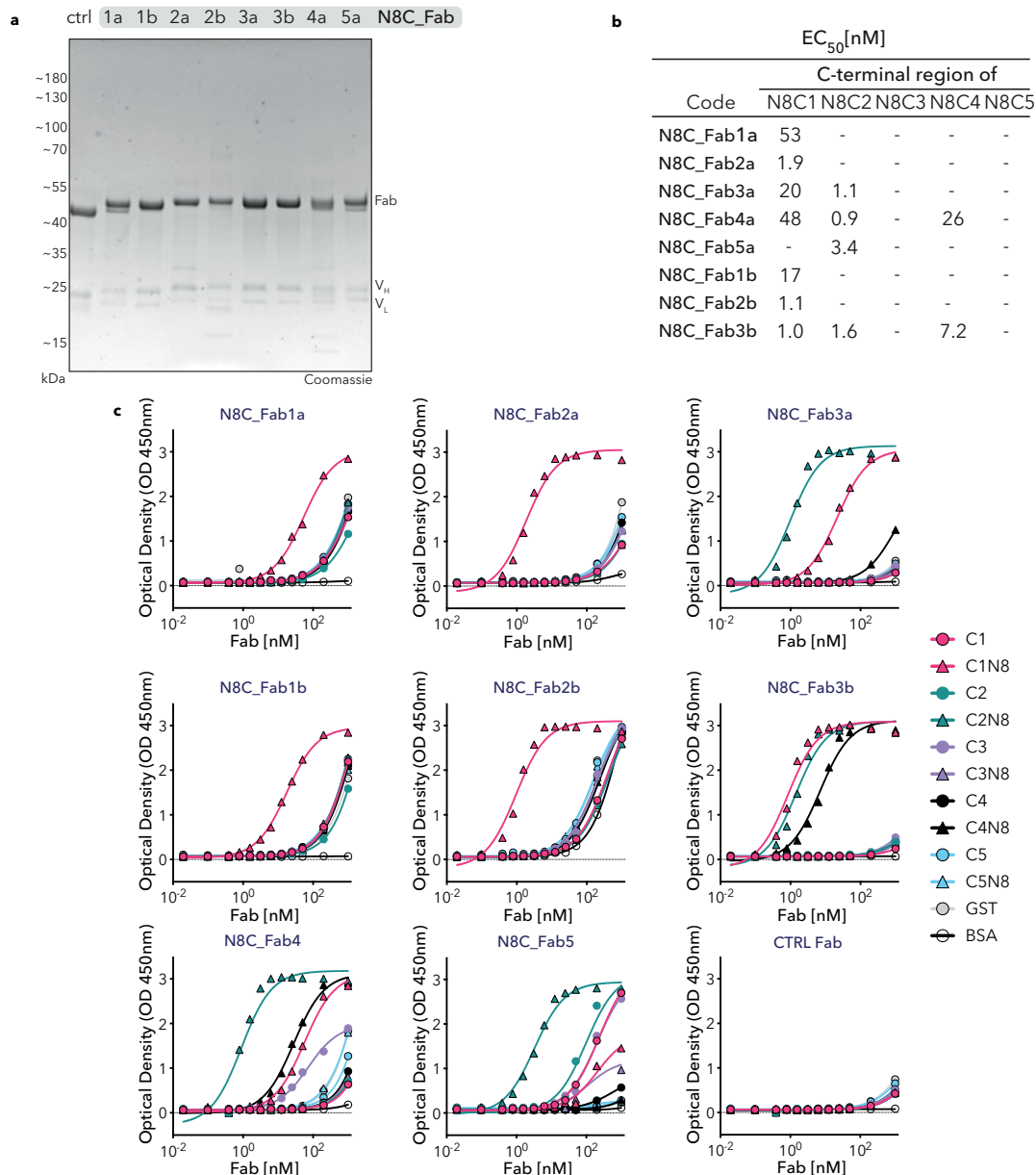
Signal peptide   CDRs

c

CDR-L3
WT: S S Y S L I
Library F: X$_{(3-7)}$ — P/L F/I

CDR-H1
WT: F S S S S I
Library F: I/L Y/S Y/S Y/S Y/S I/M

CDR-H2
WT: S I S S S Y G Y T Y
Library F: Y/S I/Y Y/P Y/S Y/S Y/S G Y/S T Y/S

CDR-H3
WT: T V R G S K K P Y F S G W A M
Library F: X$_{(1-17)}$ — A/G F/I/L/M

d

Code	bait	L3	H1	H2	H3
N8C_Fab1a	NEDD8-CUL1-RBX1	AASLI	LYYSSM	YISSSSGYTS	HFYWAM
N8C_Fab2a	NEDD8-CUL1-RBX1	WGWFSFPI	LYYSSM	YISSSSGYTS	SYGGSGAGYWYAL
N8C_Fab3a	NEDD8-CUL2-RBX1	SSYSLI	IYYSSI	SISSSYGYTY	GYFSWAAHGVGL
N8C_Fab4a	NEDD8-CUL2-RBX1	GYAFWHPI	LSYYSM	SISPYYSYTY	SHWASYYAGAF
N8C_Fab5a	NEDD8-CUL2-RBX1	SSYSLI	FSSSSI	SIYSSSYTS	SAVSSFWYFSSGM
N8C_Fab1b	NEDD8-CUL1-RBX1	AGSLI	LYYSSM	YISSSSGYTS	HFYWAL
N8C_Fab2b	NEDD8-CUL1-RBX1	WGWFSYRI	LYYYYI	YISPYSGYTS	TYGGSGPRYWYAF
N8C_Fab3b	NEDD8-CUL1-RBX1	SSYSLI	FSSSSI	SISSSYGYTY	DPFGWAAHGVGL
hIgG1 WT		SSYSLI	FSSSSI	SISSSYGYTY	TVRGSKKPYFSGWAM

Figure 27 Selection of Fabs targeting neddylated cullins. a, Schematic diagram depicting the negative-negative-positive selection strategy employed to produce synthetic antibody fragments (Fabs) specifically targeting neddylated cullins, but not their non-neddylated counterparts. The steps yielding specific antibodies are indicated. Selections were conducted utilizing neddylated C-terminal regions of CUL1 or CUL2 bound to RBX1. **b**, The DNA and amino acid sequences of the library F Fab scaffold are presented, with complementarity-determining regions (CDRs) highlighted in red. **c**, An overview of the CDR diversity within library F is provided, with allowed amino acids for each position indicated. For the position labeled with X, amino acids Tyr, Ser, Gly, Ala, Phe, Trp, His, Pro, or Val were permitted. **d**, The sequence information of the Fabs generated using the selection strategy outlined in a is shown, along with details of the baits utilized for their selection. Figure adapted from Henneberg, Duda, Singh et. al 2023.

the bait exhibited broader interactions, one also recognizing neddylated CUL1-RBX1, and another both neddylated CUL1- and neddylated CUL4-RBX1.

To enhance affinities for CUL1 and explore the potential of orthogonal selection to broaden the spectrum of recognized neddylated cullins by a single Fab, we conducted an additional round of selections using the neddylated CUL1 fragment

a

| | ctrl | 1a | 1b | 2a | 2b | 3a | 3b | 4a | 5a | N8C_Fab |

b

	EC50 [nM]				
	C-terminal region of				
Code	N8C1	N8C2	N8C3	N8C4	N8C5
N8C_Fab1a	53	-	-	-	-
N8C_Fab2a	1.9	-	-	-	-
N8C_Fab3a	20	1.1	-	-	-
N8C_Fab4a	48	0.9	-	26	-
N8C_Fab5a	-	3.4	-	-	-
N8C_Fab1b	17	-	-	-	-
N8C_Fab2b	1.1	-	-	-	-
N8C_Fab3b	1.0	1.6	-	7.2	-

Figure 28 Characterization of Fabs targeting neddylated cullins. a, Coomassie-stained gel of the indicated Fabs from the N8C_Fab suite. **b**, The EC50 values for binding between the indicated Fabs and the C-terminal regions of neddylated cullins 1-5 (N8 C1 = NEDD8-modified CUL1, and so on) were determined using ELISA. **c**, ELISA curves from Fab binding titrations against both neddylated and non-neddylated versions of cullins 1-5, GST, and BSA which were used to determine binding specificities as shown in Figure 26b. The corresponding EC50 values are displayed above in panel b. Figure adapted from Henneberg, Duda, Singh et. al 2023.

bound to RBX1 as the bait. The new libraries were derived from the sequences of N8C_Fab1a, N8C_Fab2a, and N8C_Fab3a, with the sequences of their complementarity-determining regions (CDRs)-L3 and H3 being diversified via soft randomization. Selections based on the framework of Fabs gained from CUL1-RBX1 selections (N8C_Fab1a and N8C_Fab2) yielded new Fabs exhibiting up to a threefold increase in affinity compared to their original counterparts (Figure 28b). From the selections using the library based on N8C_Fab3a, for which CUL2-RBX1 was originally used as the bait, resulted in N8C_Fab3b. This Fab showcased the following remarkable properties in ELISA: sustained interaction with neddylated CUL2–RBX1, a 20-fold improvement in EC50 towards neddylated CUL1–RBX1, and newfound recognition of neddylated CUL4A–RBX1. Additionally, N8C_Fab3b co-
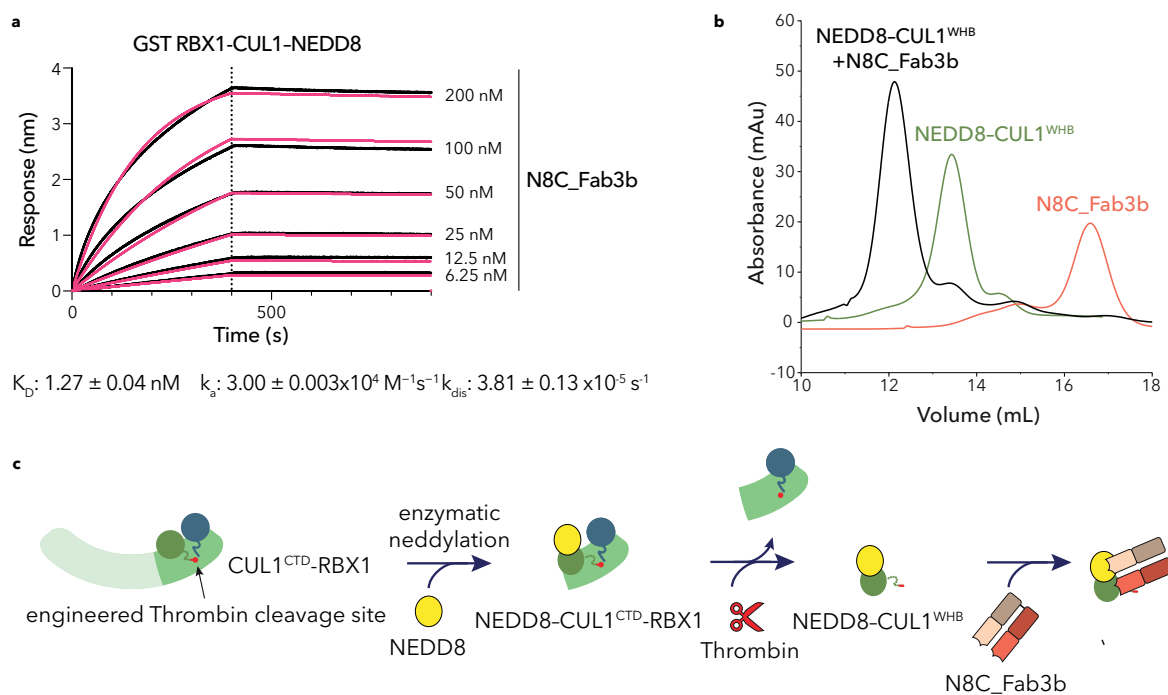
Figure 29 Crystallization of a complex of the neddylated CUL1 WHB domain and N8C_Fab3b. a, The Biolayer Interferometry sensorgram (in black) and the corresponding curve fitting (in red) from the binding of N8C_Fab3b (analyte) to GST RBX1-CUL1−NEDD8 (ligand, using GST biosensors). Calculated values for the equilibrium constant (KD) and rates of association and dissociation (ka and kdis) are provided below. **b**, Size exclusion chromatograms comparing the migration profiles of N8C_Fab3b, NEDD8−CUL1WHB, and the complex formed between the two, visualized by total absorbance at 280 nm. The purified complex was subsequently utilized for structure determination. **c**, Overview of the strategy employed to generate the isolated neddylated CUL1 WHB subdomain is presented. A mutant version of the complex between RBX1 and CUL1's C-terminal region (CTD) was engineered to include a thrombin cleavage site upstream of CUL1's WHB subdomain. Following enzymatic neddylation of RBX1 bound to CUL1, thrombin cleavage released the NEDD8−CUL1WHB unit, which was then mixed with N8C_Fab3b for further experimentation. Figure adapted from Henneberg, Duda, Singh et. al 2023.

purified with CUL1-RBX1 in size-exclusion chromatography (SEC) experiments. Association and dissociation rates of $\sim 3 \times 10^4\,M^{-1}\,s^{-1}$ and $\sim 3.8 \times 10^{-5}\,s^{-1}$, respectively, were determined via Bio-Layer Interferometry measurements, indicating a nanomolar affinity of N8C_Fab3b for neddylated CUL1-RBX1 (Figure 29a).
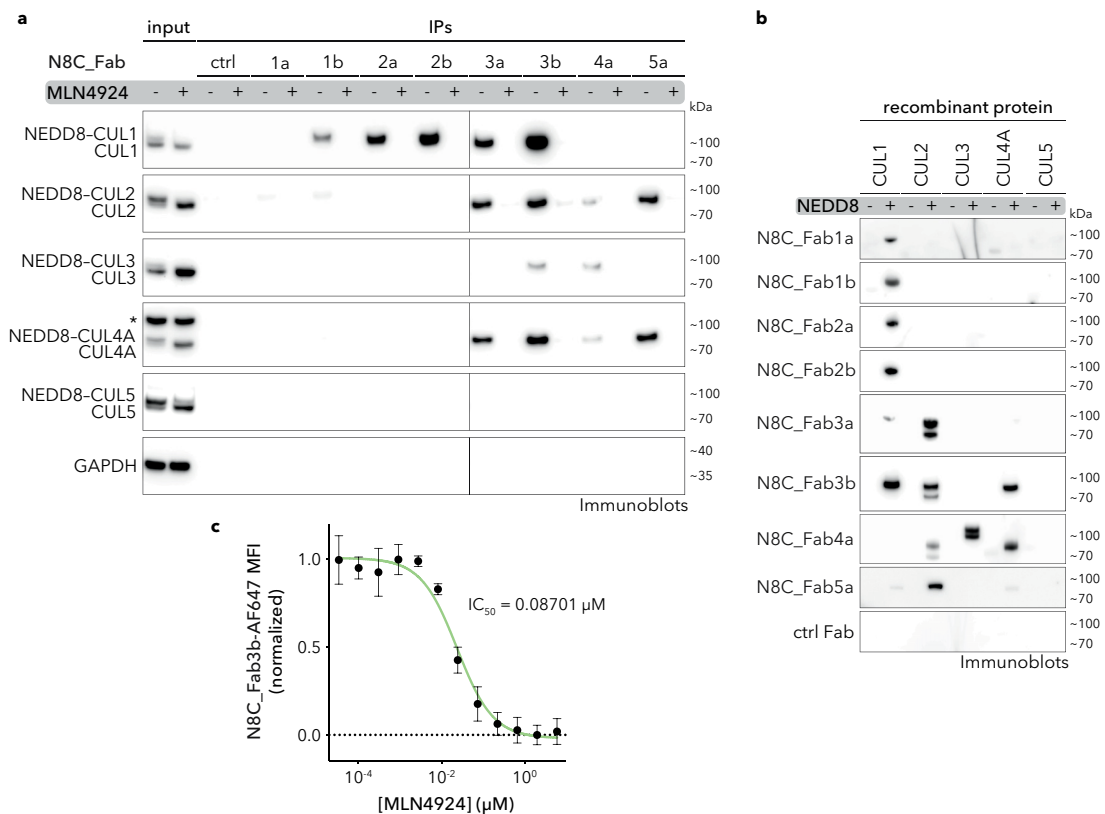
Figure 30 Generated Fabs are specific for neddylated cullins. a, Immunoblots of indicated recombinant cullins either modified with NEDD8 (+) or not (-) using the indicated Fabs as primary binders. b, Immunoprecipitations from K562 cells treated with DMSO or the neddylation inhibitor MLN4924 using the indicated Fabs. The slower migrating forms of cullins, which are diminished following MLN4924 treatment, are presumed to be NEDD8-modified, whereas the faster-migrating forms of cullins that accumulate upon MLN4924 treatment are considered to be unneddylated. An asterisk denotes a band that cross-reacts with the anti-CUL4 antibody. GAPDH is employed as a control for sample processing. The immunoblot results presented in panels a and b represent data from two separate experiments. c, Dose-response curve of MLN4924 for K562 cells measured by flow cytometry using fluorescently labeled N8C_Fab3b (Alexa Fluor 647) as a direct readout of levels of neddylated cullins ($n = 3$ biologically independent samples, data are shown as mean values ± s.d.). Figure adapted from Henneberg, Duda, Singh et. al 2023.

In total, eight Fabs were gained from the selections, with some specifically recognizing neddylated CUL1-RBX1 or neddylated CUL2-RBX1, while others bind several neddylated cullin-RBX1 complexes with low nanomolar EC_{50}s.

## N8C_Fabs selectively detect neddylated cullins

We evaluated the ability of purified version of the Fabs to selectively detect neddylated cullins in different assays. All Fabs specifically recognized neddylated cullins when used in immunoblots (Figure 30b). The observed cullin preferences aligned with those seen in ELISA using phage-displayed Fabs. This correlation persisted in immunoprecipitation (IP) experiments using K562 cell lysates, followed by immunoblotting with commercial cullin-specific antibodies (Figure 30a). Neddylation dependence was confirmed as interactions were abolished by treating cells with the neddylation inhibitor MLN4924. While ELISA did not detect neddylated CUL3–RBX1 interacting with any Fabs, it was detected by purified N8C_Fab4a in immunoblot and was enriched by both N8C_Fab3b and N8C_Fab4a in IPs from cell lysates.

We assessed the utility of N8C_Fab3b in flow cytometry due to its ability to bind multiple different cullin scaffolds and high specificity for neddylated over non-neddylated cullins. As a benchmark we selected treatment with MLN4924, which should lead to loss of signal if N8C_Fab3b directly detects neddylated cullins. Indeed, half-maximal inhibitory concentration (IC50) determined by dose–response curves in K562 cells of approximately ~87 nM (Figure 30c) were consistent with the reported <100 nM based on NEDD8 migration detected in immunoblots as a proxy for conjugate formation[188].

Effects of N8C_Fabs on neddylated CRL activities

With neddylation serving as the activating mutations of cullins it significantly influences the binding partners and function of cullin-RING complexes. To ensure that binding of N8C_Fabs does not prevent ubiquitylation competent CRLs to form we tested addition of Fabs to activity assays. Initially, we investigated whether Fab binding could prevent deconjugation of the fragile NEDD8 modification by CSN.
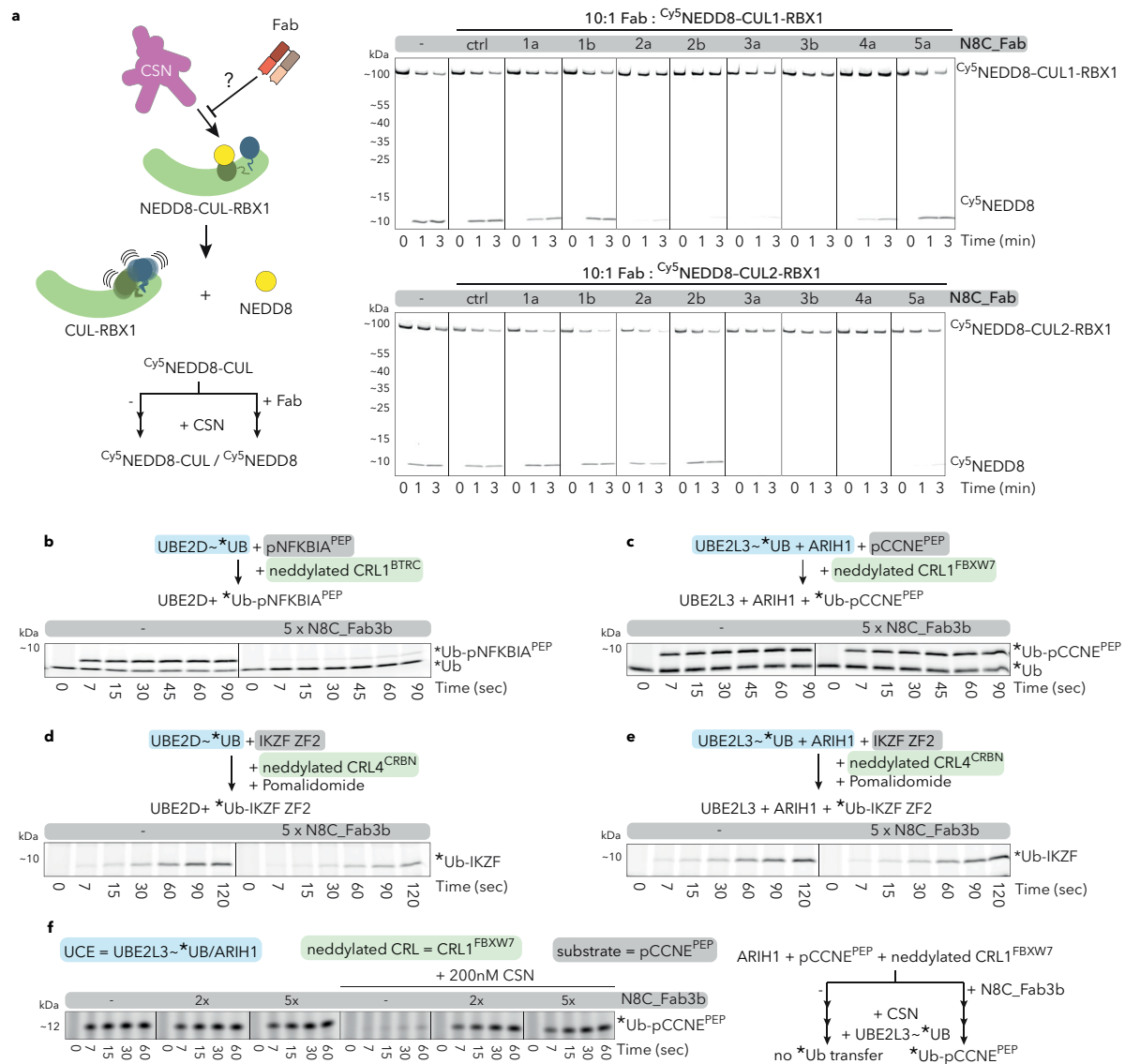
Figure 31 Impact of neddylated cullin targeting Fabs on activity of CRLs. a, The CSN-catalyzed deconjugation of fluorescent NEDD8 from CUL1 is monitored by observing the loss of signal for ^{Cy5}NEDD8-CUL1 RBX1 and the accumulation of free NEDD8 over time by SDS-PAGE. The depicted assay tests the protective effects of incubating the C-terminal regions of either CUL1 or CUL2 in complex with RBX1 (as indicated) with 10x molar excess of indicated Fabs. **b**, Impact of N8C_Fab3b binding on ubiquitylation by neddylated CRL1^{BTRC}-UBE2D was determined by monitoring the transfer of fluorescent ubiquitin (*Ub) to a substrate peptide derived from phospho-NFKBIA (pNFKBIA^{PEP}) via SDS−PAGE. **c**, Similar to b, the effects of N8C_Fab3b binding were evaluated, but this time, the transfer of *Ub by neddylated CRL1FBXW7-UBE2L3/ARIH1 to a substrate peptide derived from phospho-Cyclin E (pCCNEPEP) was monitored. **d**, Similar to b, but assessing the pomalidomide-induced transfer of *Ub by neddylated CRL4^{CRBN}-UBE2D to an IKZF ZF2 substrate. **e**, Similar to d, but monitoring the pomalidomide-induced transfer of *Ub by neddylated CRL4^{FBXW7}-UBE2L3/ARIH1 to an IKZF ZF2 substrate. **f**, Similar to c, but comparing *Ub transfer in the absence and presence of CSN, with or without prior incubation with N8C_Fab3b. For schemes of reactions in panels b−f, the ubiquitin-conjugating enzyme (UCE) is highlighted in blue, the substrate is depicted in gray, and the neddylated cullin is shown in green. Gel panels (a−f) represent data from two independent experiments. Figure adapted from Henneberg, Duda, Singh et. al 2023.

complexes, the addition of several N8C_Fabs to these reactions retarded deneddylation (Figure 31a). The ability to preserve the NEDD8 linkage was largely associated with Fab binding as determined by ELISA, with a few exceptions (Figure 28). For instance, N8C_Fab4a offered solid protection for neddylated CUL1 compared to N8C_Fab1b, even though its EC50 value was nearly triple that of N8C_Fab1b. One plausible explanation for these variations could be that only a portion of the Fabs binds in a way that prevents CSN from accessing the NEDD8–cullin bond

We chose N8C_Fab3b for further study due to its ability to bind a wide array of neddylated cullins and its capability to sustain cullin neddylation in the presence of CSN. We then examined the impact of N8C_Fab3b on ubiquitylation reactions that have been structurally characterized. In the selected reactions either an E2 (UBE2D) or E3 (ARIH1, which works together with the E2 UBE2L3 to ubiquitylate CRL substrates) served as the UCE. Addition of N8C_Fab3b to neddylated CRL1^{BTRC} together with UBE2D inhibited ubiquitylation of a peptide substrate derived from phospho-NFKBIA (Figure 31b). On the other hand, the ubiquitylation of a peptide substrate derived from phospho-Cyclin E by neddylated CRL1^{FBXW7} in combination with UBE2L3/ARIH1 was unaffected by addition of N8C_Fab3b (Figure 31c). Testing the effects of N8C_Fab3b addition to pomalidomide-induced ubiquitylation of a peptide substrate based on the Ikaros degron by CRL4^{CRBN} confirmed that the effects of N8C_Fab3b correlated with the UCE used in the reactions (Figure 31d, e).

We next tested whether the lack of effect of N8C_Fab3b on ARIH1 based reactions is due to N8C_Fab3b not binding during ARIH1-dependent ubiquitylation or N8C_Fab3b biding being compatible with ubiquitylation by ARIH1. To that extend we performed an experiment combining competition between N8C_Fab3b and deneddylation, with the requirement for CRL neddylation for ARIH1-mediated

ubiquitylation (Figure 31f). UBE2L3/ARIH1-mediated ubiquitylation was eliminated when CSN was added at a concentration overcoming CRL substrate inhibition. However, addition of N8C_Fab3b restored ubiquitylation activity. This indicates, that N8C_Fab3b bind during ARIH1-mediated ubiquitylation and protects the neddylated CRL1 complex.

N8C_Fab3b captures the active conformation of NEDD8–CUL1

To understand the mode of binding permitting selective recognition of neddylated cullins by N8C_Fab3b, we sought out to determine the structure of N8C_Fab3b in complex with NEDD8–CUL1-RBX1. To obtain this complex in a form that could be crystallized, we devised a strategy relying on introducing a Thrombin cleavage site into the cullin (Figure 29b, c). This allowed enzymatic neddylation of CUL1^{CTD} (Thrombin 676/677)–RBX1 and subsequently separate the neddylated WHB domain from the remaining CUL1^{CTD}. This allowed us to gain a crystal structure of N8C_Fab3b in complex with NEDD8–CUL1^{WHB} resulting in a structure at 2.7 Å resolution (Table 1).

Table 1 Crystallographic data collection and refinement statistics. Table adapted from Henneberg, Duda, Singh et. al 2023.

	N8C_Fab3b-NEDD8-CUL1^{WHB}
Data collection	
Space group	P 21 21 21
Cell dimensions	
a, b, c (Å)	102.37, 106.87,180.65
a, f3, y (°)	90.00, 90.00, 90.00
Resolution (Å)	90.33 - 2.66 (2.70 - 2.66) *
R_{sym} or R_{merge}	0.06
I / aI	1.72 (at 2.65Å)
Completeness (%)	98.3
Redundancy	6.7
Refinement	

Resolution (Å)	2.66
No. reflections	56649
R_{work} / R_{free}	0.217/ 0.263
No. atoms	8808
Protein	8808
Ligand/ion	0
Water	0
B-factors	
Protein	77.01
Ligand/ion	
Water	
R.m.s. deviations	
Bond lengths (Å)	0.0094
Bond angles (°)	1.1774

*Values in parentheses are for highest-resolution shell.

The structure reveals how N8C_Fab3b specifically recognizes neddylated over non-neddylated cullin. A unique surface spanning both NEDD8 and CUL1 is recognized by N8C_Fab3b (Figure 32a). Specifically, Tyr55 and Trp103 of N8C_Fab3b, located in CDR-H2 and H3, respectively, intricately fit into a groove situated between NEDD8's Ile36 patch and the CUL1 WHB domain. This groove is defined by the isopeptide linkage between NEDD8 and CUL1 on one side and noncovalent NEDD8–CUL1 contacts on the other (Figure 32b). The stability of the complex is reinforced by numerous hydrogen bonds formed between the Fab CDRs and either NEDD8 or CUL1 (Figure 33a). Furthermore, Tyr93 of CDR-L3 plays a crucial role by securely grasping the edge of CUL1's WHB domain (Figure 32c). Consequently, N8C_Fab3b selectively binds to a specific arrangement of NEDD8 and its associated CUL1 WHB domain.
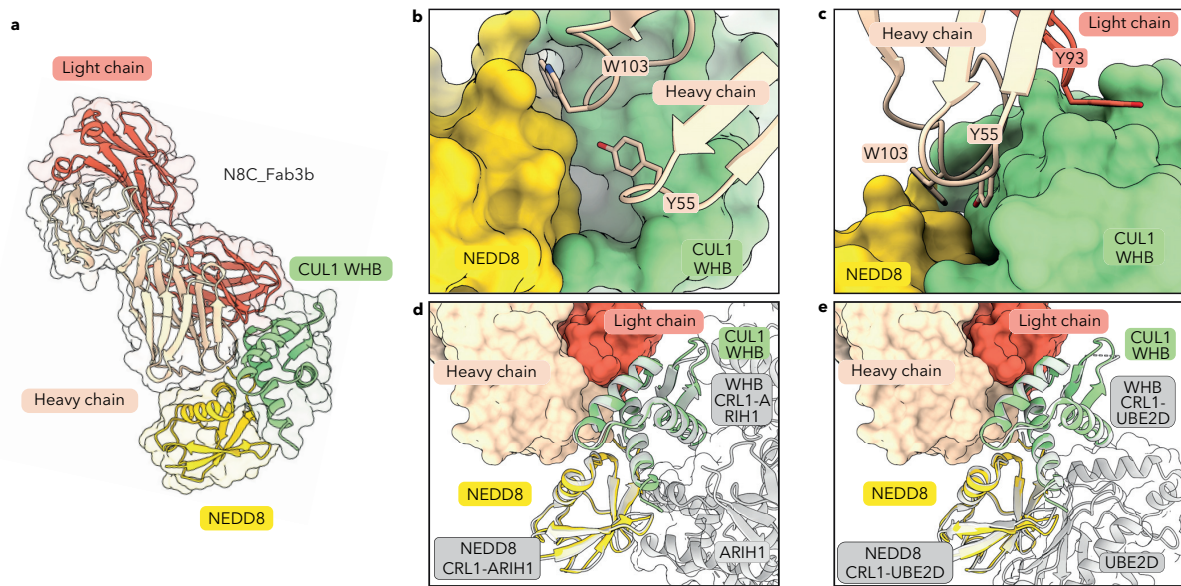
Figure 32 N8C_Fab3b captures the active conformation of the neddylated CUL1 WHB domain.
a, Crystal structure of N8C_Fab3b in complex with the neddylated CUL1 WHB domain (CUL1 WHB). A unique interface spanning both NEDD8 and CUL1 is recognized by N8C_Fab3b. **b**, Zoom-in of Y55 and W103 of the N8C_Fab3b heavy chain buried in a groove formed between the CUL1 WHB domain and NEDD8. **c**, Zoom-in of Y93 of the N8C_Fab3b light chain hooking into the edge of the CUL1 WHB domain. **d**, Superposition of the neddylated CUL1 WHB domain from the structure of N8C_Fab3b-bound complex with the one seen in an active CRL1[FBXW7]-UBE2L3/ARIH1 complex (PDB 7B5L). The active conformation of NEDD8 at the covalently linked CUL1 WHB domain is captured by N8C_Fab3b. **e**, Superposition of the neddylated CUL1 WHB domain from the structure of N8C_Fab3b-bound complex with the one seen in an active CRL1[BTRC]-UBE2D2 complex (PDB 6TTU). Figure adapted from Henneberg, Duda, Singh et. al 2023.

Remarkably, the conformation of the neddylated CUL1 WHB domain captured by N8C_Fab3b matches the one seen in structures of NFKBIA ubiquitylation by CUL1[BTRC] with the E2 UBE2D[170], and CDKN1B and CCNE ubiquitylation by CRL1[SKP2] and CRL1[FBXW7] together with the E2/E3 combination UBE2L3/ARIH1[171], respectively (Figure 32d, e). The residues of the WHB domain essential for mediating noncovalently binding to NEDD8 are conserved in CUL1-4 (Figure 33b). However, CUL5's sequence is not conducive to forming such a complex; NEDD8 and CUL5's WHB domain take on a different conformation in neddylated CRL5 E3s[268] (Figure 33c). Hence, the specificity is shaped not only by the interactions directly facilitated

by N8C_Fab3b but also by the neddylated CRL's capability to assume the active conformation between NEDD8 and the cullin's WHB domain.
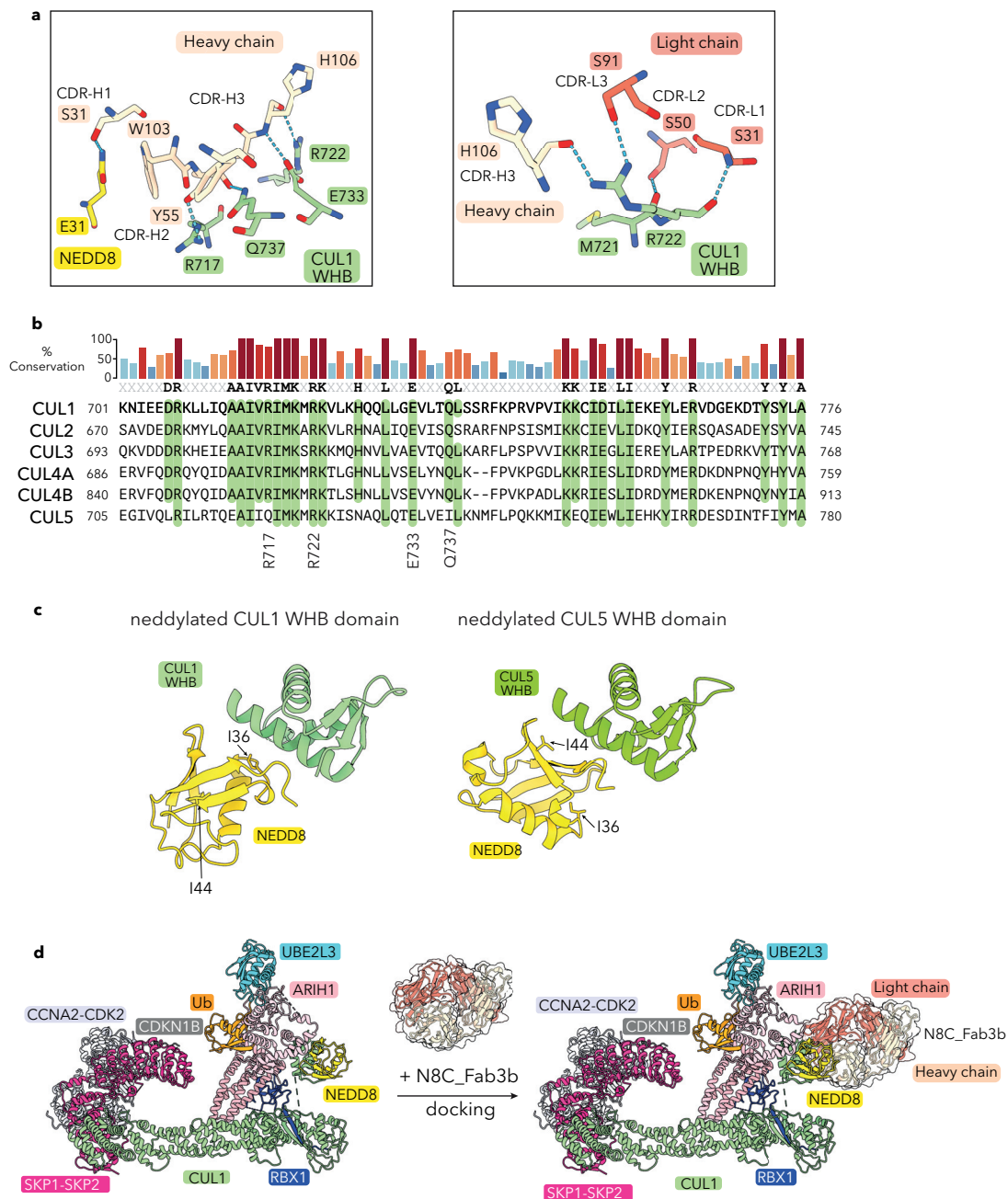
Figure 33 Structure of the complex of N8C_Fab3b with the neddylated CUL1 WHB domain. **a**, Detailed views depicting the interactions between the light and heavy chains of N8C_Fab3b and NEDD8 and the CUL1 WHB domain. **b**, Sequence alignment of the CUL1 WHB domains of CUL1-5. Conserved residues are highlighted in green and key residues involved in the interaction with N8C_Fab3b are indicated below. The bars on top indicate the percentage of sequence conservation. **c**, Structural comparison showing the arrangement of NEDD8 and its linked WHB domain from CUL1 (structure shown in Fig. 3) and CUL5 (PDB: 7ONI). **d**, Modeling of N8C_Fab3b on the structure of the neddylated CRL1[SKP2]-UBE2L3/ARIH1 complex (PDB: 7B5L) is shown. Alignment was performed on NEDD8 linked to the CUL1 WHB domain from both structures. Figure adapted from Henneberg, Duda, Singh et. al 2023.

In a neddylated CRL1 complex, NEDD8 and CUL1's WHB domain are suspected to adopt multiple conformations. Previous cryo-EM structures without an UCE did not capture these conformations, and for activation of UBE2D or ARIH1 the NEDD8–CUL1 WHB domain unit takes on different relative positions[170,171]. Modelling N8C_Fab3b into previously solved structures of ubiquitylation complexes showed that, during ubiquitin transfer from UBE2D to an SBM-bound substrate the Fab would clash, but it can capture an ARIH1-bound CRL complex without interfering with complex formation (Figure 33d). This explains the impact of N8C_Fab3b binding on different ubiquitylation reactions (Figure31b-e). The structure of N8C_Fab3b also hints at an inherent preference of NEDD8 and a cullin's WHB domain to bind each other in the active conformation. In sum, the findings show that N8C_Fab3b captures the active conformation between NEDD8 and cullin domain it modifies, thereby highlighting the Fabs potential to investigate NEDD8-triggered CRLs.

A pipeline probing cellular repertoires of neddylated CRLs

Given the capability of N8C_Fab3b IPs to enrich NEDD8-activated CRLs, we proceeded to refine the methodology, considering several key criteria. Initially, our focus was on identifying proteins that specifically interact with neddylated cullins. To achieve this, we distinguished between the effects of treating cells with DMSO as a control versus MLN4924[188], eliminating cullin neddylation. Additionally, we explored the impact of increasing the levels of neddylated cullins by employing the CSN inhibitor CSN5i-3[276].

Secondly, we recognized the intricate dynamics of the CRL assembly and disassembly pathway, where the cellular pool of cullin–RBX1 subcomplexes undergoes shuffling among excess SBMs in a deneddylation-dependent process[162,163,184]. CRL disassembly experiences a temporary pause due to the NEDD8

being retained on complexes bound to substrates. To maintain the cellular inventory of neddylated CRLs, we implemented the 'N8-block'-strategy. This involved applying MLN4924 and CSN5i-3 during cell harvesting, including them in lysis and wash buffers[162].
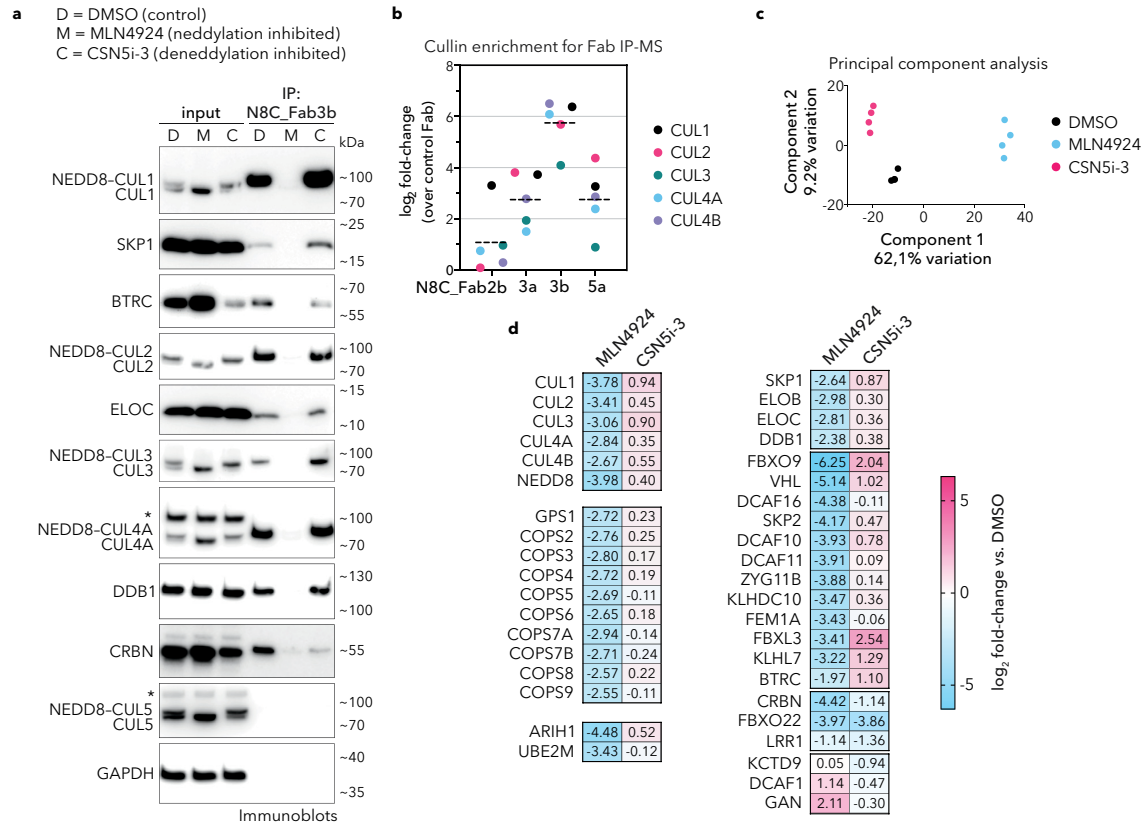
Figure 34 Probing the cellular repertoire of active CRLs. a, Immunoprecipitations from K562 cells using N8C_Fab3b. Cells were treated with either DMSO (D), the neddylation inhibitor MLN4924 (M) or the cullin deneddylase inhibitor CSN5i-3 (C) for 2 h. Indicated CRL components were probed for by immunoblotting. The slower migrating forms of cullins, which are diminished following MLN4924 treatment, are presumed to be NEDD8-modified, whereas the faster-migrating forms of cullins that accumulate upon MLN4924 treatment are considered to be unneddylated. An asterisk denotes bands that cross-react with the anti-CUL4 or anti-CUL5 antibodies. GAPDH is used as a sample processing control. The immunoblot results presented in panels a and b represent data from two separate experiments. b, Comparing the levels of cullins detected by mass spectrometry in immunoprecipitations with Fabs N8C_Fab2b, N8C_Fab3a, N8C_Fab3b and N8C_Fab5a compared to a control Fab (n = 3 biological independent samples). Mean $\log_2$ fold-change is indicated by a dashed line. c, Principal component analysis based on protein groups identified by mass spectrometry in immunoprecipitation experiments using N8C_Fab3b from 293T cells treated with DMSO (black), MLN4924 (blue), or CSN5i-3 (magenta) for 2h. All measurements were done as biological triplicates (n = 3). d, Heatmap showing selected proteins differentially identified by mass spectrometry in N8C_Fab3b immunoprecipitation from 293T cells treated with either MLN4924, or CSN5i-3 and compared to a DMSO control (n = 3). Figure adapted from Henneberg, Duda, Singh et. al 2023.

Conducting IPs with N8C_Fab3b utilizing N8-block, followed by immunoblotting, successfully demonstrated neddylation-dependent enrichment of known CRL components. including adapter proteins like SKP1, ELOC, and DDB1, as well as SBMs like BTRC and CRBN (Figure 34a). To further validate the suitability of N8C_Fab3b for profiling active CRL interactors, comparable IPs were conducted using N8C_Fab2b, N8C_Fab3a, and N8C_Fab5a, followed by library-free data-independent acquisition (DIA) MS. These experiments showed that all the Fabs significantly enriched cullins and SBMs in a manner dependent on neddylation (Figure 34b and 36a). The specificity of cullins bound in these experiments closely matched their in vitro binding properties (Figure 28c). Notably, N8C_Fab3b exhibited an enrichment of known cullin-associated proteins that was on average tenfold greater than that of the next best Fab. This led to the selection of N8C_Fab3b for profiling the cellularly activated CRL-omes (Figure 34b).

Subsequently, we employed unbiased DIA proteomics to explore which proteins are enriched by N8C_Fab3b. IPs from 293T cells, treated with DMSO, MLN4924, or CSN5i-3, showed cleanly separated populations by principal component analysis, underscoring reproducibility and neddylation dependence across four biological replicates (Figure 34c). Interactors known to vary under the distinct neddylation states induced by the inhibitors could be effectively pinpointed, serving as positive controls (Figure 34d).

Apart from the cullins and NEDD8, significant dependence on neddylation level was seen for components of the COP9 signalosome, the RBX1-specific NEDD8 E2 UBE2M, and UCE ARIH1, as well as adapter proteins SKP1, ELOB, ELOC, and DDB1. Notably, the NEDD8 E2 UBE2F and UCE ARIH2 specific to CUL5–RBX2 were absent, indicating that the interactors are associated with neddylated cullins 1–4, the targets recognized by N8C_Fab3b.

Identified SBMs can be categorized into three groups regarding the impact of impact of MLN4924-induced neddylation inhibition or CSN5-i3-induced deneddylation inhibition on their levels of enrichment by N8C_Fab3b (Figure 34d). Most showed a decrease with MLN4924, and either maintained similar or increased binding after CSN5i-3 treatments, aligning with the established model of regulation involving neddylation, deneddylation, assembly, and disassembly processes[160,162,163]. Some SBMs decrease upon inhibiting either neddylation or deneddylation, a phenomenon reported previously and attributed to autoubiquitylation-mediated degradation, as observed for CRBN[183,186]. Lastly, following the treatment with MLN4924, KCTD9, DCAF1, and GAN were observed to increase in IPs. Their preferential association with neddylated cullins in the absence of ongoing neddylation suggests that these SBMs have unconventional means to obstruct CSN. This characteristic, in conjunction with the autoubiquitylation of SBMs, has been previously reported for another neddylated CRL subject to pleiotropic regulation[187]. Remarkably, KCTD9, DCAF1, and GAN all form higher-order assemblies, and unneddylated CRL4^{DCAF1} oligomerizes, sequestering its CUL4 from neddylation and CSN[185,277,278]. This leads to the hypothesis that this third class of SBMs creates specialized assemblies that retain neddylated cullins post-MLN4924 treatment. However, to fully understand the precise molecular mechanisms behind this, further research is necessary.

Profiling CRL complexes activated by extracellular signals

The findings from Figure 34d indicated that N8C_Fab3b might be able to reveal CRL complexes undergoing changes in neddylation state in response to external stimuli. To delve deeper into this aspect, we examined three types of stimuli known to trigger neddylated CRL-dependent protein degradation in combination with a protocol that inhibits protein turnover.

Considering the growing significance of neddylated CRLs in targeted protein degradation[191,279], we investigated responses to degrader drugs. Firstly, we tested the molecular glue Indisulam, which utilizes neddylated CRL4^{DCAF15} to degrade RBM39[205,208] (Figure 35a). Indisulam was chosen as a benchmark due to its established dependence on neddylation and deneddylation, as well as the CRL assembly/disassembly machinerie[162,183]. Indeed, profiling with N8C_Fab3b after Indisulam treatment revealed an increased association of DCAF15 with neddylated cullins (Figure 36b). Remarkably, this was the sole significant change induced by Indisulam (Figure 35b). Next, we investigated the effects of a bivalent degrader, MZ1, which forms complexes between CRL2^{VHL} and members of the bromodomain and extraterminal domain (BET) family, BRD2, BRD3, and BRD4[280] (Figure 35c). Profiling of active CRLs showed that MZ1 led to an enrichment of VHL (Figure 36c). Additionally, it revealed an increased association of BRD2, BRD3, and BRD4 with a neddylated CRL in response to MZ1 (Figure 35d). Hence, our profiling method can identify the CRL activated by a degrader drug and, in some instances, targets for degradation as well. This indicates that the profiling method can identify CRLs activated by a degrader drug and, in some cases, the targets for degradation as well. The preferential enrichment of BRD4 over BRD2 and BRD3 aligns with MZ1-targeted degradation rather than its affinity for these neosubstrates[280], suggesting that the architecture of the CRL complex, rather than substrate binding, drives degradation[279,281]. Thus, our profiling method can pinpoint which CRL is activated by a degrader drug and, in certain instances, also reveal the substrate targeted for degradation.
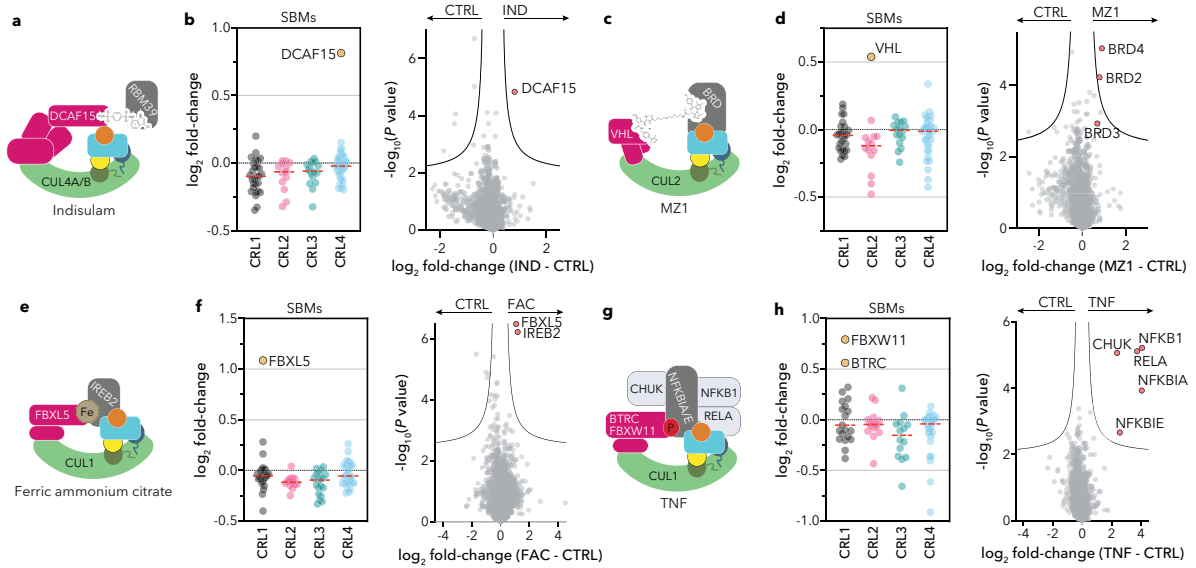
Figure 35 Profiling of CRL complexes activated by extracellular stimuli. a, Cartoon representation of the neddylated CRL4^{DCAF15} complex, in which the molecular glue Indisulam recruits RBM39 as a neo-substrate. NEDD8, cullin WHB domain, RBX1 RING domain, ubiquitin and UCE are colored yellow, dark green, blue, orange and cyan, respectively, as in Figure 16. **b**, The log$_2$ fold-change of SBMs associated with CUL1, CUL2, CUL3, and CUL4 (left panel), as well as a volcano plot showing all protein groups (right) identified in N8C_Fab3b immunoprecipitations from 293T cells treated with 2 µM Indisulam for 1h, as compared DMSO (CTRL). The mean log$_2$ fold-change is depicted by a dashed line (left plot). In the volcano plot, the curve corresponds to 5% FDR (FDR controlled, two-sided t test, randomizations = 250, s0 = 0.1). **c**, Cartoon representation of the neddylated CRL2^{VHL} complex, in which the bivalent degrader MZ1 recruits a BRD protein as a neo-substrate. **d**, same as b, except with a different stimulus: 1 h with 1µM MZ1 compared to a DMSO control. **e**, Cartoon representation of the neddylated CRL1^{FBXL5} complex, in which the substrate IREB2 is recruited in an iron-dependent manner. **f**, same as in b, but with a different stimulus: 90 min with 100 µM ferric ammonium citrate (FAC) compared to PBS (CTRL). **g**, Stimulation with TNF triggers phosphorylation of NFKBIA and NFKBIE, leading to their CRL1^{BTRC} and CRL1^{FBXW11} mediated ubiquitylation. The fully assembled complex of neddylated CRL1^{BTRC} or CRL1^{FBXW11} (here shown as a singular SBM) with phosphorylated NFKBIA or NFKBIE is shown as a cartoon. **h**, same as in b, but with a different cells and stimulus: 5 min treatment of K562 cells with 25 ng ml^{-1} TNF compared to PBS (CTRL). All experiments shown in **b**, **d**, **f** and **h** included $n = 4$ biological independent samples. Figure adapted from Henneberg, Duda, Singh et. al 2023.

Responses by the cellular CRL pool are essential for proper function of several signaling pathways critical for cell health. First, we looked at a metabolic signaling pathway to validate if profiling using N8C_Fab3b allows capturing such regulation. Exposure to high iron levels has been found to induce CRL1^{FBXL5}-dependent degradation of the iron regulatory protein 2 (IREB2)[282,283] (Figure 35e). Indeed, cells treated with ferric ammonium citrate showed a twofold increase in neddylated cullin association only for FBXL5 and IREB2 (Figures 35f, 36d). Lastly, we profiled the cellular response towards stimulation with a cytokine. Phosphorylation and

subsequent degradation of NFKBIA and NFKBIE by CRL1^{BTRC} and CRL1^{FBXW11} (also referred to as CRL1^{βTRCP1} and CRL1^{βTRCP2}) is induced by TNF (Figure 32g). Accordingly, after treating cells with TNF, our active CRL profiling workflow selectively identified these SBMs and substrates (Figures 35h, 36e). Notably, as
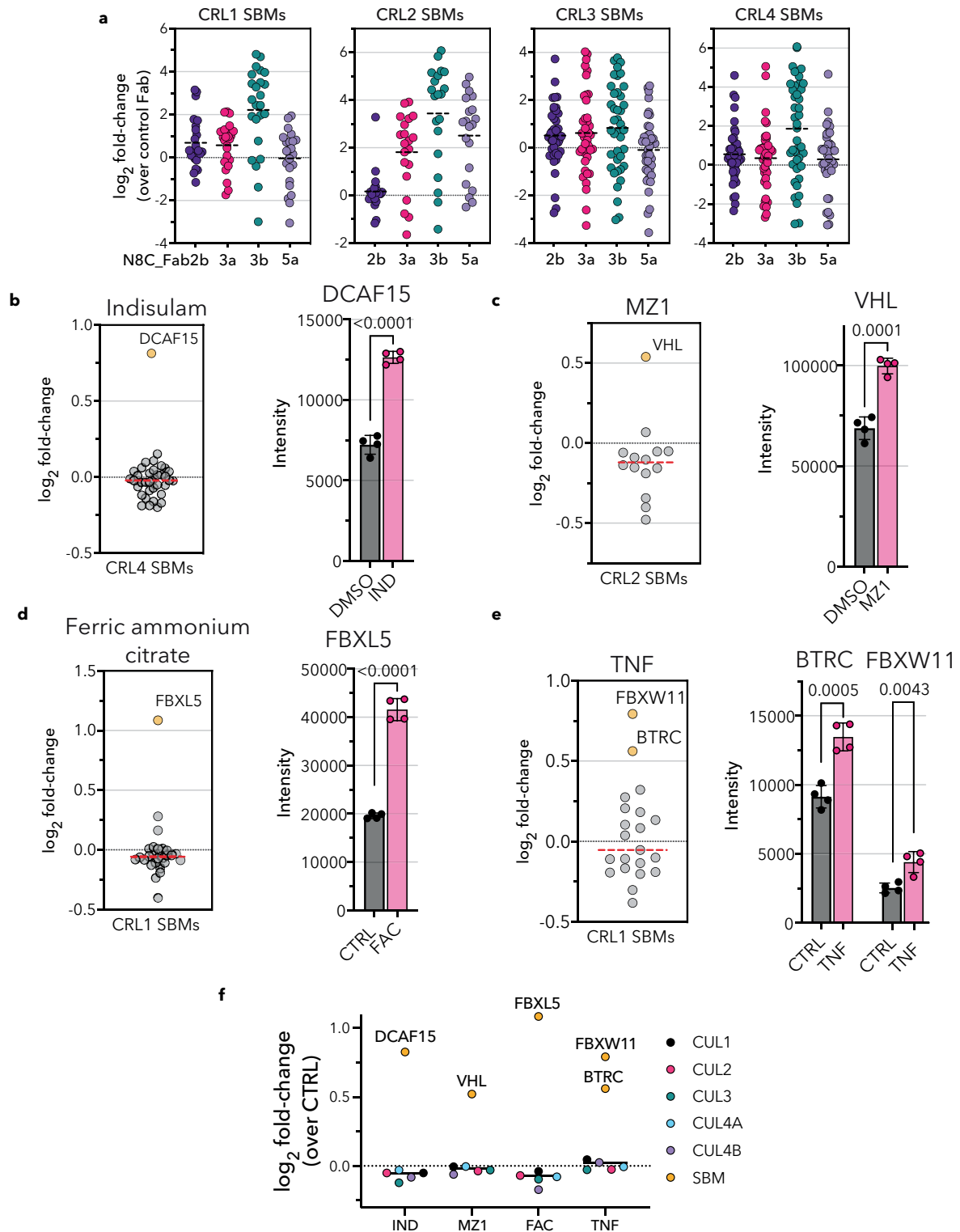
Figure 36 Using N8C_Fab3b for IP-MS experiments. a, Comparison of SBMs (for CRL1-4) enriched in IP-MS experiments using Fabs N8C_Fab2b, 3a, 3b, and 5a, compared to a control Fab. Plots are made from the same data used for Figure 34a (n = 3 biological independent samples). The $\log_2$ fold-change is depicted. Each dot represents one SBM known to associate with the indicated cullin. **b-f**. Further analysis of data shown in Figure 35 (n = 4 biological independent samples, data shown as mean +/- SD). **b**, Reshaping of the CRL network by the molecular glue degrader Indisulam. 293T cells were treated for 1 hour with 2 µM Indisulam (IND) compared to control (DMSO) as determined by SBMs identified in N8C_Fab3b IP-MS experiments. In the plot on the left, each dot represents one CRL4 SBM, and the $\log_2$ fold-change between treated samples and the control (DMSO) is shown. The bar graph on the right is showing differences in protein group intensity for the indicated SBM, with the p-value determined by a two-sided Student's t-test. **c**, Reshaping of the CRL network by the bivalent degrader MZ1. 293T cells were treated for 1 hour with 1 µM MZ1 compared to control (DMSO) as determined by SBMs identified in N8C_Fab3b IP-MS experiments. In the plot on the left, each dot represents one CRL2 SBM, and the $\log_2$ fold-change between treated samples and the control (DMSO) is shown. The bar graph on the right is showing differences in protein group intensity for the indicated SBM, with the p-value determined by a two-sided Student's t-test. **d**, Reshaping of the CRL network by a metabolic signal (excess iron). 293T cells were treated for 90 min with 100 µM ferric ammonium citrate (FAC) compared to control (PBS) as determined by SBMs identified in N8C_Fab3b IP-MS experiments. In the plot on the left, each dot represents one CRL1 SBM, and the $\log_2$ fold-change between treated samples and the control (DMSO) is shown. The bar graph on the right is showing differences in protein group intensity for the indicated SBM, with the p-value determined by a two-sided Student's t-test. **e**, Reshaping of the CRL network by a cytokine signal. K562 cells were treated for 5 min with 25 ng ml^{-1} compared to control (PBS) as determined by SBMs identified in N8C_Fab3b IP-MS experiments. In the plot on the left, each dot represents one CRL1 SBM, and the $\log_2$ fold-change between treated samples and the control (DMSO) is shown. The bar graph on the right is showing differences in protein group intensity for the indicated SBM, with the p-value determined by a two-sided Student's t-test. **f**, $\log_2$ fold-change for the experiments in panels b-e, of each cullin (shown as dots, CUL1 in black, CUL2 in magenta, CUL3 in green, CUL4A in blue, CUL4B in purple) and the SBM of interest (shown in yellow). The cellular stimulus is indicated below. Figure adapted from Henneberg, Duda, Singh et. al 2023.

found with other stimuli, our profiling method identified the precise SBM-containing complex that responded to the signal, despite the fact that cellular levels of neddylated cullins remained constant (Figure 36f). Remarkably, in this instance, the CRL profiling also identified additional critical components of TNF-induced degradation and signaling pathways, including the kinase CHUK, which generates the NFKBIA and NFKBIE phosphor-degrons, as well as the transcription factors NFKB1 and RELA that are trapped in the cytosol by NFKBIA and NFKBIE.

Baseline active CRL repertoire primes cellular response

We then addressed the fundamental question of whether active CRL repertoires varied across cell types by quantitatively comparing the cellular landscapes of neddylated CRLs without endogenous cullin labeling. We examined neddylated

CRL repertoires in a panel of ten cell lines derived from kidney, tongue, brain, blood, lung, ovary, and prostate using the proteomics pipeline. To correct for intrinsic differences between cell lines (Figure 37), we evaluated the relative loss of SBMs in N8C_Fab3b IPs following 2-hour MLN4924 treatment. Remarkably, in at least one cell line, the relative levels of 83 SBMs shifted significantly (Figure 38a). Several SBMs, including as BTRC, KLHL12, and CRBN, exhibit considerable variability in neddylated CRL occupancies between cell lines, whereas VHL showed high occupancy in all cell lines except for CAL33 cells (Figure 38b).
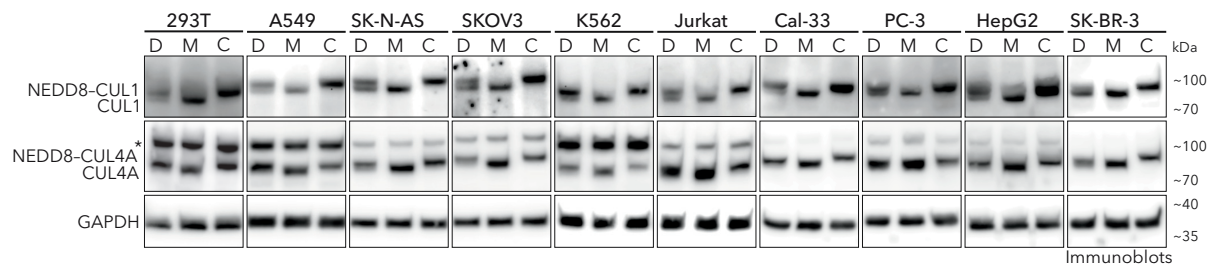
Figure 37 Levels of cullin neddylation across different cell lines. Immunoblots showing cellular neddylation levels for CUL1 and CUL4A after 2h treatment with DMSO (D), MLN4924 (M), and CSN5i-3 (C) for 293T, A549, SK-N-AS, SKOV3, K562, Jurkat, CAL-33, PC-3, HepG2, and SK-BR-3 cells. GAPDH serves as the sample processing control. Slower migrating forms of cullins lost upon MLN4924 treatment are interpreted as NEDD8-modified, whereas faster-migrating forms of cullins increased after MLN4924 treatment are interpreted as unneddylated. * denotes a band cross-reacting with the anti-CUL4 antibody. The presented results are representative of data obtained from two independent experiments. Figure adapted from Henneberg, Duda, Singh et. al 2023.

Is the response to a degradation signal impacted by the levels of pre-assembled active CRL? To test this, we looked at BRD4 degradation induced by dBET6, which recruits neddylated CRL4^{CRBN} (Figure 38c). This system was selected based on the following criteria: (1) CRL4^{CRBN} is a major E3 frequently used in targeted protein degradation strategies[191,279]; (2) CRBN is regulated by NEDD8 in a multimodal manner[183]; and (3) the degradation activity of the bivalent degrader molecule dBET6, which uses CRBN, depends on the cellular machineries regulating neddylation/deneddylation and CRL assembly/disassembly[183,284]. Four cell lines representative of the range of CRBN occupancy levels were selected: high levels in 293T and Jurkat, lower levels in SK-N-AS, and very low levels in CAL33. Total

proteome analysis of the selected cell lines showed that CRBN occupancy levels determined by N8C_Fab3b IP strongly correlate with CRBN expression levels (Figure 38d). However, SK-N-AS and CAL33 cells showed different levels of CRBN assembled in active complexes, despite having near identical CRBN quantities, indicating that factors beyond protein level impact the formation of neddylated CRL4[CRBN]. The levels of degradation efficiency seen in the different cells correlated most strongly with the levels of CRBN assembled in neddylated CRLs as determined by our probe (Figure 38e)
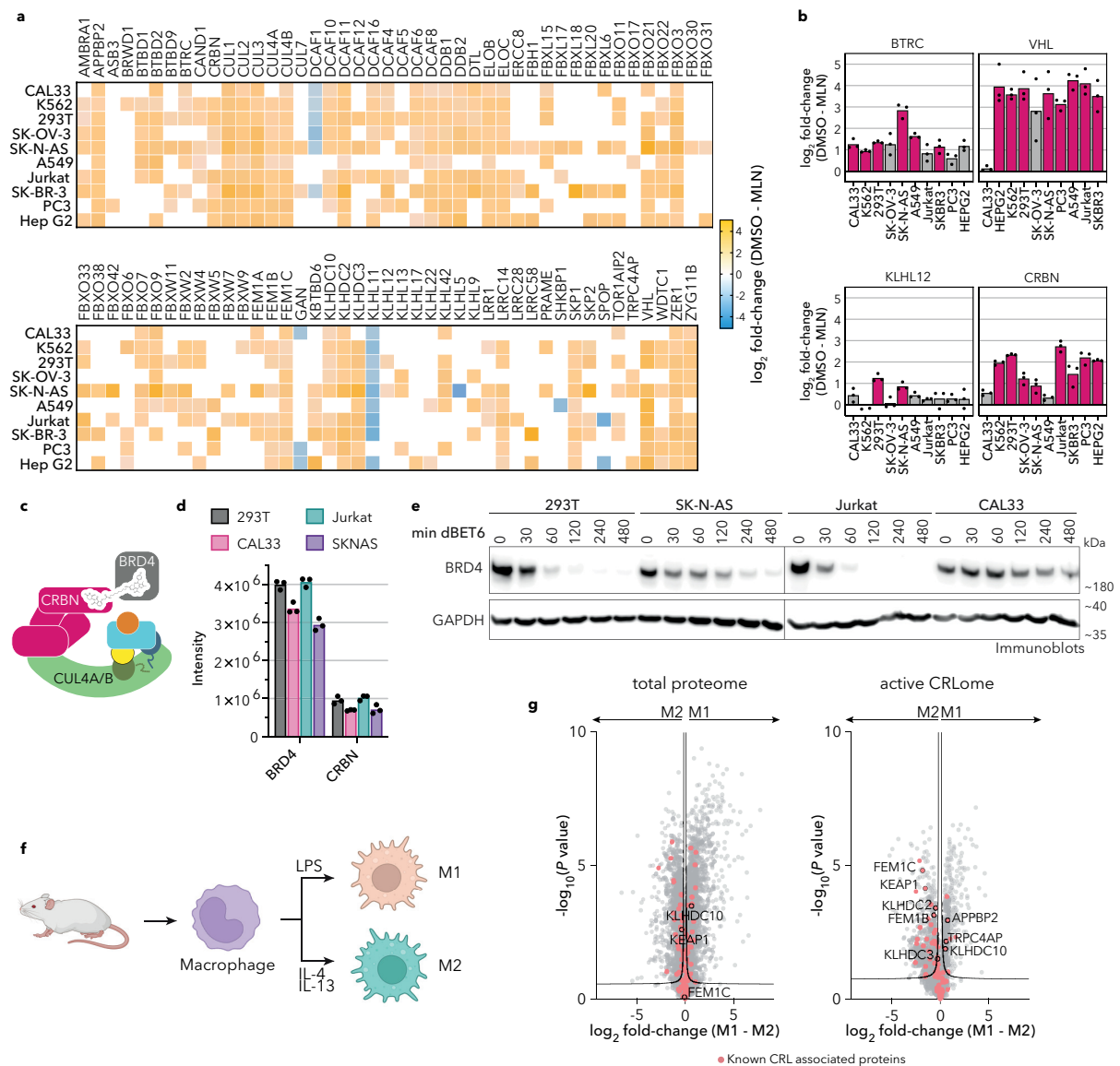
Figure 38 The baseline repertoire of neddylated CRLs primes the cellular response. a, Heatmap showing the results of N8C_Fab3b based CRL profiling performed in different cell lines. The $\log_2$ fold-change comparing a DMSO control to MLN4924 treated cells is shown. All listed SBMs are significantly enriched compared to control in at least one cell line (n = 3 biological independent samples, FDR controlled at 5% cutoff, two-sided t test, randomizations = 250, s0 = 0.1). SBMs not significantly enriched compared to control in a particular cell line are not colored. b, Bar graphs based on data shown in a show the differences in identified levels of selected CRL1, CRL2, CRL3, and CRL4 SBMs (BTRC, VHL, KLHL12 and CRBN, respectively) to highlight variations in the CRL repertoire of different cell lines. Data are shown as mean values. When the difference in N8C_Fab3b enrichment between DMSO and MLN4924 treatment is significant (5% FDR cutoff) bars are colored in pink. c, Cartoon representation of the neddylated CRL4^{CRBN} complex, in which the bivalent degrader dBET6 recruits a BRD4 as a neo-substrate. d, Protein group intensities from total proteomics experiments of 293T, CAL33, Jurkat and SKNAS as a readout of cellular protein levels (n = 3 biological independent samples, data are shown as mean values). e, Immunoblots of BRD4 and GAPDH (loading control) to monitor BRD4 degradation induced by treatment with 0.1 µM dBet6 for indicated durations. BRD4 degradation was monitored in 293T, SK-N-AS, Jurkat and CAL33 cells. Shown results are representative of two independent experiments. f, Schematic illustrating the production of mouse bone marrow-derived macrophages and using treatment with LPS or a combination of IL-4 and IL-13 to activate M1 and M2 states, respectively. Figure made with assets from biorender.com. g, Volcano plots showing differences between the total proteome (left, n = 4) and active CRLome (right, n = 4, as determined by N8C_Fab3b profiling) of M1 and M2 mouse macrophages. Known CRL components are colored red. SBMs known to be associated with the redox stress response and/or recognition of C-degrons are labeled with their names. Both volcano plots show the curve for 5% FDR (FDR controlled, two-sided t test, randomizations = 250, s0 = 0.1). Figure adapted from Henneberg, Duda, Singh et. al 2023.

The sequences of the cullin WHB domain and NEDD8 are conserved across mammalian species (Figure 39), suggesting that our active CRL profiling workflow could also be applied to cells derived from different source organisms. Indeed, performing IPs with N8C_Fab3b from mouse cells also enriched cullins, adapter proteins and SBMs in a neddylation dependent manner (meaning, enrichment was lost upon MLN4924 treatment) (Figure 40a). This made it possible to investigate the active CRL repertoire of cells derived from a primary source (Figure 40b). To make use of this opportunity, we examined how the active CRL repertoire differs between macrophages with anti-microbial (M1) or anti-helminth and tissue reparative (M2) activities, which can be studied using a robust ex vivo model of macrophage activation[285,286]. To that extend, macrophages were generated by differentiating bone marrow progenitor cells with CSF1. The resulting macrophages we then either left unstimulated (M0) or treated with LPS or IL-4 + IL-13 to produce the M1 and M2

Figure 39 The sequences of the CUL1 WHB domain and NEDD8 are conserved across mammals. a, Sequence alignment of the CUL1 WHB domain from various species (human, mouse, rat, rabbit, chimpanzee, macaque, and bovine). The degree of sequence conservation is highlighted by red bars. **b**, Sequence alignment of NEDD8 from the same organisms as in panel a. Figure adapted from Henneberg, Duda, Singh et. al 2023.

activation stages (Figure 38f, 40c), respectively. Analysis of the total proteome revealed that the levels of CRL components in M1 and M2 macrophages are generally comparable. N8C_Fab3b profiling on the other hand showed notable differences in the neddylated CRL repertoires of the two macrophage activation states (Figure 38g). It is noteworthy that six out of eight SBMs known to bind "C-degrons", a specific set of sequences at the C-termini of proteins[287,288], are amongst the 37 SBMs identified to differ between the M1 and M2 activation states. Prior studies suggest that C-degrons are produced during stress conditions that trigger mistranslation or proteolytic cleavage. Notably, KLHDC10 helps nascent chain clearing from stalled ribosomes, whereas APPBP2, FEM1C, KLHDC2, and KLHDC3 are linked to the degradation of selenoproteins which are prematurely truncated in selenium-limiting conditions[288,289]. Standing out amongst the identified SBMs are the redox sensing SBMs KEAP1[290,291] and FEM1B[138,292], which are maintained between M0 and M2 but show a relative decrease in active CRL occupancy for M1.

This observation aligns with the distinct metabolic profiles and roles of different macrophage states in inflammatory responses[285,286,293]. Our data suggests that the different stress pathways experienced by macrophages in the M1 and M2 activation states activate distinct CRLs.
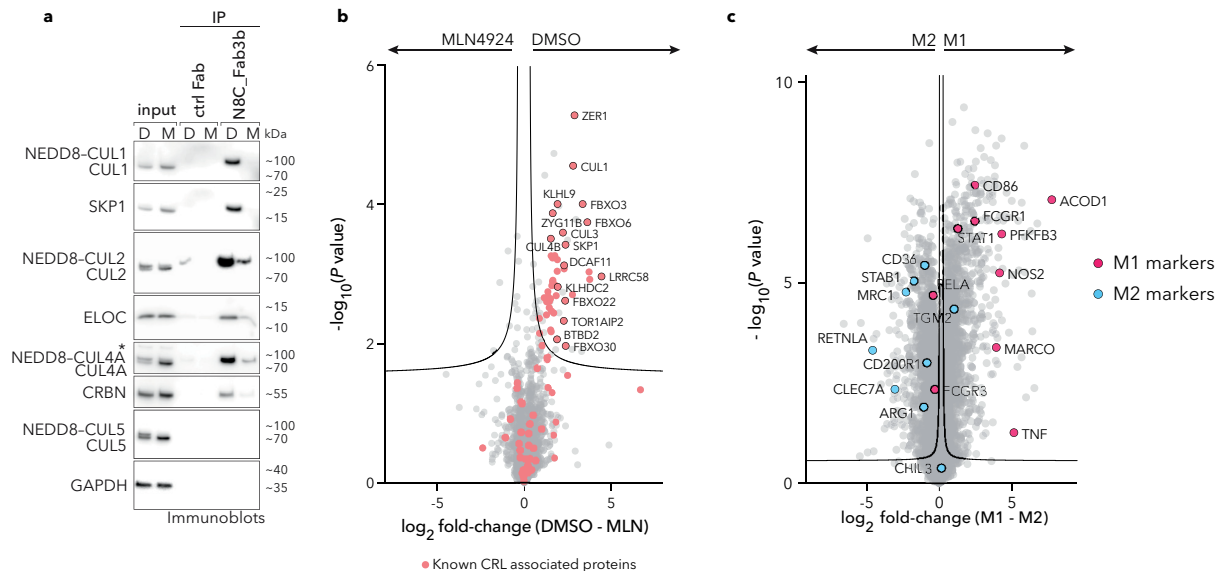
Figure 40 N8C_Fab3b based profiling in mouse cells. a, Immunoblots of IP experiments using N8C_Fab3b or a control Fab from 3T3 murine cells treated with DMSO (D) or MLN4924 (M) for 2 hours. Detected proteins include known CRL complex components and the GAPDH sample processing control. Slower migrating forms of cullins observed upon MLN4924 treatment are interpreted as NEDD8-modified, while faster-migrating forms are considered unneddylated. The presented results are representative of two independent experiments. b, Volcano plot of N8C_Fab3b IP-MS experiments performed with mouse bone marrow-derived macrophages after treatment with DMSO or MLN4924 (MLN) for 2 hours (n = 3 biological independent samples). Known components of CRLs and the ubiquitin-proteasome system are highlighted in red. Selected proteins of interest are labeled with their protein names, and the curve for 5% FDR is shown (FDR controlled, two-sided t-test, randomizations = 250, s0 = 0.1). c, Volcano plot of total proteome experiments from mouse bone marrow-derived macrophages activated to M1 or M2 states by treatment with LPS or a combination of IL-4 and IL-13, respectively (based on results shown for Figure 38, n = 4 biological independent samples). Known marker proteins of he M1 and M2 activation states are highlighted in pink and light blue, respectively. The curve for 5% FDR is shown (FDR controlled, two-sided t-test, randomizations = 250, s0 = 0.1). Figure adapted from Henneberg, Duda, Singh et. al 2023.

Discussion

In this work we investigate CRLs as dynamic systems that are able to adjust their composition to the current requirements of the cell. Cryo-EM and biochemical studies revealed the structural trajectory by which CAND1 enables the disassembly of one CRL and the reciprocal formation of a new one[184]. By investigating how different CAND1 β-hairpin mutants affect the TNF induced degradation of phosphorylated NFKBIA, a process dependent on the assembly of a CRL, we were able to validate the structural mechanism in cells (Figure 24). Profiling the landscape of CUL1-associated F-box proteins in cells expressing different CAND1 mutants further revealed the mechanism of CAND1 mediated assembly and disassembly regulates CRL complex formation at a systemwide level (Figure 25).

After investigating how CAND1 enables a CRL landscape with high plasticity, we next thought out to characterize the composition of active neddylated CRLs. To that extend we developed eight affinity reagents with the capacity to selectively bind neddylated cullins both in solution and immunoblots. Six of these were able to immunoprecipitated neddylated cullins and provided protection against CSN-mediated deneddylation for CUL1 and/or CUL2. Of the generated reagents, N8C_Fab3b was extensively characterized and emerged as a promising candidate, capable of recovering neddylated CUL1, CUL2, CUL3, and CUL4, along with their associated proteins in IPs (Figure 34).

Crucially, N8C_Fab3b does not function merely as a coincidental detector of NEDD8 and a cullin; instead, it selectively binds to the active conformation (Figure 32). So far, this active conformation had only been structurally visualized for CUL1-based complexes with UCEs[170,171], but the binding of N8C_Fab3b provides biochemical evidence that this active conformation is conserved for NEDD8-linked CUL1–CUL4. Remarkably, N8C_Fab3b leaves NEDD8's I44-patch exposed, allowing

it to bind ARIH1 during ubiquitylation (Figure 32d and Figure 31f). Unlike E2 enzymes, which disengage after performing ubiquitylation, ARIH1 retains high affinity for neddylated CRLs[265], copurifying with numerous CRLs in a neddylation-dependent manner and mediating their biological regulation[186,265]. This dual recognition capability of N8C_Fab3b, capturing both a ubiquitin-like protein and its target, aligns with the characteristics of downstream effectors[170,171,294-297], underscoring its unique utility in this context. While E2 enzymes detach upon completing their role in the ubiquitylation reaction, ARIH1 exhibits a sustained high affinity for neddylated cullins, playing a crucial role in the biological activity of multiple CRLs and co-purifying with them in a neddylation-dependent manner. Hence the ability to capture ARIH1-bound CRLs complexes might be crucial for exploring the landscapes of neddylated CRLs within cells. N8C_Fab3bs capacity in this regard is further demonstrated by our mechanistic data. This also highlights that an affinity reagent can be used to simultaneously recognize both a ubiquitin-like protein and its target, a distinctive feature commonly found in downstream effectors, all the while allowing such an effector to bind.

By conducting IPs with N8C_Fab3b in different settings, we unveiled essential features of the neddylated CRL network. For instance, the impact of inhibiting neddylation or deneddylation does not affect SBM association with cullins uniformly across the CRL system (Figure 34d). These data underscore the varied mechanisms governing the assembly, disassembly, activation, and deactivation of distinct CRLs. While the majority of SBMs detected in N8C_Fab3b IPs followed the expected pattern of decreasing upon MLN4924 treatment, a subset exhibited distinct behavior. However, some SBMs saw reduced association with neddylated cullins under both MLN4924 and CSN5i-3 treatments, while others demonstrated an increase with MLN4924 and a decrease with CSN5i-3. The former group likely includes SBMs subject to autoubiquitylation-dependent degradation, which would

be sensitive to MLN4924-induced elimination of neddylation and enhanced by CSN5i-3-induced increases in neddylation[183]. Meanwhile, the latter category underscores the varied regulation of CRL neddylation status, which for certain SBMs is further affected by interconversion between alternative assemblies[185,187].

Given that previous studies have demonstrated shifts in the repertoire of SBMs co-purifying with endogenously tagged CUL1 or CUL4 in response to various extracellular stimuli[162,163], we hypothesized that N8C_Fab3b IPs could serve as a tool to identify pathways activated by signals, obviating the need for endogenous tagging. It's worth noting that the expression of the Fab in cells may introduce unwanted complexities, as Fab-binding interferes with CSN-mediated deneddylation and substrate ubiquitylation by UBE2D-family E2s. Despite this, N8C_Fab3b demonstrated utility in affinity purification from lysates. While the steric bulk of the Fab might result in the preferential recognition of certain CRL complexes over others, our data demonstrate that N8C_Fab3b IPs can effectively pinpoint pathways responding to diverse signals without requiring endogenous tagging. This expands upon concepts established in studies focused on complexes with a single endogenously tagged cullin[162,163], showcasing that the extensive network of CRL1, CRL2, CRL3, and CRL4 complexes orchestrates precise rearrangements in response to small molecule degraders and signaling pathways.

Our robust and versatile proteomics pipeline, utilizing N8C_Fab3b, has the capability to identify SBMs and, in certain instances, their associated substrates in response to signals. Notably, in the case of the TNF treatment, our pipeline successfully identified the kinase responsible for generating the substrate phospho-degron necessary for SBM binding, along with components of the transcriptional complex regulated by the neddylated CRL (Figure 35). This underscores the ability of our workflow to shed light on entire signaling pathways. While the assembly of

neddylated CRL1[SKP2] with the cyclin–CDK2–CKSHS1 kinase, which phosphorylates its substrate p27, was previously recognized[126,171], our findings suggest that kinase–substrate–E3 ligase signaling complexes may be more prevalent than previously acknowledged.

An essential characteristic of our pipeline is its generic applicability to mammalian systems. We observed significant variation in the repertoires of over 70 SBMs across different cell lines (Figure 38a). Looking at targeted protein degradation strategies making use of a specific SBM (CRBN), we identified a general correspondence between its protein levels and degradation efficiency. However, the efficiency of targeted protein degradation exhibited a stronger correlation with CRBN's association with neddylated cullins than it did with CRBN protein levels. Furthermore, our approach allowed us to gain novel insights into a system originating from a mouse, that is not easily amenable to endogenous tagging. Our investigation unveiled variations in neddylated CRL repertoires across macrophage activation states. This effect was particularly notable in E3s associated with quality control, selenium, and redox stress responses, especially those recognizing C-degrons (Figure 38g). Therefore, our findings not only suggest that CRL networks dynamically rearrange to drive cellular signaling but also allow us to propose that CRL repertoires may adapt to address stresses arising from toxic effectors, crucial for macrophage activities such as microbial killing, efferocytosis, and tissue repair[285,286,293].

In conclusion, this research underscores the potential of employing binders that recognize specific biologically relevant conformations or an activating PTM in combination with its target. Such binders allow the selection of active complexes from broader pools of constituent molecules. We demonstrate the efficacy of conformation-specific affinity probes in capturing E3 complexes that lack residues

easily targeted by reactive chemical moieties. Our approach, which selectively targets a site-specific modification and conformation, provides new insights into dynamic E3 ligase systems and targeted protein degradation pathways.

Materials and Methods

Protein Production

All proteins are of human origin.

Cullin expression and purification

To produce the baits for Fab selection, soluble versions of the cullin C-terminal regions bound to RBX1 were expressed[166,265]. The following solubilizing mutations were introduced: solubilizing substitutions L421E, V451E, V452K and Y455K for the CUL1 C-terminal region including residues 411-776; solubilizing substitutions L390E, T420E, V421K and Y424K for the CUL2 C-terminal region including residues 380-776; solubilizing substitutions V417K and L418K for the CUL3 C-terminal region including residues 382-768; solubilizing substitutions L408K, I438D, L439D and F442Y for the CUL4A C-terminal region including residues 400-759; and with solubilizing substitutions L407E, L439K and V440K for the CUL5 C-terminal region including residues 411-780. To allow for the removal of RBX1 at a later stage while still permitting neddylation a Thrombin cleavage site was inserted in the CUL1 C-terminal region between K676 and N677. All cullin C-terminal regions were expressed as N-terminal GST-fusions co-expressed with MBP-TEV-RBX1 in *E. coli* BL21Gold (DE3) cells. For expression cells were grown to an OD600 of 0.8 and then induced with 0.6 µM isopropyl-β-D-thiogalactopyranoside (IPTG) for 17 h at 16 °C. Purification involved an initial glutathione affinity step with wash buffer (50 mM Tris pH 8, 200 mM NaCl, 5 mM DTT) and elution buffer (50 mM Tris pH 8, 200 mM NaCl, 5 mM DTT and 10 mM reduced glutathione). Fractions containing the target protein were pooled and cleaved by addition of TEV at a ratio of 1:100 w/w overnight at 4°C. Cullin C-terminal region-RBX1 complexes were then purified by cation exchange chromatography using 50 mM HEPES pH 7, 1 M NaCl and 1 mM DTT as the bump elution buffer.

To produce full-length cullin-RBX complexes, wild-type CUL1 CUL1, CUL2, CUL3, CUL4A, CUL5, GST–TEV–RBX1 (residues 5-C) and GST–TEV–RBX2 (residues 5-C) were cloned into pFastBac. Each cullin was co-expressed with its matching GST-RBX in High-Five (Hi5) insect cells by coinfection with separate baculoviruses produced in SF9 cells, CUL1, CUL2, CUL3, and CUL4A with GST-tagged RBX1 and. CUL5 with GST-tagged RBX2. A similar purification strategy as used for the cullin C-terminal regions was employed to produce pure full-length cullin-RBX complexes. Initial batch purification by glutathione affinity chromatography was followed by TEV-protease cleavage (unless indicated otherwise) and subsequently further purified by ion exchange and SEC.

Fab expression and purification

Both the heavy and light chains contained a periplasmic leader sequence derived from E. coli heat-stable enterotoxin II at their N-termini. Both chains were tagged C-terminally, the light chain with a FLAG and the heavy chain with a hexahistidine tag. Fabs were produced using bicistronic expression bicistronic expression using a pET vector. *E. coli* Rosetta (DE3) cells were grown in Terrific Broth to an OD600 of ~0.8 at which point they were induced with with 1 mM IPTG for 17 h at 18 °C. Cells were lysed by sonication in 50 mM HEPES pH 7.4 and 300 mM NaCl and Fabs purified using Ni_{2+}-affinity purification followed by ion exchange and pooled fractions buffer exchanged into 30 mM HEPES pH 7.4 and 150 mM NaCl by spin concentration. To produce biotinylated Fabs an AviTag-hexa-histidine tag with a GS-linker between the heavy chain and the tag was installed on the heavy chain C-terminus in lieu of the hexa-histidine tag. Site-specific biotinylation of the Avi-tag was carried out after the initial Ni_{2+}-affinity-purification step *in vitro* using BirA ligase. For this Fabs were diluted to ~80 µM by addition of bicine (pH 8.3) to 50 mM, ATP to 10 mM and Mg(OAc)2 to 10 mN. Recombinant BirA ligase was added at a molar ratio of 1:100 and biotin (Sigma-Aldrich B4501) at 1 mM and the reaction was incubated overnight

at 4 °C. The success of the biotinylation reaction was validated by testing binding of the biotinylated Fab to recombinant Streptavidin (ThermoFisher Scientific, 434301). Subsequently, Fabs were purified following the scheme described above.

The labeling of N8C_Fab3b with Alexa Fluor 647 was achieved using Alexa Fluor 647 NHS Ester (Succinimidyl Ester; Thermo Fisher Scientific, A20006), following the manufacturer's recommended protocols.

<u>Other proteins</u>

GST-Thrombin versions of Ubiquitin, NEDD8, NAE1, and UBE2F, as well as GST-TEV versions of UBE2D3, UBE2L3, and ARIH1 were expressed in BL21 Gold (DE3) *E. coli*[170,171,268]. His-MBP-TEV-BTRC[(175-C)] and GST-TEV-FBXW7[(263-C)] were produced in BL21 Gold (DE3) *E. coli* co-expression with SKP1[170]. GST-3C-IKZF1[ZF2]-Strep (residues 141–169, K157R,K165R, 140K) was expressed in BL21 Gold (DE3)[170]. UBE2M-His and GST-TEV-UBA1 were produced in Hi5 cells[170]. For preparation of CSN all subunits were co-expressed[180]. His-TEV–DDB1 and GST-TEV-CRBN were produced by co-expression in Hi5 cells[170]. The proteins were initially batch purified using either glutathione or Ni-NTA affinity resin. Subsequently, they underwent proteolytic cleavage with the specified protease. Following this step, further purification was carried out using ion exchange and size exclusion chromatography techniques[171,268].

Cullins (CUL1-4) were neddylated in reactions containing 16 µM cullin, 80 µM NEDD8, 4 µM UBE2M and 700 nM NAE1 in 30 mM Tris pH 7.6, 50 mM NaCl, 10 mM ATP, 10 mM $MgCl_2$. After 8 min at RT the reaction was quenched with 10 mM DTT. To neddylated CUL5 UBE2F was used instead of UBE2M. To fluorescently label ubiquitin (*Ub) the N-terminal RRASV sequence was replaced with RRACV and Fluorescein-5-Maleimide (Thermo Scientific, #62245) was used for labeling

following following manufacturer's instructions. To produce fluorescently labeled NEDD8 (^{Cy5}NEDD8) a Sortase-mediated reaction (50 μM NEDD8, 10 μM Sortase and 200 μM peptide in 50 mM Tris pH 7.5, 150 mM NaCl, 10 mM CaCl$_2$) was used to conjugate a Cy5 labeled peptide (Cy5-(PEG)$_5$-LPETGG) to NEDD8

Biochemical assays

CSN deneddylation assays

Reactions were performed in a buffer comprised of 50 mM Tris (pH 7.5), 50 mM NaCl, and 2.5 mM MgCl2. For robust detection of loss of neddylation CUL1 or CUL2 neddylated with Cy5-NEDD8 were used and preincubated for 10 min with 10x molar excess of Fab. To initiate the reactions, 10 nM CSN was added, and the reaction allowed to proceed at room temperature. Samples were taken at indicated time points by quenching with SDS sample buffer. After separation of the reactions products by SDS-PAGE, the fluorescence signal was detected using an Amersham Typhoon imager (Cytiva).

Substrate ubiquitylation assays

To avoid the effects of the UBA1-dependent formation of the E2~Ub intermediate experiments were performed in a pulse-chase format. To probe the ubiquitin transfer from UBE2D3 to NFKBIA mediated by CRL1^{BTRC}, thioester-linked UBE2D3~Ub was produced in a pulse reaction incubated for 10 min at room temperature. The reaction was done in a buffer buffer of 50 mM Tris pH 7.5, 50 mM NaCl, 2.5 mM MgCl2 and 1.5 mM ATP and contained 10 μM UBE2D3, 15 μM fluorescent ubiquitin and 0.2 μM UBA1. Reactions were quenched by addition of 25 mM EDTA and subsequently diluted in 25 mM MES pH 6.5 and 150 mM NaCl to a final concentration of 100 nM UBE2D3. CRL1 (NEDD8-CUL1-RBX1-SKP1-BTRC) and substrate (phosphorylated peptide derived from NFKBIA, KKERLLDDRHD(pS)GLD(pS)MKDEE)[170] were mixed in 25 mM MES pH 6.5 and 150

mM NaCl at 400 nM and 1µM respectively and incubated on ice. To investigate the impact of Fab binding on CRL reactivity, Fab was introduced into the chase mix at a designated molar excess compared to CRL. The quenched pulse reaction and chase mixes were combined at a 1:1 ratio, resulting in a final concentration of 200 nM neddylated CRL1[BTRC] and 50 nM UBE2D3~Ub. Samples were collected at specified time points, and the reaction was halted by adding 3× SDS–PAGE sample buffer. Separation of reaction products occurred through SDS–PAGE, and fluorescence signaling was detected using an Amersham Typhoon imager (Cytiva).

Similar reaction conditions were used for ARIH1/CRL1[FBXW7]-dependent ubiquitin transfer from UBE2L3 to CCNE. Concentrations for the pulse mix were kept identical, while 400 nM ARIH1 was added besides CRL to the chase mix (equimolar with the CRL, 200 nM final concentration) and 2 µM phosphorylated peptide derived from CCNE (KAMLSEQNRASPLPSGLL(pT)PPQ(pS)GRRASY)[265] was used as the substrate.

For reactions with CRL4[CRBN] similar conditions were used. Final reaction concentrations were 100 nM E2~Ub, 500 nM CRL4[CRBN] (and ARIH1 when indicated), 5 µM pomalidomide and 2.5 µM IKZF ZF2 as a substrate. Reactions were performed at room temperature.

NFKBIA substrate ubiquitylation assay in the presence of CSN
For these reactions only minor modifications were made to the parameters for ARIH1/CRLFBXW7 based reactions described above. The chase mix was incubated with indicated molar excess of N8C_Fab3b relative to CRL1. Then 200nM CSN (equimolar with CRL1) was added and the samples incubated for 5 min on ice. Pulse mix was added and the samples taken at indicated time points.

Selection of Fabs by phage display

Established protocols were used for phage selections. Plates (96-well MaxiSorp plates, Thermo Fisher Scientific, 12565135) were coated with purified NEDD8–CUL^{CTD}–RBX1 complexes at 5 µg ml^{-1} by incubating overnight at 4°C. Five rounds of selection were performed starting from the Fab library F to produce binders specific to neddylated cullins. To remove phage that bound nonspecifically, a negative-negative-positive selections strategy was used. To that extend phage were sequentially incubated on plates coated with NEDD8, uneddylated cullin and neddylated cullin. Clones specifically binding neddylated cullins were selected via clonal phage ELISA and identified by DNA sequencing.

Affinity maturation

Affinity-matured libraries were assembled by oligonucleotide-directed mutagenesis, employing the Kunkel mutagenesis method[298]. The CDR-L3 and CDR-H3 regions of the phagemid template were mutated using degenerate oligonucleotides that contained a 70% ratio of the wildtype nucleotide and a 10% ratio of the remaining three nucleotides, following a soft randomization strategy. The diversity of the library was 1.5 x 10^9, with an incorporated diversity of 64% in the CDR-L3 region and 74% in the CDR-H3 region.

ELISAs

Both Page and protein ELISAs were conducted using immobilized proteins. Proteins, at a concentration of 2 µg ml-1, were coated on 384-well MaxiSorp plates (Thermo Fisher Scientific, 12665347) overnight at 4°C. Phage bound to protein were identified using the anti-M13-HRP antibody (1:5,000; GE Healthcare, 27-9421-01) and anti-Kappa-HRP (1:5,000; Southern Biotech, 2060-05). The binding affinities of the purified Fab proteins were determined as EC50 values, which represent the concentration of Fab at which 50% of binding was observed by ELISA. These EC50

values were computed using the GraphPad Prism software, applying a nonlinear regression model algorithm.

Cell culture

Trichoplusnia ni High-Five and Sf9 insect cells were cultured in Ex-cell 420 medium. *E. coli* bacterial cells (BL21 Gold (DE3) and Rosetta (DE3)) were cultured in LB or TB medium.

All mammalian cells were cultured in media containing 10% fetal bovine serum (Gibco, A3160802), 4 mM GlutaMAX (Gibco, 35050038), 1 mM sodium pyruvate (Gibco, 11360070; 100 units per ml penicillin) and 100 µg ml^{-1} streptomycin (Gibco, 15140122) at 37 °C and 5% carbon dioxide. Specific media were used for different cell types: Dulbecco's Modified Eagle Medium (DMEM; Gibco, 11960044) for CAL33, 293T, SK-N-AS, A549, and Hep G2 cells; Iscove's Modified Dulbecco's Medium (Gibco, 12440053) for K562s; RPMI 1640 (Gibco, 72400021) for Jurkat cells; McCoy's 5A (modified) Medium (Gibco, 26600023) for SK-OV-3 cells; and Ham's F-12 Nutrient Mixture (Gibco, 21127022) for PC3 cells. All cells were routinely tested for mycoplasma using MycoAlert (Lonza, LT07-318) kits.

Generation of stable cell lines

The Flp-In™ T-REx™ 293 3xFLAG-Cul1 WT and CAND null cells (CAND1 and CAND2 knockout) used to make stable cell lines were generously provided by Xing Liu[160,163]. To generate lentivirus for both WT and mutant CAND1 constructs, co-transfection of the packaging (psPAX2) and enveloping (pMD.2G) plasmids into HEK293T cells was performed using Lipofectamine 3000 (Invitrogen, L3000015). After 72 h, supernatants containing viral particles were harvested and the relative viral titer determined using Lenti-X GoStix (Takara, 631280). The Flp-In™ T-REx™ 293 3xFLAG-CUL1 CAND null cells were infected with 5 µl of the normalized virus

and, after 48 h, transferred to T75 flasks with media containing 100 µg/ml hygromycin B (GIBCO, 10687010). Cells were selected for 10 days, after which hygromycin B-resistant colonies were isolated and screened for the expression of WT or mutant CAND1 through immunoblotting. Cells demonstrating CAND1 expression levels approaching that of endogenous CAND1 were selected for further experiments.

IκBα (NFKBIA) degradation assay

The experimental procedure closely followed previously described methodologies[160]. In brief, ~0.7 million cells were plated in 6-well dishes and allowed to grow overnight. Subsequently, the media was replaced with FBS-free DMEM for a 3-hour period. The cells were then exposed to 100 µg/ml cycloheximide (Sigma-Aldrich, 239765) for 10 minutes before the addition of 25 ng/ml of TNF. At specified intervals post-TNF treatment, cells underwent PBS washes and lysis in 3x SDS sample buffer, followed by boiling for 5 minutes at 98°C and brief sonication. The samples were subjected to SDS-PAGE and later analyzed through immunoblotting. For plotting the relative phospho-IκBα levels, phospho-IκBα band intensities were quantified in Fiji and normalized to the Vinculin loading control. The maximal normalized phospho-IκBα band intensity per replicate was set as 1, and the minimal normalized phospho-IκBα band intensity as 0, to derive relative phospho-IκBα levels. The data are depicted as mean±SEM of three biological replicates (n=3).

Immunoblots

Immunoblots were carried out using peroxidase-conjugated secondary antibodies in conjunction with the SuperSignal West Pico PLUS Chemiluminescent Substrate (Thermo Fisher Scientific, 34580). Images of the blots were taken using an Amersham ImageQuant 800 (Cytiva). The secondary antibodies used for detection

included goat anti-rabbit-HRP (1:5,000; Thermo Fisher Scientific, 31460), donkey anti-mouse-HRP (1:5,000; Jackson ImmunoResearch, 715-035-150), and Streptavidin-HRP (1:5,000; Cell Signaling Technology, 3999).

Primary antibodies used in the study were anti-CUL1 (1:1,000; Santa Cruz Biotechnology, sc–17775), anti-CUL2 (1:1,000; Abcam, ab166917), anti-CUL3 (1:1,000; Bethyl Laboratories, A301-109A), anti-CUL4A (1:1,000; Bethyl Laboratories, A300-739A), anti-CUL5 (1:1,000; Abcam, ab184177), anti-SKP1 (1:1,000; Cell Signaling Technology, 2156), anti-BTRC (1:1,000; Cell Signaling Technology, 4394), anti-ELOC (1:1,000; Biolegend, 613101), anti-DDB1 (1:1,000; Abcam, ab109027), anti-CRBN (1:1,000; Sigma, HPA045910), anti-BRD4 (1:1,000; Cell Signaling Technology, 13440), and anti-GAPDH (1:5,000; Cell Signaling Technology, 2118).

To test the N8C_Fabs ability to detect neddylated cullins specifically in a western blot format, neddylated or unneddylated CUL1-5 (200 ng) were probed using 2 µg/ml biotinylated Fabs as the primary binder and Strepavidin-HRP as a secondary binder. All immunoblots used PVDF membranes, and for blocking and incubation with the secondary antibodies (except Strepavidin-HRP) 5% nonfat dry milk in TBST (20 mM Tris pH 7.4, 150 mM NaCl, 0.1% Tween-20) was used. Incubation with primary antibodies and Strepavidin-HRP was performed in 5% bovine serum albumin in TBST. The brightness and contrast of raw images were adjusted in Fiji.

N8C_Fab Affinity-purification experiments

During collection cells were subjected to an "N8-block" treatment (3 min treatment with 1 µM MLN4924 (MedChemExpress, HY-70062) and 1 µM CSN5i-3 (MedChemExpress, HY-112134) in media) to conserve their active CRL repertoire for IP[162]. Following this, cells were washed in PBS (Gibco, 14190094) and lysed in lysis buffer (25 mM HEPES pH 7.4, 100 mM NaCl, 0.5% IGEPAL CA-630, 5% glycerol, 1× protease inhibitor (Sigma-Aldrich, 11836145001), 1 µM MLN4924 and 1 µM

CSN5i-3). The lysates were homogenized by brief sonication (10 seconds, 1 second on/off, 10% amplitude, Bandelin Sonopuls HD 4200, TS 103) and then cleared by centrifugation at 20,000g for 3 minutes at 4 °C. High Capacity Magne Streptavidin Beads (Promega, V7820) were coated with the indicated biotinylated Fabs according to the manufacturer's instructions. An equivalent of 6 µl of bead slurry of the Fab-coated beads was added to the cleared cell lysates and incubated for 45 minutes at 4 °C while rotating. After the incubation, the beads were washed twice with the lysis buffer, twice with a wash buffer (the lysis buffer without IGEPAL CA-630), and twice with HBS (25 mM HEPES pH 7.4 and 150 mM NaCl). After the final wash, all buffer was removed and the beads were resuspended in a reducing sample buffer for analysis by immunoblotting.

Flow cytometry

After this, the cells were washed twice with PBS and then fixed with paraformaldehyde (Thermo Fisher Scientific, 28908) for 10 minutes at room temperature. This was followed by cell permeabilization using ice-cold methanol at -20 °C for 1 hour, and two subsequent washes with PBS–BSA (PBS containing 0.5% BSA and 0.1% sodium azide). Cells were then incubated with 0.002 mg ml^{-1} N8C_Fab3b-Alexa Fluor 647 in PBS–BSA for 1 hour at room temperature while shaking. After this, the samples were washed twice with PBS–BSA and analyzed on an Attune NxT (Thermo Fisher Scientific) flow cytometer, collecting a total of 10,000 events. FlowJo (BD Bioscience) was used to extract mean fluorescent intensities (MFIs) and the values were normalized to the minimal and maximal MFI as averaged across replicates. The samples were then plotted in Prism 9 (GraphPad), and the dose–response curve was generated using the 'sigmoidal dose–response' analysis function.

Bio-Layer Interferometry measurements

An Octet K2 system (ForteBio) was used for Bio-Layer Interferometry measurements. The temperature was set to 30°C with shaking at 1,000 rpm. Proteins were first diluted into the BLI reaction buffer, which consisted of 25 mM HEPES (pH 7.5), 150 mM NaCl, 0.1 mg/ml BSA, and 0.01% Tween-20. Anti-GST biosensors (Sartorius, 18-5097) were utilized for all measurements. The ligand, GST RBX1–CUL1–NEDD8, was immobilized on the biosensors, while His-tagged N8C_Fab3b was used as the analyte. Six dilutions of N8C_Fab3b, varying from 200 to 6.25 nM, were used for the measurement. The raw data was processed using the Octet Data Analysis HT software (Release 11.1). A 1:1 binding model was assumed for analysis of both association and dissociation and a global (group) fitting with linked R_{max} values was performed. The reported dissociation constant (K_D), association rate (k_a) and dissociation rate (k_{dis}) are shown as calculated by the software. The processed data and fitted curves were visualized using Prism (version 9).

Complex formation and purification for crystallization

*Crystallization experiments were performed by David Duda

To produce the neddylated CUL1 WHB domain used for crystallization 16 µM CUL1^{CTD} (Thrombin 676/677)–RBX1 was neddylated as described above. After quenching with 10mM DTT, 500 µg ml^{-1} of Thrombin and 2.5 mM CaCl$_2$ were added and the mixture incubated for 1h at 16°C. The remaining CUL1^{CTD} was separated from N8-CUL1^{WHB} by two rounds of SEC using a Superdex 200 column with 25 mM Tris pH 7.6 and 200 mM NaCl as the buffer. For complex formation equimolar concentrations of N8C_Fab3b and N8-CUL1^{WHB} were mixed and incubated on ice for 15 min. The complex was then purified by SEC into a final buffer of 25 mM Tris pH 7.6 and 200 mM NaCl using a Superdex 200 column.

Crystallization

*Crystallization experiments were performed by David Duda

Crystals of N8C_Fab3b-bound NEDD8–CUL1^{WHB} were obtained by hanging drop vapor diffusion at room temperature. N8C_Fab3b–NEDD8–CUL1^{WHB} at 12.5 mg ml^{-1} was mixed in a 1:1 ratio with well buffer (2.1 M AmSO$_4$, 100 mM citrate pH 6, 10 mM tris(2-carboxyethyl)phosphine (TCEP)).

Crystallographic data collection and structure determination

Diffraction data were collected at the NE-CAT beamline (24-ID-E) of the Advanced Photon Source (APS). The crystallographic dataset was integrated and scaled using XDS (version: 3 November 2014)[299]. Phases were solved by molecular replacement with Phaser (v.2.5.6)[300] using the structure of the Fab isolated from HER2 bound to Herceptin (Protein Data Bank (PDB): 1N8Z) as the search model. Each asymmetric unit contained two molecules of Fab-bound NEDD8-CUL1WHB, with crystals forming in the P2$_1$2$_1$2$_1$ spacegroup with unit cell edges $a = 101.9$ Å, $b = 107.2$ Å and $c = 185.1$ Å. Crystallographic refinement and rebuilding were performed for multiple rounds using COOT (v.0.8)[301] and Phenix (v.1.9-1692)[302]. Structural quality measurements and diffractions as well as refinement statistics are listed in Table 1. Structures were analyzed and visualized using UCSF ChimeraX (v.1.2.5)[303].

Affinity-purification mass spectrometry

For enrichments with N8C_Fabs Around 75 µL of compacted cells were lysed in 400 µl lysis buffer to be used for AP-MS experiments. The IP procedure was performed similarly as described under "IP experiments". For AP-MS experiments lysates were further cleared by an adding a filtration step using 0.22 µm spin filters (Corning, 8161). After the final wash, the beads were resuspended in 45 µl denaturing lysis buffer (100 mM Tris pH 8.5 and 1% SDC) and heated to 98 °C for 5 minutes. TCEP

and 2-Chloroacetamide were added to final concentrations of 10 mM and 40 mM, respectively, and samples were incubated at 45 °C for 5 minutes. Samples were digested by adding Trypsin (Sigma-Aldrich, T6567) and LysC (FUJIFILM Wako, 125-05061) at 1:100 w/w and incubating overnight at 37 °C while shaking (1,200 rpm). Clean-up of digested samples was done using SDB-RPS StageTips[304]. For this, samples were first diluted 5× in loading buffer (1% trifluoroacetic acid (TFA) in isopropanol) and then loaded onto the StageTips. After a single wash with the loading buffer and two washes with 200 µl of StageTips wash buffer (0.2% TFA/2% acetonitrile), the samples were eluted with 60 µl 1.25% ammonium hydroxide in 80% ACN. The eluted samples were dried in a SpeedVac centrifuge and dried samples reconstituted in buffer A* (0.2% TFA and 2% ACN), standardizing to a peptide concentration of 0.1 mg ml^{-1} based on absorbance at 280 nm.

Total proteome analysis

For total proteome analysis, cells underwent four washes with PBS prior to the addition of a denaturing lysis buffer. The lysates were then heated at 98°C for 5 minutes and sonicated briefly (3 seconds, 20% amplitude) to ensure complete lysis. The clarified lysates, obtained by centrifugation, were then subjected to the same digestion and clean-up procedures as described in "AP-MS".

LC–MS/MS measurements

Peptides were separated by loading onto a reverse-phase column (50 cm length, 75 µm inner diameter, packed in-house with ReproSil-Pur C18-AQ 1.9 µm resin (Dr. Maisch HPLC GmbH)). A custom-made column oven was used to maintain the column temperature at 50°C. An EASY-nLC 1200 system directly connected to the mass spectrometer (Orbitrap Exploris 480, Thermo Fisher Scientific) via a nano-electrospray source was used for nano-flow liquid chromatography. Each measurement involved loading 200 ng of peptides and separating them using a

binary buffer system comprised of buffer A (0.1% formic acid (FA)) and buffer B (0.1% FA, 80% ACN) at 300 nl min^{-1}. For separation of IP samples, a 60-min gradient at starting at 5% buffer B, followed by a stepwise increase to 30% in 45 min, 65% in 8 min and 95% in 2 min, staying at 95% for 5 min. Total proteome samples underwent separation using a 120-min gradient, starting at 5% buffer B, followed by a stepwise increase to 30% in 90 min, 65% in 16 min, and 95% in 4 min, staying at 95% for 10 min. MS data were acquired in DIA mode, comprising one MS1 full scan followed by 32 MS2 windows. MS1 full scans (300–1,650 m/z range) were obtained at a resolution of 120,000 at 200 m/z, with the automatic gain control (AGC) target set to 3×10^6 at a maximum injection time of 20 ms (60 min gradient) or 60 ms (120 min gradient). Each MS2 scan was collected at a resolution of 30,000 at m/z 200, with AGC adjusted to 10×10^6, maximum injection time set to 54 ms, and the normalized HCD collision energy at 28% (60 min gradient) or 27% (120 min gradient). The default charge state was 2, and RF lens was set to 40%. All spectra were recorded in profile mode.

MS data analysis

DIA raw files underwent processing using Spectronaut[305] (version 15, Figures 34b , 36a and 38a,b; version 16, Figures 34c,d, 35b,d,f,h, 36b–f, 38d–g and 40b,c) with default settings for directDIA. Data were further analyzed using the Perseus software package (v.1.6.7.0). After log$_2$ transformation of protein group intensities, datasets were filtered to retain a minimum of 50% valid values in at least one experimental condition. A normal distribution with a width of 0.3 and a downshift of 1.8 was used to impute missing values.

For CUL1-repertiore profiling experiments the protein group intensities for CUL1, SKP1, CAND1 and F-box proteins were extracted and filtered for an average coefficient of variation within experimental conditions of less than 15%. After

normalizing the protein group intensities for FLAG-immunopurifications to the CUL1 levels the $\log_2$-fold-changes were calculated and plotted in GraphPad Prism. To plot the percentage of CUL1-associated compared to free F-box proteins the CUL1 normalized protein group intensities were corrected based on their total eluate volume as compared to the FLAG-immunopurifications. The total F-box level was calculated by summing the corrected GST-pulldown and FLAG-immunopurification protein group intensities. The protein group intensities of FLAG-immunopurifications were taken as the level of CUL1 bound F-box proteins.

For N8C_Fab experiments, intensities for CUL1–CUL4, their adapter proteins, known substrate-binding motifs (SBMs), and other proteins associated with CRLs (Supplementary Data) were extracted and, when specified, filtered for an average coefficient of variation within experimental conditions of 15%. Singular values of the log2 fold change were calculated by subtracting the average of the log2-transformed protein group intensities of the replicates of one experimental condition from the other. For Figure 38b, $\log_2$(fold changes) were determined by subtracting the $\log_2$-transformed protein group intensities of individual replicates between experimental conditions. Replicates of DMSO- and MLN4924-treated cells were paired based on the order they were measured in. Volcano plots were generated using the function included in Perseus, which was also utilized to produce curves highlighting a 5% false discovery rate (FDR; s0 = 0.1). In the cell line panel, raw files were processed collectively, and SBMs exhibited significant enrichment (t test, FDR = 5%, s0 = 0.1) between the DMSO- and MLN4924-treated samples in at least one cell line extracted.

CRL repertoire

For Figure 34b, AP-MS experiments were performed as described in "AP-MS" with indicated N8C_Fabs as compared to a control Fab with wildtype CDRs. For Figure 34d, 293T cells underwent a 2-hour treatment with a DMSO control, 1 µM MLN4924, or 1 µM CSN5i-3, before being subjected to the standard AP-MS workflow. For Figure 34c, the Perseus principal component analysis function was used, incorporating the $\log_2$-transformed protein group intensities of all experiment-identified protein groups. Each dot on the plot represents an individual biological replicate.

Profiling CRL repertoire changes

With CRL complex stability strongly depending on the presence of substrate, we aimed to prevent substrate degradation and complex dissociation within cells. Accordingly, cells were treated with 10 µM of the proteasome inhibitor MG132 (MedChemExpress, HY-13259) and 10 µM of the VCP inhibitor CB-5083 (MedChemExpress, HY-12861) for 5 min before the initiation of the treatment with the stimulus of interest. To validate our workflow, we employed treatment with the molecular glue Indisulam, previously reported to reshape the CRL4 network[162]. To that extend, 293T cells were treated with 2 µM Indisulam (MedChemExpress, HY-13650) for 1 h, followed by collection and preparation for AP–MS experiments as described above. To assess whether the reshaping of the CRL network extends to other degraders and CRLs utilizing different cullin backbones, we further examined the bivalent degrader MZ1, that recruits a CRL2 complex, by treating 293T cells with 1 µM MZ1 (MedChemExpress, HY-107425) for 1 h. Beyond degraders, numerous cellular pathways rely on CRL activity, such as iron homeostasis[282]. To explore whether metabolic pathways also reshape the cellular CRL network, cells were supplied with an excess of iron through treatment with 100 µM ferric ammonium citrate (Sigma-Aldrich, F5879) for 90 min. Another stimulus known to depend on

CRL activity is cytokine signaling. K562 cells were subjected to our AP–MS workflow after 3-hour serum starvation, followed by treatment with 25 ng ml−1 human TNF (PeproTech, 300-01A) for 5 min. *P* values for direct comparisons of substrate-binding motifs (SBMs) were calculated in GraphPad Prism (v.9) using the t-test function (unpaired, two-tailed, 95% confidence level).

CRBN degradation efficiencies

To determine how different levels of Cereblon associated with active CRLs affects the degradation efficiency indicated cells lines were plated in six-well plates and treated for indicated durations with 0.1 µM dBET6 (MedChemExpress, HY-112588). Cells were lysed in reducing sample buffer. The levels of BRD4 were determined by immunoblotting and GAPDH was used as a loading control.

Bone marrow-derived macrophages

Male wild-type C57BL/6N mice were housed in pathogen-free conditions at the Max Planck Institute of Biochemistry's animal facility. The use of the mice for organ isolation was approved by the Government of Upper Bavaria. Mice resided in open cages at 22 °C and 55% humidity, following a 14-hour light cycle/10-hour dark cycle. For collection of mouse bone marrow, the femurs and tibiae of 8- to 10-week-old mice were flushed with PBS. Differentiation into BMDMs was done by culturing in DMEM with 50 ng ml^{-1} human recombinant CSF1 (produced in-house) for 7 days[306]. BMDMs seeded overnight in media containing 100 ng ml−1 CSF1 were activated by 24 h stimulation with 10 ng ml^{-1} LPS from E. coli O55:B5 (Sigma-Aldrich, L2880) or a combination of 10 ng ml^{-1} mouse recombinant IL-4 (produced in-house) and 10 ng ml^{-1} IL-13 (PeproTech, 210-13). For Figure 40b, BMDMs were treated with 1 µM MLN4924 for 2 h before processing for active CRL profiling, as described above. BMDMs in their nonactivated and activated states were collected and

processed for total proteome (Figure 38g, left, and Figure 40b) or active CRL repertoire analysis (Figure 38g, right), as previously detailed.

Permissions

In alignment with my rights as an author material from the following publications in Elsevier journals (https://www.elsevier.com/about/policies-and-standards/copyright#1-author-rights) have been used in this thesis:

1) Systemwide disassembly and assembly of SCF ubiquitin ligase complexes, Baek K, Scott DC, **Henneberg LT**, King MT, Mann M, Schulman BA., Cell. 2023 Apr 27;186(9):1895-1911.e21. doi: 10.1016/j.cell.2023.02.035. Epub 2023 Apr 6.
   *Thesis contains work from this published paper.

2) Decoding the messaging of the ubiquitin system using chemical and protein probes, **Henneberg LT**, Schulman BA., Cell Chem Biol. 2021 Jul 15;28(7):889-902. doi: 10.1016/j.chembiol.2021.03.009. Epub 2021 Apr 7.

In alignment with my rights as an author material from the following publication in a Springer Nature journal (https://www.nature.com/nature-portfolio/reprints-and-permissions/permissions-requests) has been used in this thesis:

1) Activity-based profiling of cullin-RING ligase networks by conformation-specific probes, **Henneberg LT**, Singh J, Duda DM, Baek K, Yanishevski D, Murray PJ, Mann M, Sidhu SS, Schulman B., bioRxiv. 2023 Jan 17:2023.01.14.524048. doi: 10.1101/2023.01.14.524048. Preprint.
   *Thesis contains work from this published paper.

References

1   Balazsi, G., van Oudenaarden, A. & Collins, J. J. Cellular decision making and biological noise: from microbes to mammals. *Cell* **144**, 910-925 (2011). https://doi.org:10.1016/j.cell.2011.01.030

2   Bludau, I. & Aebersold, R. Proteomic and interactomic insights into the molecular basis of cell functional diversity. *Nat Rev Mol Cell Bio* **21**, 327-340 (2020). https://doi.org:10.1038/s41580-020-0231-2

3   Beadle, G. W. & Tatum, E. L. Genetic control of biochemical reactions in neurospora. *Proc. Natl Acad. Sci. USA* **27** (1941).

4   Collins, F. S., Lander, E. S., Rogers, J. & Waterson, R. H. Finishing the euchromatic sequence of the human genome. *Nature* **431** (2004).

5   Carter, H., Hofree, M. & Ideker, T. Genotype to phenotype via network analysis. *Curr. Opin. Genet. Dev.* **23** (2013).

6   Rauscher, B., Valentini, E., Hardeland, U. & Boutros, M. Phenotype databases for genetic screens in human cells. *J. Biotechnol.* **261** (2017).

7   Amberger, J., Bocchini, C. & Hamosh, A. A new face and new challenges for Online Mendelian Inheritance in Man (OMIM®). *Hum. Mutat.* **32** (2011).

8   Arkin, A. P. & Schaffer, D. V. Network news: innovations in 21st century systems biology. *Cell* **144** (2011).

9   Thompson, D., Regev, A. & Roy, S. Comparative analysis of gene regulatory networks: from network reconstruction to evolution. *Annu. Rev. Cell Dev. Biol.* **31** (2015).

10   Bernadskaya, Y. & Christiaen, L. Transcriptional control of developmental cell behaviors. *Annu. Rev. Cell Dev. Biol.* **32** (2016).

11   Kilchert, C., Wittmann, S. & Vasiljeva, L. The regulation and functions of the nuclear RNA exosome complex. *Nat. Rev. Mol. Cell Biol.* **17** (2016).

12   Magnuson, B., Bedi, K. & Ljungman, M. Genome stability versus transcript diversity. *DNA Repair* **44** (2016).

13   Schneider, C., Kudla, G., Wlotzka, W., Tuck, A. & Tollervey, D. Transcriptome-wide analysis of exosome targets. *Mol. Cell* **48** (2012).

14   Popp, M. W. & Maquat, L. E. Nonsense-mediated mRNA decay and cancer. *Curr. Opin. Genet. Dev.* **48** (2018).

15   Wong, J. J. L. Orchestrated intron retention regulates normal granulocyte differentiation. *Cell* **154** (2013).

16   Kurosaki, T., Popp, M. W. & Maquat, L. E. Quality and quantity control of gene expression by nonsense-mediated mRNA decay. *Nat. Rev. Mol. Cell Biol.* **20** (2019).

17   Machnicka, M. A. MODOMICS: a database of RNA modification pathways – 2013 update. *Nucleic Acids Res.* **41** (2012).

18   Zhao, B. S., Roundtree, I. A. & He, C. Post-transcriptional gene regulation by mRNA modifications. *Nat. Rev. Mol. Cell Biol.* **18** (2017).

19   Ranjan, N. & Leidel, S. A. The epitranscriptome in translation regulation: mRNA and tRNA modifications as the two sides of the same coin? *FEBS Lett.* **593** (2019).

20   Zaccara, S., Ries, R. J. & Jaffrey, S. R. Reading, writing and erasing mRNA methylation. *Nat. Rev. Mol. Cell Biol.* **20** (2019).

21   Roundtree, I. A., Evans, M. E., Pan, T. & He, C. Dynamic RNA modifications in gene expression regulation. *Cell* **169** (2017).

22   Bentley, D. L. Coupling mRNA processing with transcription in time and space. *Nat. Rev. Genet.* **15** (2014).

23   Klerk, E. & 't Hoen, P. A. C. Alternative mRNA transcription, processing, and translation: insights from RNA sequencing. *Trends Genet.* **31** (2015).

24   Garieri, M. The effect of genetic variation on promoter usage and enhancer activity. *Nat. Commun.* **8** (2017).

25 Reyes, A. & Huber, W. Alternative start and termination sites of transcription drive most transcript isoform differences across human tissues. *Nucleic Acids Res.* **46** (2018).

26 Proudfoot, N. J., Furger, A. & Dye, M. J. Integrating mRNA processing with transcription. *Cell* **108** (2002).

27 Wang, E. T. Alternative isoform regulation in human tissue transcriptomes. *Nature* **456** (2008).

28 Pan, Q., Shai, O., Lee, L. J., Frey, B. J. & Blencowe, B. J. Deep surveying of alternative splicing complexity in the human transcriptome by high-throughput sequencing. *Nat. Genet.* **40** (2008).

29 Tress, M. L. The implications of alternative splicing in the ENCODE protein complement. *Proc. Natl Acad. Sci. USA* **104** (2007).

30 Shi, Y. Mechanistic insights into precursor messenger RNA splicing by the spliceosome. *Nat. Rev. Mol. Cell Biol.* **18** (2017).

31 Tress, M. L., Abascal, F. & Valencia, A. Alternative splicing may not be the key to proteome complexity. *Trends Biochem. Sci.* **42** (2017).

32 Wan, Y. & Larson, D. R. Splicing heterogeneity: separating signal from noise. *Genome Biol.* **19** (2018).

33 Liu, Y., Beyer, A. & Aebersold, R. On the dependency of cellular protein levels on mRNA abundance. *Cell* **165** (2016).

34 Dikic, I. Proteasomal and autophagic degradation systems. *Annu. Rev. Biochem.* **86** (2017).

35 Varshavsky, A. N-degron and C-degron pathways of protein degradation. *Proc. Natl Acad. Sci. USA* **116** (2019).

36 Harper, J. W. & Bennett, E. J. Proteome complexity and the forces that drive proteome imbalance. *Nature* **537** (2016).

37 Zhang, B. Proteogenomic characterization of human colon and rectal cancer. *Nature* **513** (2014).

38   Liu, Y. Multi-omic measurements of heterogeneity in HeLa cells across laboratories. *Nat. Biotechnol.* (2019). https://doi.org:10.1038/s41587-019-0037-y

39   Malmström, J. Proteome-wide cellular protein concentrations of the human pathogen Leptospira interrogans. *Nature* **460** (2009).

40   Milo, R. What is the total number of protein molecules per cell volume? A call to rethink some published values. *BioEssays* **35** (2013).

41   Brar, G. A. Beyond the triplet code: context cues transform translation. *Cell* **167** (2016).

42   Kearse, M. G. & Wilusz, J. E. Non-AUG translation: a new start for protein synthesis in eukaryotes. *Genes Dev.* **31** (2017).

43   Loftfield, R. B. & Vanderjagt, D. The frequency of errors in protein biosynthesis. *Biochem. J.* **128** (1972).

44   Walsh, C. T., Garneau-Tsodikova, S. & Gatto, G. J. Protein posttranslational modifications: the chemistry of proteome diversifications. *Angew. Chem. Int. Ed.* **44** (2005).

45   Wolan, D. W., Zorn, J. A., Gray, D. C. & Wells, J. A. Small-molecule activators of a proenzyme. *Science* **326** (2009).

46   Shalini, S., Dorstyn, L., Dawar, S. & Kumar, S. Old, new and emerging functions of caspases. *Cell Death Differ.* **22** (2015).

47   Puente, X. S., Sánchez, L. M., Overall, C. M. & López-Otín, C. Human and mouse proteases: a comparative genomic approach. *Nat. Rev. Genet.* **4** (2003).

48   Blume-Jensen, P. & Hunter, T. Oncogenic kinase signalling. *Nature* **411** (2001).

49   Aebersold, R. How many human proteoforms are there? *Nat. Chem. Biol.* **14** (2018).

50   Wang, X. *et al.* Three-dimensional reconstruction of protein networks provides insight into human genetic disease. *Nature biotechnology* **30**, 159-164 (2012).

51   Sahni, N. *et al.* Widespread macromolecular interaction perturbations in human genetic disorders. *Cell* **161**, 647-660 (2015).

52   Kristensen, A. R., Gsponer, J. & Foster, L. J. A high-throughput approach for measuring temporal changes in the interactome. *Nat Methods* **9**, 907-909 (2012). https://doi.org:10.1038/nmeth.2131

53   Shirasaki, D. I. *et al.* Network organization of the huntingtin proteomic interactome in mammalian brain. *Neuron* **75**, 41-57 (2012). https://doi.org:10.1016/j.neuron.2012.05.024

54   Pankow, S. *et al.* ΔF508 CFTR interactome remodelling promotes rescue of cystic fibrosis. *Nature* **528**, 510-516 (2015). https://doi.org:10.1038/nature15729

55   Marsh, J. A. & Teichmann, S. A. Structure, dynamics, assembly, and evolution of protein complexes. *Annu. Rev. Biochem.* **84** (2015).

56   Levy, E. D. & Pereira-Leal, J. B. Evolution and dynamics of protein interactions and networks. *Curr. Opin. Struct. Biol.* **18** (2008).

57   Pennington, K., Chan, T., Torres, M. & Andersen, J. The dynamic and stress-adaptive signaling hub of 14-3-3: emerging mechanisms of regulation and context-dependent protein–protein interactions. *Oncogene* **37** (2018).

58   Chen, S., Synowsky, S., Tinti, M. & MacKintosh, C. The capture of phosphoproteins by 14-3-3 proteins mediates actions of insulin. *Trends Endocrinol. Metab.* **22** (2011).

59   Collins, B. C. Quantifying protein interaction dynamics by SWATH mass spectrometry: application to the 14-3-3 system. *Nat. Methods* **10** (2013).

60   Goldstein, G. *et al.* Isolation of a polypeptide that has lymphocyte-differentiating properties and is probably represented universally in living

cells. *Proc Natl Acad Sci U S A* **72**, 11-15 (1975). https://doi.org:10.1073/pnas.72.1.11

61   Sharp, P. M. & Li, W. H. Ubiquitin genes as a paradigm of concerted evolution of tandem repeats. *J Mol Evol* **25**, 58-64 (1987). https://doi.org:10.1007/BF02100041

62   Graham, R. W., Jones, D. & Candido, E. P. UbiA, the major polyubiquitin locus in Caenorhabditis elegans, has unusual structural features and is constitutively expressed. *Mol Cell Biol* **9**, 268-277 (1989). https://doi.org:10.1128/mcb.9.1.268-277.1989

63   Catic, A. & Ploegh, H. L. Ubiquitin--conserved protein or selfish gene? *Trends Biochem Sci* **30**, 600-604 (2005). https://doi.org:10.1016/j.tibs.2005.09.002

64   Goldknopf, I. L. & Busch, H. Isopeptide linkage between nonhistone and histone 2A polypeptides of chromosomal conjugate-protein A24. *Proc Natl Acad Sci U S A* **74**, 864-868 (1977). https://doi.org:10.1073/pnas.74.3.864

65   Goldknopf, I. L., French, M. F., Musso, R. & Busch, H. Presence of protein A24 in rat liver nucleosomes. *Proc Natl Acad Sci USA* **74** (1977).

66   Hershko, A., Heller, H., Elias, S. & Ciechanover, A. Components of ubiquitin-protein ligase system. Resolution, affinity purification, and role in protein breakdown. *J Biol Chem* **258**, 8206-8214 (1983).

67   Hershko, A., Ciechanover, A. & Rose, I. A. Identification of the active amino acid residue of the polypeptide of ATP-dependent protein breakdown. *J Biol Chem* **256**, 1525-1528 (1981).

68   Hershko, A., Ciechanover, A., Heller, H., Haas, A. L. & Rose, I. A. Proposed role of ATP in protein breakdown: conjugation of protein with multiple chains of the polypeptide of ATP-dependent proteolysis. *Proc Natl Acad Sci U S A* **77**, 1783-1786 (1980). https://doi.org:10.1073/pnas.77.4.1783

69   Ciechanover, A., Elias, S., Heller, H. & Hershko, A. "Covalent affinity" purification of ubiquitin-activating enzyme. *J Biol Chem* **257**, 2537-2542 (1982).

70   Ciehanover, A., Hod, Y. & Hershko, A. A heat-stable polypeptide component of an ATP-dependent proteolytic system from reticulocytes. *Biochem Biophys Res Commun* **81**, 1100-1105 (1978). https://doi.org:10.1016/0006-291x(78)91249-4

71   Glickman, M. H. & Ciechanover, A. The ubiquitin-proteasome proteolytic pathway: destruction for the sake of construction. *Physiol Rev* **82**, 373-428 (2002). https://doi.org:10.1152/physrev.00027.2001

72   Waxman, L., Fagan, J. M. & Goldberg, A. L. Demonstration of two distinct high molecular weight proteases in rabbit reticulocytes, one of which degrades ubiquitin conjugates. *J Biol Chem* **262**, 2451-2457 (1987).

73   Hough, R., Pratt, G. & Rechsteiner, M. Purification of two high molecular weight proteases from rabbit reticulocyte lysate. *J Biol Chem* **262**, 8303-8313 (1987).

74   Vijay-Kumar, S., Bugg, C. E. & Cook, W. J. Structure of ubiquitin refined at 1.8 A resolution. *J Mol Biol* **194**, 531-544 (1987). https://doi.org:10.1016/0022-2836(87)90679-6

75   Tatham, M. H., Plechanovova, A., Jaffray, E. G., Salmen, H. & Hay, R. T. Ube2W conjugates ubiquitin to alpha-amino groups of protein N-termini. *Biochem J* **453**, 137-145 (2013). https://doi.org:10.1042/BJ20130244

76   Wang, X. *et al.* Ube2j2 ubiquitinates hydroxylated amino acids on ER-associated degradation substrates. *J Cell Biol* **187**, 655-668 (2009). https://doi.org:10.1083/jcb.200908036

77   Clague, M. J., Heride, C. & Urbé, S. The demographics of the ubiquitin system. *Trends in Cell Biology* **25**, 417-426 (2015). https://doi.org:10.1016/j.tcb.2015.03.002

78   Cappadocia, L. & Lima, C. D. Ubiquitin-like Protein Conjugation: Structures, Chemistry, and Mechanism. *Chem Rev* **118**, 889-918 (2018). https://doi.org:10.1021/acs.chemrev.6b00737

79   Kim, W. *et al.* Systematic and quantitative assessment of the ubiquitin-modified proteome. *Mol Cell* **44**, 325-340 (2011). https://doi.org:10.1016/j.molcel.2011.08.025

80   Wagner, S. A. *et al.* A Proteome-wide, Quantitative Survey of In Vivo Ubiquitylation Sites Reveals Widespread Regulatory Roles. *Molecular & Cellular Proteomics* **10**, M111.013284-M013111.013284 (2011). https://doi.org:10.1074/mcp.m111.013284

81   Peng, J., Schwartz, D. & Elias, J. E. A proteomics approach to understanding protein ubiquitination. *Nat Biotechnol* **21** (2003).

82   Stewart, M. D., Ritterhoff, T., Klevit, R. E. & Brzovic, P. S. E2 enzymes: more than just middle men. *Cell Res* **26**, 423-440 (2016). https://doi.org:10.1038/cr.2016.35

83   Buetow, L. & Huang, D. T. Structural insights into the catalysis and regulation of E3 ubiquitin ligases. *Nature reviews. Molecular cell biology* **17**, 626-642 (2016). https://doi.org:10.1038/nrm.2016.91

84   Metzger, M. B., Pruneda, J. N., Klevit, R. E. & Weissman, A. M. RING-type E3 ligases: master manipulators of E2 ubiquitin-conjugating enzymes and ubiquitination. *Biochimica et biophysica acta* **1843**, 47-60 (2014). https://doi.org:10.1016/j.bbamcr.2013.05.026

85   Spratt, D. E., Walden, H. & Shaw, G. S. RBR E3 ubiquitin ligases: new structures, new insights, new questions. *Biochem J* **458**, 421-437 (2014). https://doi.org:10.1042/BJ20140006

86   Weber, J., Polo, S. & Maspero, E. HECT E3 Ligases: A Tale With Multiple Facets. *Front Physiol* **10**, 370 (2019). https://doi.org:10.3389/fphys.2019.00370

87   Horn-Ghetko, D. & Schulman, B. A. New classes of E3 ligases illuminated by chemical probes. *Curr Opin Struct Biol* **73**, 102341 (2022). https://doi.org:10.1016/j.sbi.2022.102341

88   Mevissen, T. E. T. & Komander, D. Mechanisms of Deubiquitinase Specificity and Regulation. *Annu Rev Biochem* **86**, 159-192 (2017). https://doi.org:10.1146/annurev-biochem-061516-044916

89   Popovic, D., Vucic, D. & Dikic, I. Ubiquitination in disease pathogenesis and treatment. *Nature Medicine* **20**, 1242-1253 (2014). https://doi.org:10.1038/nm.3739

90   Ashida, H., Kim, M. & Sasakawa, C. Exploitation of the host ubiquitin system by human bacterial pathogens. *Nature Reviews Microbiology* **12**, 399-413 (2014). https://doi.org:10.1038/nrmicro3259

91   Isaacson, M. K. & Ploegh, H. L. Ubiquitination, Ubiquitin-like Modifiers, and Deubiquitination in Viral Infection. *Cell Host and Microbe* **5**, 559-570 (2009). https://doi.org:10.1016/j.chom.2009.05.012

92   Randow, F. & Lehner, P. J. Viral avoidance and exploitation of the ubiquitin system. *Nature Cell Biology* **11**, 527-534 (2009). https://doi.org:10.1038/ncb0509-527

93   Hochstrasser, M. Origin and function of ubiquitin-like proteins. *Nature* **458**, 422-429 (2009). https://doi.org:10.1038/nature07958

94   Walden, H. *et al.* The structure of the APPBP1-UBA3-NEDD8-ATP complex reveals the basis for selective ubiquitin-like protein activation by an E1. *Mol Cell* **12**, 1427-1437 (2003). https://doi.org:10.1016/s1097-2765(03)00452-0

95   Harper, J. W. & Schulman, B. A. Structural complexity in ubiquitin recognition. *Cell* **124**, 1133-1136 (2006). https://doi.org:10.1016/j.cell.2006.03.009

96   Swatek, K. N. & Komander, D. Ubiquitin modifications. *Cell Research* **26**, 399-422 (2016). https://doi.org:10.1038/cr.2016.39

97   Komander, D. & Rape, M. The ubiquitin code. *Annual Review of Biochemistry* **81**, 203-229 (2012). https://doi.org:10.1146/annurev-biochem-060310-170328

98   Kaiser, S. E. *et al.* Protein standard absolute quantification (PSAQ) method for the measurement of cellular ubiquitin pools. *Nat Methods* **8**, 691-696 (2011). https://doi.org:10.1038/nmeth.1649

99   Ziv, I. *et al.* A perturbed ubiquitin landscape distinguishes between ubiquitin in trafficking and in proteolysis. *Mol Cell Proteomics* **10**, M111 009753 (2011). https://doi.org:10.1074/mcp.M111.009753

100   Dammer, E. B. *et al.* Polyubiquitin linkage profiles in three models of proteolytic stress suggest the etiology of Alzheimer disease. *J Biol Chem* **286**, 10457-10465 (2011). https://doi.org:10.1074/jbc.M110.149633

101   Xu, P. *et al.* Quantitative Proteomics Reveals the Function of Unconventional Ubiquitin Chains in Proteasomal Degradation. *Cell* **137**, 133-145 (2009). https://doi.org:10.1016/j.cell.2009.01.041

102   Choudhary, C., Kumar, C. & Gnad, F. Lysine acetylation targets protein complexes and co-regulates major cellular functions. *Science* **325** (2009).

103   Lundby, A., Lage, K. & Weinert, B. T. Proteomic analysis of lysine acetylation sites in rat tissues reveals organ specificity and subcellular patterns. *Cell Rep* **2** (2012).

104   Ohtake, F., Saeki, Y. & Sakamoto, K. Ubiquitin acetylation inhibits polyubiquitin chain elongation. *Embo Rep* **16** (2015).

105   Weinert, B. T., Schölz, C. & Wagner, S. A. Lysine succinylation is a frequently occurring modification in prokaryotes and eukaryotes and extensively overlaps with acetylation. *Cell Rep* **4** (2013).

106   Lee, H. J. *et al.* Quantitative analysis of phosphopeptides in search of the disease biomarker from the hepatocellular carcinoma specimen. *Proteomics* **9** (2009).

107 Zhou, H., Di Palma, S. & Preisinger, C. Toward a comprehensive characterization of a human cancer cell phosphoproteome. *J Proteome Res* **12** (2013).

108 Lundby, A., Secher, A. & Lage, K. Quantitative maps of protein phosphorylation sites across 14 different rat organs and tissues. *Nat Commun* **3** (2012).

109 Swaney, D. L., Beltrao, P. & Starita, L. Global analysis of phosphorylation and ubiquitylation cross-talk in protein degradation. *Nat Methods* **10** (2013).

110 Rikova, K., Guo, A. & Zeng, Q. Global survey of phosphotyrosine signaling identifies oncogenic kinases in lung cancer. *Cell* **131** (2007).

111 Olsen, J. V., Blagoev, B. & Gnad, F. Global, in vivo, and site-specific phosphorylation dynamics in signaling networks. *Cell* **127** (2006).

112 Galisson, F., Mahrouche, L. & Courcelles, M. A novel proteomics approach to identify SUMOylated proteins and their modification sites in human cells. *Mol Cell Proteomics* **10** (2011).

113 Lamoliatte, F., Bonneil, E. & Durette, C. Targeted identification of SUMOylation sites in human proteins using affinity enrichment and paralog-specific reporter ions. *Mol Cell Proteomics* **12** (2013).

114 Hendriks, I. A. *et al.* Uncovering global SUMOylation signaling networks in a site-specific manner. *Nature Structural and Molecular Biology* **21**, 927-936 (2014). https://doi.org:10.1038/nsmb.2890

115 Carroll, E. C., Greene, E. R., Martin, A. & Marqusee, S. Site-specific ubiquitination affects protein energetics and proteasomal degradation. *Nat Chem Biol* **16**, 866-875 (2020). https://doi.org:10.1038/s41589-020-0556-3

116 Husnjak, K. & Dikic, I. Ubiquitin-binding proteins: decoders of ubiquitin-mediated cellular functions. *Annu Rev Biochem* **81**, 291-322 (2012). https://doi.org:10.1146/annurev-biochem-051810-094654

117   Smeenk, G. & Mailand, N. Writers, Readers, and Erasers of Histone Ubiquitylation in DNA Double-Strand Break Repair. *Front Genet* **7**, 122 (2016). https://doi.org:10.3389/fgene.2016.00122

118   Dikic, I., Wakatsuki, S. & Walters, K. J. Ubiquitin-binding domains - from structures to functions. *Nature reviews. Molecular cell biology* **10**, 659-671 (2009). https://doi.org:10.1038/nrm2767

119   Ciechanover, A., Heller, H., Elias, S., Haas, A. L. & Hershko, A. ATP-dependent conjugation of reticulocyte proteins with the polypeptide required for protein degradation. *Proc Natl Acad Sci U S A* **77**, 1365-1368 (1980). https://doi.org:10.1073/pnas.77.3.1365

120   Aebersold, R. *et al.* How many human proteoforms are there? *Nat Chem Biol* **14**, 206-214 (2018). https://doi.org:10.1038/nchembio.2576

121   Yao, T. & Cohen, R. E. A cryptic protease couples deubiquitination and degradation by the proteasome. *Nature* **419**, 403-407 (2002). https://doi.org:10.1038/nature01071

122   Alberts, B. *et al. Molecular biology of the cell*. Sixth edition edn, 1 volume (various pagings) : illustrations (chiefly color) ; 29 cm (Garland Science, Taylor and Francis Group, 2015).

123   Montes de Oca Luna, R., Wagner, D. S. & Lozano, G. Rescue of early embryonic lethality in mdm2-deficient mice by deletion of p53. *Nature* **378**, 203-206 (1995). https://doi.org:10.1038/378203a0

124   Moroishi, T., Nishiyama, M., Takeda, Y., Iwai, K. & Nakayama, K. I. The FBXL5-IRP2 axis is integral to control of iron metabolism in vivo. *Cell Metab* **14**, 339-351 (2011). https://doi.org:10.1016/j.cmet.2011.07.011

125   Wakabayashi, N. *et al.* Keap1-null mutation leads to postnatal lethality due to constitutive Nrf2 activation. *Nat Genet* **35**, 238-245 (2003). https://doi.org:10.1038/ng1248

126   Skaar, J. R., Pagan, J. K. & Pagano, M. Mechanisms and function of substrate recruitment by F-box proteins. *Nature reviews. Molecular cell biology* **14**, 369-381 (2013). https://doi.org:10.1038/nrm3582

127   Watson, E. R., Brown, N. G., Peters, J. M., Stark, H. & Schulman, B. A. Posing the APC/C E3 Ubiquitin Ligase to Orchestrate Cell Division. *Trends Cell Biol* **29**, 117-134 (2019). https://doi.org:10.1016/j.tcb.2018.09.007

128   Yau, R. & Rape, M. The increasing complexity of the ubiquitin code. *Nat Cell Biol* **18**, 579-586 (2016). https://doi.org:10.1038/ncb3358

129   Horn-Ghetko, D. *et al.* Ubiquitin ligation to F-box protein targets by SCF–RBR E3–E3 super-assembly. *Nature*, 1-6 (2021). https://doi.org:10.1038/s41586-021-03197-9

130   Haakonsen, D. L. & Rape, M. Branching Out: Improved Signaling by Heterotypic Ubiquitin Chains. *Trends Cell Biol* **29**, 704-716 (2019). https://doi.org:10.1016/j.tcb.2019.06.003

131   Winston, J. T. *et al.* The SCFbeta-TRCP-ubiquitin ligase complex associates specifically with phosphorylated destruction motifs in IkappaBalpha and beta-catenin and stimulates IkappaBalpha ubiquitination in vitro. *Genes Dev* **13**, 270-283 (1999). https://doi.org:10.1101/gad.13.3.270

132   Donato, V. *et al.* The TDH-GCN5L1-Fbxo15-KBP axis limits mitochondrial biogenesis in mouse embryonic stem cells. *Nat Cell Biol* **19**, 341-351 (2017). https://doi.org:10.1038/ncb3491

133   Shemorry, A., Hwang, C. S. & Varshavsky, A. Control of protein quality and stoichiometries by N-terminal acetylation and the N-end rule pathway. *Mol Cell* **50**, 540-551 (2013). https://doi.org:10.1016/j.molcel.2013.03.018

134   Ivan, M. *et al.* HIFalpha targeted for VHL-mediated destruction by proline hydroxylation: implications for O2 sensing. *Science* **292**, 464-468 (2001). https://doi.org:10.1126/science.1059817

135   Jaakkola, P. *et al*. Targeting of HIF-alpha to the von Hippel-Lindau ubiquitylation complex by O2-regulated prolyl hydroxylation. *Science* **292**, 468-472 (2001). https://doi.org:10.1126/science.1059796

136   Zhang, Y. *et al*. RNF146 is a poly(ADP-ribose)-directed E3 ligase that regulates axin degradation and Wnt signalling. *Nat Cell Biol* **13**, 623-629 (2011). https://doi.org:10.1038/ncb2222

137   Yoo, Y. D. *et al*. N-terminal arginylation generates a bimodal degron that modulates autophagic proteolysis. *Proc Natl Acad Sci U S A* **115**, E2716-E2724 (2018). https://doi.org:10.1073/pnas.1719110115

138   Manford, A. G. *et al*. A Cellular Mechanism to Detect and Alleviate Reductive Stress. *Cell* **183**, 46-61 e21 (2020). https://doi.org:10.1016/j.cell.2020.08.034

139   Csizmok, V. *et al*. An allosteric conduit facilitates dynamic multisite substrate recognition by the SCF(Cdc4) ubiquitin ligase. *Nat Commun* **8**, 13943 (2017). https://doi.org:10.1038/ncomms13943

140   Tang, X. *et al*. Suprafacial orientation of the SCFCdc4 dimer accommodates multiple geometries for substrate ubiquitination. *Cell* **129**, 1165-1176 (2007). https://doi.org:10.1016/j.cell.2007.04.042

141   Werner, A., Baur, R., Kaya, D., Teerikorpi, N. & Rapé, M. Multivalent substrate recognition by an E3 ligase is essential for neural crest specification. *Elife*, e35407 (2018).

142   Mena, E. L. *et al*. Structural basis for dimerization quality control. *Nature* **586**, 452-456 (2020). https://doi.org:10.1038/s41586-020-2636-7

143   Mena, E. L. *et al*. Dimerization quality control ensures neuronal development and survival. *Science* **362** (2018). https://doi.org:10.1126/science.aap8236

144   Eddins, M. J., Carlile, C. M., Gomez, K. M., Pickart, C. M. & Wolberger, C. Mms2-Ubc13 covalently bound to ubiquitin reveals the structural basis of

linkage-specific polyubiquitin chain formation. *Nat Struct Mol Biol* **13**, 915-920 (2006). https://doi.org:10.1038/nsmb1148

145 Koegl, M. *et al.* A novel ubiquitination factor, E4, is involved in multiubiquitin chain assembly. *Cell* **96**, 635-644 (1999). https://doi.org:10.1016/s0092-8674(00)80574-7

146 Wickliffe, K. E., Lorenz, S., Wemmer, D. E., Kuriyan, J. & Rape, M. The mechanism of linkage-specific ubiquitin chain elongation by a single-subunit E2. *Cell* **144**, 769-781 (2011). https://doi.org:10.1016/j.cell.2011.01.035

147 Yau, R. G. *et al.* Assembly and Function of Heterotypic Ubiquitin Chains in Cell-Cycle and Protein Quality Control. *Cell* **171**, 918-933 e920 (2017). https://doi.org:10.1016/j.cell.2017.09.040

148 Rusnac, D. V. & Zheng, N. Structural Biology of CRL Ubiquitin Ligases. *Adv Exp Med Biol* **1217**, 9-31 (2020). https://doi.org:10.1007/978-981-15-1025-0_2

149 Wang, K., Deshaies, R. J. & Liu, X. Assembly and Regulation of CRL Ubiquitin Ligases. *Adv Exp Med Biol* **1217**, 33-46 (2020). https://doi.org:10.1007/978-981-15-1025-0_3

150 Harper, J. W. & Schulman, B. A. Cullin-RING Ubiquitin Ligase Regulatory Circuits: A Quarter Century Beyond the F-Box Hypothesis. *Annual Review of Biochemistry* **90**, 403-429 (2021). https://doi.org:10.1146/annurev-biochem-090120-013613

151 Bai, C. *et al.* SKP1 connects cell cycle regulators to the ubiquitin proteolysis machinery through a novel motif, the F-box. *Cell* **86**, 263-274 (1996). https://doi.org:10.1016/s0092-8674(00)80098-7

152 Hao, B., Oehlmann, S., Sowa, M. E., Harper, J. W. & Pavletich, N. P. Structure of a Fbw7-Skp1-cyclin E complex: multisite-phosphorylated substrate recognition by SCF ubiquitin ligases. *Mol Cell* **26**, 131-143 (2007). https://doi.org:10.1016/j.molcel.2007.02.022

153 Schulman, B. A. *et al.* Insights into SCF ubiquitin ligases from the structure of the Skp1–Skp2 complex. *Nature* **408**, 381-386 (2000).

154 Skowyra, D., Craig, K. L., Tyers, M., Elledge, S. J. & Harper, J. W. F-box proteins are receptors that recruit phosphorylated substrates to the SCF ubiquitin-ligase complex. *Cell* **91**, 209-219 (1997). https://doi.org:10.1016/s0092-8674(00)80403-1

155 Winston, J. T., Koepp, D. M., Zhu, C., Elledge, S. J. & Harper, J. W. A family of mammalian F-box proteins. *Curr Biol* **9**, 1180-1182 (1999). https://doi.org:10.1016/S0960-9822(00)80021-4

156 Goldenberg, S. J. *et al.* Structure of the Cand1-Cul1-Roc1 complex reveals regulatory mechanisms for the assembly of the multisubunit cullin-dependent ubiquitin ligases. *Cell* **119**, 517-528 (2004).

157 Liu, J., Furukawa, M., Matsumoto, T. & Xiong, Y. NEDD8 modification of CUL1 dissociates p120(CAND1), an inhibitor of CUL1-SKP1 binding and SCF ligases. *Mol Cell* **10**, 1511-1518 (2002). https://doi.org:10.1016/s1097-2765(02)00783-9

158 Zheng, J. *et al.* CAND1 binds to unneddylated CUL1 and regulates the formation of SCF ubiquitin E3 ligase complex. *Mol Cell* **10**, 1519-1526 (2002). https://doi.org:10.1016/s1097-2765(02)00784-0

159 Zheng, N. *et al.* Structure of the Cul1-Rbx1-Skp1-F boxSkp2 SCF ubiquitin ligase complex. *Nature* **416**, 703-709 (2002). https://doi.org:10.1038/416703a

160 Liu, X. *et al.* Cand1-Mediated Adaptive Exchange Mechanism Enables Variation in F-Box Protein Expression. *Mol Cell* **69**, 773-786.e776 (2018). https://doi.org:10.1016/j.molcel.2018.01.038

161 Pierce, Nathan W. *et al.* Cand1 Promotes Assembly of New SCF Complexes through Dynamic Exchange of F Box Proteins. *Cell* **153**, 206-215 (2013). https://doi.org:https://doi.org/10.1016/j.cell.2013.02.024

162   Reichermeier, K. M. *et al.* PIKES Analysis Reveals Response to Degraders and Key Regulatory Mechanisms of the CRL4 Network. *Mol Cell* **77**, 1092-1106.e1099 (2020). https://doi.org:10.1016/j.molcel.2019.12.013

163   Reitsma, J. M. *et al.* Composition and Regulation of the Cellular Repertoire of SCF Ubiquitin Ligases. *Cell* **171**, 1326-1339.e1314 (2017). https://doi.org:https://doi.org/10.1016/j.cell.2017.10.016

164   Zemla, A. *et al.* CSN- and CAND1-dependent remodelling of the budding yeast SCF complex. *Nat Commun* **4**, 1641 (2013). https://doi.org:10.1038/ncomms2628

165   Wu, S. *et al.* CAND1 controls in vivo dynamics of the cullin 1-RING ubiquitin ligase repertoire. *Nat Commun* **4**, 1642 (2013). https://doi.org:10.1038/ncomms2636

166   Duda, D. M. *et al.* Structural insights into NEDD8 activation of cullin-RING ligases: conformational control of conjugation. *Cell* **134**, 995-1006 (2008). https://doi.org:10.1016/j.cell.2008.07.022

167   Saha, A. & Deshaies, R. J. Multimodal Activation of the Ubiquitin Ligase SCF by Nedd8 Conjugation. *Mol Cell* **32**, 21-31 (2008). https://doi.org:10.1016/j.molcel.2008.08.021

168   Yamoah, K. *et al.* Autoinhibitory regulation of SCF-mediated ubiquitination by human cullin 1's C-terminal tail. *P Natl Acad Sci USA* **105**, 12230-12235 (2008). https://doi.org:10.1073/pnas.0806155105

169   Scott, D. C. *et al.* Two Distinct Types of E3 Ligases Work in Unison to Regulate Substrate Ubiquitylation. *Cell* **166**, 1198-1214 e1124 (2016). https://doi.org:10.1016/j.cell.2016.07.027

170   Baek, K. *et al.* NEDD8 nucleates a multivalent cullin–RING–UBE2D ubiquitin ligation assembly. *Nature* **578**, 461-466 (2020). https://doi.org:10.1038/s41586-020-2000-y

171   Horn-Ghetko, D. *et al.* Ubiquitin ligation to F-box protein targets by SCF-RBR E3-E3 super-assembly. *Nature* **590** (2021). https://doi.org:10.1038/s41586-021-03197-9

172   Monda, J. K. *et al.* Structural conservation of distinctive N-terminal acetylation-dependent interactions across a family of mammalian NEDD8 ligation enzymes. *Structure* **21**, 42-53 (2013). https://doi.org:10.1016/j.str.2012.10.013

173   Scott, D. C. *et al.* A dual E3 mechanism for Rub1 ligation to Cdc53. *Mol Cell* **39**, 784-796 (2010). https://doi.org:10.1016/j.molcel.2010.08.030

174   Scott, D. C., Monda, J. K., Bennett, E. J., Harper, J. W. & Schulman, B. A. N-terminal acetylation acts as an avidity enhancer within an interconnected multiprotein complex. *Science* **334**, 674-678 (2011). https://doi.org:10.1126/science.1209307

175   Angers, S. *et al.* Molecular architecture and assembly of the DDB1-CUL4A ubiquitin ligase machinery. *Nature* **443**, 590-593 (2006). https://doi.org:10.1038/nature05175

176   Cardote, T. A. F., Gadd, M. S. & Ciulli, A. Crystal Structure of the Cul2-Rbx1-EloBC-VHL Ubiquitin Ligase Complex. *Structure* **25**, 901-911 e903 (2017). https://doi.org:10.1016/j.str.2017.04.009

177   Bornstein, G., Ganoth, D. & Hershko, A. Regulation of neddylation and deneddylation of cullin1 in SCFSkp2 ubiquitin ligase by F-box protein and substrate. *Proc Natl Acad Sci U S A* **103**, 11515-11520 (2006). https://doi.org:10.1073/pnas.0603921103

178   Fischer, Eric S. *et al.* The Molecular Basis of CRL4DDB2/CSA Ubiquitin Ligase Architecture, Targeting, and Activation. *Cell* **147**, 1024-1039 (2011). https://doi.org:https://doi.org/10.1016/j.cell.2011.10.035

179   Emberley, E. D., Mosadeghi, R. & Deshaies, R. J. Deconjugation of Nedd8 from Cul1 is directly regulated by Skp1-F-box and substrate, and the COP9

signalosome inhibits deneddylated SCF by a noncatalytic mechanism. *J Biol Chem* **287**, 29679-29689 (2012). https://doi.org:10.1074/jbc.M112.352484

180   Enchev, Radoslav I. *et al.* Structural Basis for a Reciprocal Regulation between SCF and CSN. *Cell Reports* **2**, 616-627 (2012). https://doi.org:https://doi.org/10.1016/j.celrep.2012.08.019

181   Cavadini, S. *et al.* Cullin–RING ubiquitin E3 ligase regulation by the COP9 signalosome. *Nature* **531**, 598-603 (2016). https://doi.org:10.1038/nature17416

182   Mosadeghi, R. *et al.* Structural and kinetic analysis of the COP9-Signalosome activation and the cullin-RING ubiquitin ligase deneddylation cycle. *Elife* **5** (2016). https://doi.org:10.7554/eLife.12102

183   Mayor-Ruiz, C. *et al.* Plasticity of the Cullin-RING Ligase Repertoire Shapes Sensitivity to Ligand-Induced Protein Degradation. *Mol Cell* **75**, 849-858.e848 (2019). https://doi.org:https://doi.org/10.1016/j.molcel.2019.07.013

184   Baek, K. *et al.* Systemwide disassembly and assembly of SCF ubiquitin ligase complexes. *Cell* **186**, 1895-1911 e1821 (2023). https://doi.org:10.1016/j.cell.2023.02.035

185   Mohamed, W. I. *et al.* The CRL4(DCAF1) cullin-RING ubiquitin ligase is activated following a switch in oligomerization state. *Embo J* **40**, e108008 (2021). https://doi.org:10.15252/embj.2021108008

186   Zhang, Y. *et al.* Adaptive exchange sustains cullin-RING ubiquitin ligase networks and proper licensing of DNA replication. *Proc Natl Acad Sci U S A* **119**, e2205608119 (2022). https://doi.org:10.1073/pnas.2205608119

187   Scott, D. C. *et al.* E3 ligase autoinhibition by C-degron mimicry maintains C-degron substrate fidelity. *Mol Cell* **83**, 770-786 e779 (2023). https://doi.org:10.1016/j.molcel.2023.01.019

188   Soucy, T. A. *et al*. An inhibitor of NEDD8-activating enzyme as a new approach to treat cancer. *Nature* **458**, 732-736 (2009). https://doi.org:10.1038/nature07884

189   Willems, A. R., Schwab, M. & Tyers, M. A hitchhiker's guide to the cullin ubiquitin ligases: SCF and its kin. *Biochimica et biophysica acta* **1695**, 133-170 (2004).

190   Mayor-Ruiz, C. *et al*. Rational discovery of molecular glue degraders via scalable chemical profiling. *Nat Chem Biol* **16**, 1199-1207 (2020). https://doi.org:10.1038/s41589-020-0594-x

191   Wu, T. *et al*. Targeted protein degradation as a powerful research tool in basic biology and drug target discovery. *Nat Struct Mol Biol* **27**, 605-614 (2020). https://doi.org:10.1038/s41594-020-0438-0

192   Henneberg, L. T. & Schulman, B. A. Decoding the messaging of the ubiquitin system using chemical and protein probes. *Cell Chem Biol* **28**, 889-902 (2021). https://doi.org:10.1016/j.chembiol.2021.03.009

193   Dokmanovic, M. & Marks, P. A. Prospects: Histone deacetylase inhibitors. *Journal of Cellular Biochemistry* **96**, 293-304 (2005). https://doi.org:10.1002/jcb.20532

194   Knight, Z. A., Lin, H. & Shokat, K. M. Targeting the cancer kinome through polypharmacology. *Nature Reviews Cancer* **10**, 130-137 (2010). https://doi.org:10.1038/nrc2787

195   Zhang, J., Yang, P. L. & Gray, N. S. Targeting cancer with small molecule kinase inhibitors. *Nature Reviews Cancer* **9**, 28-39 (2009). https://doi.org:10.1038/nrc2559

196   Hoyt, E. A., Cal, P. M. S. D., Oliveira, B. L. & Bernardes, G. J. L. Contemporary approaches to site-selective protein modification. *Nature Reviews Chemistry* **3**, 147-171 (2019). https://doi.org:10.1038/s41570-019-0079-1

197   Hewings, D. S., Flygare, J. A., Bogyo, M. & Wertz, I. E. Activity-based probes for the ubiquitin conjugation–deconjugation machinery: new chemistries, new tools, and new insights. *FEBS Journal* **284**, 1555-1576 (2017). https://doi.org:10.1111/febs.14039

198   Sui, X. *et al.* Development and application of ubiquitin-based chemical probes. *Chemical Science* **11**, 12633-12646 (2020). https://doi.org:10.1039/d0sc03295f

199   Niphakis, M. J. & Cravatt, B. F. Enzyme inhibitor discovery by activity-based protein profiling. *Annual Review of Biochemistry* **83**, 341-377 (2014). https://doi.org:10.1146/annurev-biochem-060713-035708

200   Kelsall, I. R. *et al.* TRIAD1 and HHARI bind to and are activated by distinct neddylated Cullin-RING ligase complexes. *Embo J* **32**, 2848-2860 (2013). https://doi.org:10.1038/emboj.2013.209

201   Sakamoto, K. M. *et al.* Protacs: Chimeric molecules that target proteins to the Skp1-Cullin-F box complex for ubiquitination and degradation. *P Natl Acad Sci USA* **98**, 8554-8559 (2001). https://doi.org:10.1073/pnas.141230798

202   Sakamoto, K. M. *et al.* Development of Protacs to target cancer-promoting proteins for ubiquitination and degradation. *Molecular & cellular proteomics : MCP* **2**, 1350-1358 (2003). https://doi.org:10.1074/mcp.T300009-MCP200

203   Schneekloth, J. S. *et al.* Chemical Genetic Control of Protein Levels: Selective in Vivo Targeted Degradation. *Journal of the American Chemical Society* **126**, 3748-3754 (2004). https://doi.org:10.1021/ja039025z

204   Schneekloth, A. R., Pucheault, M., Tae, H. S. & Crews, C. M. Targeted intracellular protein degradation induced by a small molecule: En route to chemical proteomics. *Bioorganic and Medicinal Chemistry Letters* **18**, 5904-5908 (2008). https://doi.org:10.1016/j.bmcl.2008.07.114

205   Han, T. *et al.* Anticancer sulfonamides target splicing by inducing RBM39 degradation via recruitment to DCAF15. *Science* **356**, eaal3755-eaal3755 (2017). https://doi.org:10.1126/science.aal3755

206   Krönke, J. *et al.* Lenalidomide causes selective degradation of IKZF1 and IKZF3 in multiple myeloma cells. *Science* **343**, 301-305 (2014). https://doi.org:10.1126/science.1244851

207   Lu, G. *et al.* The myeloma drug lenalidomide promotes the cereblon-dependent destruction of ikaros proteins. *Science* **343**, 305-309 (2014). https://doi.org:10.1126/science.1244917

208   Uehara, T. *et al.* Selective degradation of splicing factor CAPERα By anticancer sulfonamides. *Nat Chem Biol* **13**, 675-680 (2017). https://doi.org:10.1038/nchembio.2363

209   Lv, L. *et al.* Discovery of a molecular glue promoting cdk12-ddb1 interaction to trigger cyclin k degradation. *eLife* **9**, 1-34 (2020). https://doi.org:10.7554/ELIFE.59994

210   Słabicki, M. *et al.* The CDK inhibitor CR8 acts as a molecular glue degrader that depletes cyclin K. *Nature* **585**, 293-297 (2020). https://doi.org:10.1038/s41586-020-2374-x

211   Jevtić, P., Haakonsen, D. L. & Rapé, M. An E3 ligase guide to the galaxy of small-molecule-induced protein degradation. *Cell Chem Biol* (2021). https://doi.org:https://doi.org/10.1016/j.chembiol.2021.04.002

212   Kannt, A. & Dikic, I. Expanding the arsenal of E3 ubiquitin ligases for proximity-induced protein degradation. *Cell Chem Biol* **28**, 1014-1031 (2021). https://doi.org:10.1016/j.chembiol.2021.04.007

213   Chirnomas, D., Hornberger, K. R. & Crews, C. M. Protein degraders enter the clinic - a new approach to cancer therapy. *Nat Rev Clin Oncol* **20**, 265-278 (2023). https://doi.org:10.1038/s41571-023-00736-3

214   Kohler, G. & Milstein, C. Continuous cultures of fused cells secreting antibody of predefined specificity. *Nature* **256**, 495-497 (1975). https://doi.org:10.1038/256495a0

215   Moraes, J. Z. *et al.* Hybridoma technology: is it still useful? *Curr Res Immunol* **2**, 32-40 (2021). https://doi.org:10.1016/j.crimmu.2021.03.002

216   Mitra, S. & Tomar, P. C. Hybridoma technology; advancements, clinical significance, and future aspects. *J Genet Eng Biotechnol* **19**, 159 (2021). https://doi.org:10.1186/s43141-021-00264-6

217   Jaroszewicz, W., Morcinek-Orlowska, J., Pierzynowska, K., Gaffke, L. & Wegrzyn, G. Phage display and other peptide display technologies. *FEMS Microbiol Rev* **46** (2022). https://doi.org:10.1093/femsre/fuab052

218   Ledsgaard, L., Kilstrup, M., Karatt-Vellatt, A., McCafferty, J. & Laustsen, A. H. Basics of Antibody Phage Display Technology. *Toxins (Basel)* **10** (2018). https://doi.org:10.3390/toxins10060236

219   Sidhu, S. S. & Koide, S. Phage display for engineering and analyzing protein interaction interfaces. *Curr Opin Struc Biol* **17**, 481-487 (2007). https://doi.org:https://doi.org/10.1016/j.sbi.2007.08.007

220   Pluckthun, A. Designed ankyrin repeat proteins (DARPins): binding proteins for research, diagnostics, and therapy. *Annu Rev Pharmacol Toxicol* **55**, 489-511 (2015). https://doi.org:10.1146/annurev-pharmtox-010611-134654

221   Wu, C. H., Liu, I. J., Lu, R. M. & Wu, H. C. Advancement and applications of peptide phage display technology in biomedical science. *J Biomed Sci* **23**, 8 (2016). https://doi.org:10.1186/s12929-016-0223-x

222   Shuken, S. R. An Introduction to Mass Spectrometry-Based Proteomics. *Journal of Proteome Research* **22**, 2151-2171 (2023). https://doi.org:10.1021/acs.jproteome.2c00838

223   Sinha, A. & Mann, M. A beginner's guide to mass spectrometry–based proteomics. *The Biochemist* **42**, 64-69 (2020). https://doi.org:10.1042/bio20200057

224   Aebersold, R. & Mann, M. Mass-spectrometric exploration of proteome structure and function. *Nature* **537**, 347-355 (2016). https://doi.org:10.1038/nature19949

225   Banerjee, S. & Mazumdar, S. Electrospray ionization mass spectrometry: a technique to access the information beyond the molecular weight of the analyte. *Int J Anal Chem* **2012**, 282574 (2012). https://doi.org:10.1155/2012/282574

226   Mann, M. The Rise of Mass Spectrometry and the Fall of Edman Degradation. *Clin Chem* **62**, 293-294 (2016). https://doi.org:10.1373/clinchem.2014.237271

227   Edman, P. A method for the determination of amino acid sequence in peptides. *Arch Biochem* **22**, 475 (1949).

228   Fenn, J. B., Mann, M., Meng, C. K., Wong, S. F. & Whitehouse, C. M. Electrospray ionization for mass spectrometry of large biomolecules. *Science* **246**, 64-71 (1989). https://doi.org:10.1126/science.2675315

229   Thomson, J. J. XL. Cathode Rays. *The London, Edinburgh, and Dublin Philosophical Magazine and Journal of Science* **44**, 293-316 (1897). https://doi.org:10.1080/14786449708621070

230   Karas, M., Bachmann, D., Bahr, U. & Hillenkamp, F. Matrix-assisted ultraviolet laser desorption of non-volatile compounds. *International Journal of Mass Spectrometry and Ion Processes* **78**, 53-68 (1987). https://doi.org:https://doi.org/10.1016/0168-1176(87)87041-6

231   Wien, W. Untersuchungen über die electrische Entladung in verdünnten Gasen. *Annalen der Physik* **301**, 440-452 (1898). https://doi.org:https://doi.org/10.1002/andp.18983010618

232   Fornelli, L. *et al.* Top-down proteomics: Where we are, where we are going? *J Proteomics* **175**, 3-4 (2018). https://doi.org:10.1016/j.jprot.2017.02.002

233   Nanita, S. C. & Kaldon, L. G. Emerging flow injection mass spectrometry methods for high-throughput quantitative analysis. *Anal Bioanal Chem* **408**, 23-33 (2016). https://doi.org:10.1007/s00216-015-9193-1

234   Gachumi, G., Purves, R. W., Hopf, C. & El-Aneed, A. Fast Quantification Without Conventional Chromatography, The Growing Power of Mass Spectrometry. *Analytical Chemistry* **92**, 8628-8637 (2020). https://doi.org:10.1021/acs.analchem.0c00877

235   Chekmeneva, E. *et al.* Optimization and Application of Direct Infusion Nanoelectrospray HRMS Method for Large-Scale Urinary Metabolic Phenotyping in Molecular Epidemiology. *J Proteome Res* **16**, 1646-1658 (2017). https://doi.org:10.1021/acs.jproteome.6b01003

236   Meyer, J. G., Niemi, N. M., Pagliarini, D. J. & Coon, J. J. Quantitative shotgun proteome analysis by direct infusion. *Nat Methods* **17**, 1222-1228 (2020). https://doi.org:10.1038/s41592-020-00999-z

237   Pitt, J. J. Principles and applications of liquid chromatography-mass spectrometry in clinical biochemistry. *Clin Biochem Rev* **30**, 19-34 (2009).

238   Beck, S. *et al.* The Impact II, a Very High-Resolution Quadrupole Time-of-Flight Instrument (QTOF) for Deep Shotgun Proteomics *. *Molecular & Cellular Proteomics* **14**, 2014-2029 (2015). https://doi.org:https://doi.org/10.1074/mcp.M114.047407

239   Pol, J., Strohalm, M., Havlicek, V. & Volny, M. Molecular mass spectrometry imaging in biomedical and life science research. *Histochem Cell Biol* **134**, 423-443 (2010). https://doi.org:10.1007/s00418-010-0753-3

240   Haag, A. M. Mass Analyzers and Mass Spectrometers. *Adv Exp Med Biol* **919**, 157-169 (2016). https://doi.org:10.1007/978-3-319-41448-5_7

241   Makarov, A. Electrostatic axially harmonic orbital trapping: a high-performance technique of mass analysis. *Anal Chem* **72**, 1156-1162 (2000). https://doi.org:10.1021/ac991131p

242   Meier, F. *et al*. diaPASEF: parallel accumulation-serial fragmentation combined with data-independent acquisition. *Nat Methods* **17**, 1229-1236 (2020). https://doi.org:10.1038/s41592-020-00998-0

243   Meier, F. *et al*. Online Parallel Accumulation-Serial Fragmentation (PASEF) with a Novel Trapped Ion Mobility Mass Spectrometer. *Mol Cell Proteomics* **17**, 2534-2545 (2018). https://doi.org:10.1074/mcp.TIR118.000900

244   Syka, J. E., Coon, J. J., Schroeder, M. J., Shabanowitz, J. & Hunt, D. F. Peptide and protein sequence analysis by electron transfer dissociation mass spectrometry. *Proc Natl Acad Sci U S A* **101**, 9528-9533 (2004). https://doi.org:10.1073/pnas.0402700101

245   Halim, M. A. *et al*. Combined Infrared Multiphoton Dissociation with Ultraviolet Photodissociation for Ubiquitin Characterization. *J Am Soc Mass Spectrom* **27**, 1435-1442 (2016). https://doi.org:10.1007/s13361-016-1419-8

246   Brodbelt, J. S. Photodissociation mass spectrometry: new tools for characterization of biological molecules. *Chem Soc Rev* **43**, 2757-2783 (2014). https://doi.org:10.1039/c3cs60444f

247   Antoine, R., Lemoine, J. & Dugourd, P. Electron photodetachment dissociation for structural characterization of synthetic and bio-polymer anions. *Mass Spectrom Rev* **33**, 501-522 (2014). https://doi.org:10.1002/mas.21402

248   Reilly, J. P. Ultraviolet photofragmentation of biomolecular ions. *Mass Spectrom Rev* **28**, 425-447 (2009). https://doi.org:10.1002/mas.20214

249 Olsen, J. V. *et al*. Higher-energy C-trap dissociation for peptide modification analysis. *Nat Methods* **4**, 709-712 (2007). https://doi.org:10.1038/nmeth1060

250 Ichou, F. *et al*. Comparison of the activation time effects and the internal energy distributions for the CID, PQD and HCD excitation modes. *J Mass Spectrom* **49**, 498-508 (2014). https://doi.org:10.1002/jms.3365

251 Venable, J. D., Dong, M. Q., Wohlschlegel, J., Dillin, A. & Yates, J. R. Automated approach for quantitative analysis of complex peptide mixtures from tandem mass spectra. *Nat Methods* **1**, 39-45 (2004). https://doi.org:10.1038/nmeth705

252 Purvine, S., Eppel, J. T., Yi, E. C. & Goodlett, D. R. Shotgun collision-induced dissociation of peptides using a time of flight mass analyzer. *Proteomics* **3**, 847-850 (2003). https://doi.org:10.1002/pmic.200300362

253 Bateman, R. H. *et al*. A novel precursor ion discovery method on a hybrid quadrupole orthogonal acceleration time-of-flight (Q-TOF) mass spectrometer for studying protein phosphorylation. *J Am Soc Mass Spectrom* **13**, 792-803 (2002). https://doi.org:10.1016/S1044-0305(02)00420-8

254 Masselon, C. *et al*. Accurate mass multiplexed tandem mass spectrometry for high-throughput polypeptide identification from mixtures. *Anal Chem* **72**, 1918-1924 (2000). https://doi.org:10.1021/ac991133+

255 Gillet, L. C. *et al*. Targeted data extraction of the MS/MS spectra generated by data-independent acquisition: a new concept for consistent and accurate proteome analysis. *Mol Cell Proteomics* **11**, O111 016717 (2012). https://doi.org:10.1074/mcp.O111.016717

256 Tsou, C. C. *et al*. DIA-Umpire: comprehensive computational framework for data-independent acquisition proteomics. *Nat Methods* **12**, 258-264, 257 p following 264 (2015). https://doi.org:10.1038/nmeth.3255

257   Strauss, M. T. *et al.* AlphaPept: a modern and open framework for MS-based proteomics. *Nat Commun* **15**, 2168 (2024). https://doi.org:10.1038/s41467-024-46485-4

258   Sinitcyn, P. *et al.* MaxDIA enables library-based and library-free data-independent acquisition proteomics. *Nature Biotechnology* **39**, 1563-1573 (2021). https://doi.org:10.1038/s41587-021-00968-7

259   Lyapina, S. *et al.* Promotion of NEDD-CUL1 conjugate cleavage by COP9 signalosome. *Science* **292**, 1382-1385 (2001). https://doi.org:10.1126/science.1059780

260   Enchev, R. I. *et al.* Structural basis for a reciprocal regulation between SCF and CSN. *Cell Rep* **2**, 616-627 (2012). https://doi.org:10.1016/j.celrep.2012.08.019

261   Lingaraju, G. M. *et al.* Crystal structure of the human COP9 signalosome. *Nature* **512**, 161-165 (2014). https://doi.org:10.1038/nature13566

262   Cavadini, S. *et al.* Cullin-RING ubiquitin E3 ligase regulation by the COP9 signalosome. *Nature* **531**, 598-603 (2016). https://doi.org:10.1038/nature17416

263   Wiśniewski, J. R., Hein, M. Y., Cox, J. & Mann, M. A "proteomic ruler" for protein copy number and concentration estimation without spike-in standards. *Molecular & cellular proteomics* **13**, 3497-3506 (2014).

264   Feng, S. *et al.* Arabidopsis CAND1, an Unmodified CUL1-Interacting Protein, Is Involved in Multiple Developmental Pathways Controlled by Ubiquitin/Proteasome-Mediated Protein Degradation. *The Plant Cell* **16**, 1870-1882 (2004). https://doi.org:10.1105/tpc.021949

265   Scott, D. C. *et al.* Two Distinct Types of E3 Ligases Work in Unison to Regulate Substrate Ubiquitylation. *Cell* **166**, 1198-+ (2016). https://doi.org:10.1016/j.cell.2016.07.027

266   Vogl, A. M. *et al.* Global site-specific neddylation profiling reveals that NEDDylated cofilin regulates actin dynamics. *Nat Struct Mol Biol* **27** (2020). https://doi.org:10.1038/s41594-019-0370-3

267   Lobato-Gil, S. *et al.* Proteome-wide identification of NEDD8 modification sites reveals distinct proteomes for canonical and atypical NEDDylation. *Cell Rep* **34**, 108635 (2021). https://doi.org:10.1016/j.celrep.2020.108635

268   Kostrhon, S. *et al.* CUL5-ARIH2 E3-E3 ubiquitin ligase structure reveals cullin-specific NEDD8 activation. *Nat Chem Biol* **17**, 1075-1083 (2021). https://doi.org:10.1038/s41589-021-00858-8

269   Jones, J. *et al.* A targeted proteomic analysis of the ubiquitin-like modifier nedd8 and associated proteins. *J Proteome Res* **7**, 1274-1287 (2008). https://doi.org:10.1021/pr700749v

270   Bennett, E. J., Rush, J., Gygi, S. P. & Harper, J. W. Dynamics of cullin-RING ubiquitin ligase network revealed by systematic quantitative proteomics. *Cell* **143**, 951-965 (2010). https://doi.org:10.1016/j.cell.2010.11.017

271   Matsumoto, M. L. *et al.* K11-Linked Polyubiquitination in Cell Cycle Control Revealed by a K11 Linkage-Specific Antibody. *Mol Cell* **39**, 477-484 (2010). https://doi.org:10.1016/j.molcel.2010.07.001

272   Yau, R. G. *et al.* Assembly and Function of Heterotypic Ubiquitin Chains in Cell-Cycle and Protein Quality Control. *Cell* **171**, 918-933.e920 (2017). https://doi.org:10.1016/j.cell.2017.09.040

273   Michel, M. A., Swatek, K. N., Hospenthal, M. K. & Komander, D. Ubiquitin Linkage-Specific Affimers Reveal Insights into K6-Linked Ubiquitin Signaling. *Mol Cell* **68**, 233-246.e235 (2017). https://doi.org:10.1016/j.molcel.2017.08.020

274   Yu, Y. *et al.* K29-linked ubiquitin signaling regulates proteotoxic stress response and cell cycle. *Nat Chem Biol* **17**, 896-905 (2021). https://doi.org:10.1038/s41589-021-00823-5

275   Adams, J. J. & Sidhu, S. S. Synthetic antibody technologies. *Curr Opin Struc Biol* **24**, 1-9 (2014). https://doi.org:https://doi.org/10.1016/j.sbi.2013.11.003

276   Schlierf, A. *et al.* Targeted inhibition of the COP9 signalosome for treatment of cancer. *Nat Commun* **7**, 13166-13166 (2016). https://doi.org:10.1038/ncomms13166

277   Zhuang, M. *et al.* Structures of SPOP-substrate complexes: insights into molecular architectures of BTB-Cul3 ubiquitin ligases. *Mol Cell* **36**, 39-50 (2009). https://doi.org:10.1016/j.molcel.2009.09.022

278   Ji, A. X. *et al.* Structural Insights into KCTD Protein Assembly and Cullin3 Recognition. *J Mol Biol* **428**, 92-107 (2016). https://doi.org:10.1016/j.jmb.2015.08.019

279   Cowan, A. D. & Ciulli, A. Driving E3 Ligase Substrate Specificity for Targeted Protein Degradation: Lessons from Nature and the Laboratory. *Annu Rev Biochem* **91**, 295-319 (2022). https://doi.org:10.1146/annurev-biochem-032620-104421

280   Zengerle, M., Chan, K.-H. & Ciulli, A. Selective Small Molecule Induced Degradation of the BET Bromodomain Protein BRD4. *ACS Chemical Biology* **10**, 1770-1777 (2015). https://doi.org:10.1021/acschembio.5b00216

281   Gadd, M. S. *et al.* Structural basis of PROTAC cooperative recognition for selective protein degradation. *Nat Chem Biol* **13**, 514-521 (2017). https://doi.org:10.1038/nchembio.2329

282   Vashisht, A. A. *et al.* Control of iron homeostasis by an iron-regulated ubiquitin ligase. *Science* **326**, 718-721 (2009). https://doi.org:10.1126/science.1176333

283   Salahudeen, A. A. *et al.* An E3 Ligase Possessing an Iron-Responsive Hemerythrin Domain Is a Regulator of Iron Homeostasis. *Science* **326**, 722-726 (2009). https://doi.org:10.1126/science.1176326

284   Winter, G. E. *et al*. BET Bromodomain Proteins Function as Master Transcription Elongation Factors Independent of CDK9 Recruitment. *Mol Cell* **67**, 5-+ (2017). https://doi.org:10.1016/j.molcel.2017.06.004

285   Murray, P. J. *et al*. Macrophage activation and polarization: nomenclature and experimental guidelines. *Immunity* **41**, 14-20 (2014). https://doi.org:10.1016/j.immuni.2014.06.008

286   Murray, P. J. Macrophage Polarization. *Annu Rev Physiol* **79**, 541-566 (2017). https://doi.org:10.1146/annurev-physiol-022516-034339

287   Koren, I. *et al*. The Eukaryotic Proteome Is Shaped by E3 Ubiquitin Ligases Targeting C-Terminal Degrons. *Cell* **173**, 1622-1635.e1614 (2018). https://doi.org:https://doi.org/10.1016/j.cell.2018.04.028

288   Lin, H. C. *et al*. C-Terminal End-Directed Protein Elimination by CRL2 Ubiquitin Ligases. *Mol Cell* **70**, 602-613 e603 (2018). https://doi.org:10.1016/j.molcel.2018.04.006

289   Thrun, A. *et al*. Convergence of mammalian RQC and C-end rule proteolytic pathways via alanine tailing. *Mol Cell* **81**, 2112-2122 e2117 (2021). https://doi.org:10.1016/j.molcel.2021.03.004

290   Ishii, T. *et al*. Transcription factor Nrf2 coordinately regulates a group of oxidative stress-inducible genes in macrophages. *Journal of Biological Chemistry* **275**, 16023-16029 (2000). https://doi.org:DOI 10.1074/jbc.275.21.16023

291   Dinkova-Kostova, A. T., Kostov, R. V. & Canning, P. Keap1, the cysteine-based mammalian intracellular sensor for electrophiles and oxidants. *Arch Biochem Biophys* **617**, 84-93 (2017). https://doi.org:10.1016/j.abb.2016.08.005

292   Manford, A. G. *et al*. Structural basis and regulation of the reductive stress response. *Cell* **184**, 5375-5390 e5316 (2021). https://doi.org:10.1016/j.cell.2021.09.002

293   Bakker, N. V. & Pearce, E. J. Cell-intrinsic metabolic regulation of mononuclear phagocyte activation: Findings from the tip of the iceberg. *Immunological Reviews* **295**, 54-67 (2020). https://doi.org:10.1111/imr.12848

294   Sims, J. J. & Cohen, R. E. Linkage-specific avidity defines the lysine 63-linked polyubiquitin-binding preference of rap80. *Mol Cell* **33**, 775-783 (2009). https://doi.org:10.1016/j.molcel.2009.02.011

295   Armstrong, A. A., Mohideen, F. & Lima, C. D. Recognition of SUMO-modified PCNA requires tandem receptor motifs in Srs2. *Nature* **483**, 59-63 (2012). https://doi.org:10.1038/nature10883

296   Panier, S. *et al.* Tandem protein interaction modules organize the ubiquitin-dependent response to DNA double-strand breaks. *Mol Cell* **47**, 383-395 (2012). https://doi.org:10.1016/j.molcel.2012.05.045

297   Morgan, M. T. & Wolberger, C. Recognition of ubiquitinated nucleosomes. *Curr Opin Struct Biol* **42**, 75-82 (2017). https://doi.org:10.1016/j.sbi.2016.11.016

298   Rajan, S. & Sidhu, S. S. Vol. 502 (eds K. Dane Wittrup & Gregory L. B. T. Methods in Enzymology Verdine) 3-23 (Academic Press, 2012).

299   Kabsch, W. Xds. *Acta Crystallogr D Biol Crystallogr* **66**, 125-132 (2010). https://doi.org:10.1107/S0907444909047337

300   Sliwiak, J., Jaskolski, M., Dauter, Z., McCoy, A. J. & Read, R. J. Likelihood-based molecular-replacement solution for a highly pathological crystal with tetartohedral twinning and sevenfold translational noncrystallographic symmetry. *Acta Crystallogr D Biol Crystallogr* **70**, 471-480 (2014). https://doi.org:10.1107/S1399004713030319

301   Emsley, P. & Cowtan, K. Coot: model-building tools for molecular graphics. *Acta Crystallogr D Biol Crystallogr* **60**, 2126-2132 (2004). https://doi.org:10.1107/S0907444904019158

302   Adams, P. D. *et al.* PHENIX: a comprehensive Python-based system for macromolecular structure solution. *Acta Crystallogr D Biol Crystallogr* **66**, 213-221 (2010). https://doi.org:10.1107/S0907444909052925

303   Pettersen, E. F. *et al.* UCSF ChimeraX: Structure visualization for researchers, educators, and developers. *Protein Sci* **30**, 70-82 (2021). https://doi.org:10.1002/pro.3943

304   Kulak, N. A., Pichler, G., Paron, I., Nagaraj, N. & Mann, M. Minimal, encapsulated proteomic-sample processing applied to copy-number estimation in eukaryotic cells. *Nature Methods* **11**, 319-324 (2014). https://doi.org:10.1038/nmeth.2834

305   Bruderer, R. *et al.* Extending the Limits of Quantitative Proteome Profiling with Data-Independent Acquisition and Application to Acetaminophen-Treated Three-Dimensional Liver Microtissues *[S]. *Molecular & Cellular Proteomics* **14**, 1400-1410 (2015). https://doi.org:10.1074/mcp.M114.044305

306   Dichtl, S. *et al.* Gene-selective transcription promotes the inhibition of tissue reparative macrophages by TNF. *Life Sci Alliance* **5** (2022). https://doi.org:10.26508/lsa.202101315